POLITECNICO
MILANO 1863

SCUOLA DI INGEGNERIA INDUSTRIALE
E DELL'INFORMAZIONE

1-D FLUID DYNAMIC MODELLING AND ANALYSIS OF PIPE JUNCTIONS IN IC ENGINES

TESI DI LAUREA MAGISTRALE IN
ENERGY ENGINEERING – INGEGNERIA ENERGETICA

Author: **Mirza Faizan Ali Baig (943606)**

Advisor: Prof. **Angelo Onorati**
Eng. **Andrea Massimo Marinoni**

Academic Year: 2021-22

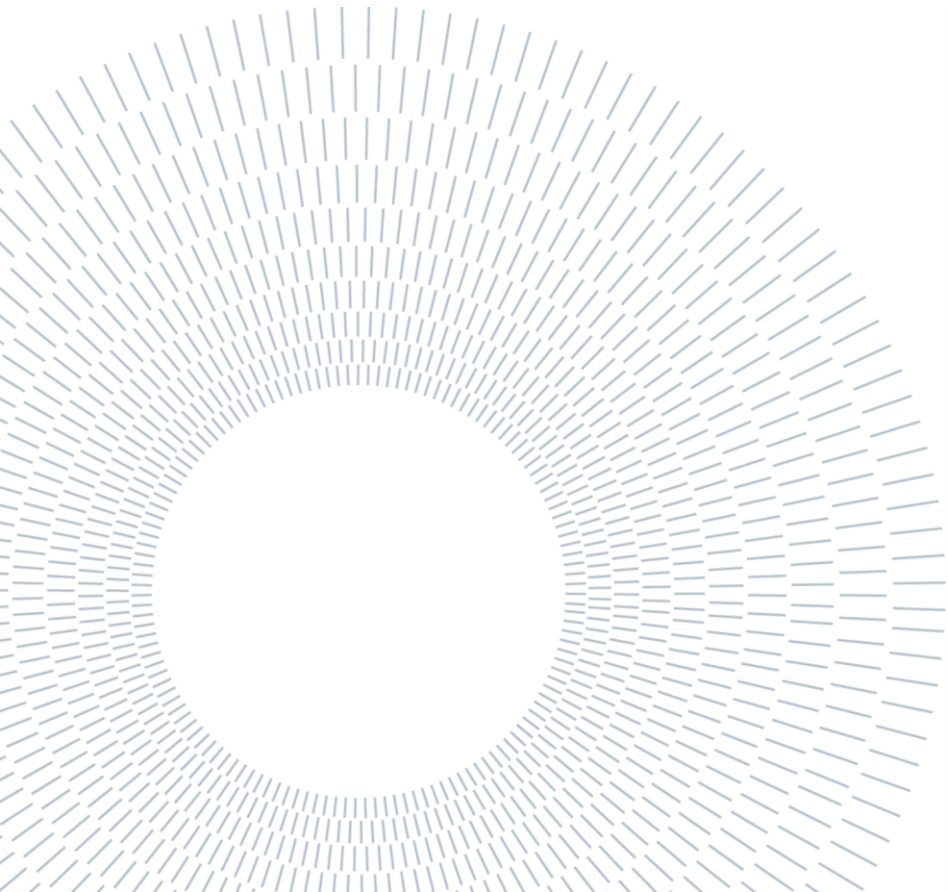

Contents

Abstract

Since the invention of the internal combustion engine, there has been continuous research for the modification and improvements in their performances adopting numerous diversified approaches with the use of various methods and technologies. Early stages for these research activities involved expensive experimental processes.

Numerical models being faster and cheaper in comparison to the experimental models were developed eventually to model the complex unsteady fluid dynamic phenomena which provide a basis in the design stages of the internal combustion engines and are used to predict the engine behaviour at various operating conditions. Multiple diversified models implemented vary in terms of their hypothesis, accuracy in results, application, and computational times.

The objective of this thesis is to analyse, improve and contribute to computational codes used by simulation tool Gasdyn for the solution of junctions in the exhaust and intake manifolds of internal combustion engines.

The fundamental conservation equations and the associated numerical techniques used for the solution are presented initially. The attention is then focussed to the various junction types and their characteristics. Different models adopted for the solution of junction boundary conditions are described and compared which includes the constant pressure model and pressure loss models. The focus is then centred on the computational codes referred to as subroutines, used for the solution of different junction types based on the theoretical constant pressure model. The application and results of the subroutines are analysed for different engine configurations. In the end, a new general subroutine is developed which is capable to provide the solution of all junction types using a single computational code and is more accurate and robust. The result from the new subroutine is validated by substituting the old computational code for each of old subroutines individually and then simultaneous substitution is performed to finally validate the new subroutine. The development of new general subroutine was successful which was verified by the results of substitution. The new subroutine has now successfully been incorporated in Gasdyn software in place of the previous subroutines for solution of different junction types.

Keywords: 1-D fluid dynamic simulation, Constant pressure junction model, Pressure Loss model, Subroutines, Duct Junction types

Abstract in lingua italiana

Dall'invenzione del motore a combustione interna, vi è stata una continua ricerca per la modifica e il miglioramento delle loro prestazioni adottando numerosi approcci diversificati con l'uso di vari metodi e tecnologie. .

I modelli numerici, essendo più veloci ed economici rispetto ai modelli sperimentali, sono stati infine sviluppati per modellare i complessi fenomeni fluidodinamici instabili che forniscono una base nelle fasi di progettazione dei motori a combustione interna e sono utilizzati per prevedere il comportamento del motore in varie condizioni operative. I molteplici modelli diversificati implementati variano in termini di ipotesi, accuratezza dei risultati, applicazione e tempi di calcolo.

L'obiettivo di questa tesi è analizzare, migliorare e contribuire ai codici computazionali utilizzati dallo strumento di simulazione Gasdyn per la soluzione delle giunzioni nei collettori di scarico e di aspirazione dei motori a combustione interna.

Inizialmente vengono presentate le equazioni fondamentali di conservazione e le relative tecniche numeriche utilizzate per la soluzione. L'attenzione è poi rivolta alle varie tipologie di giunzione e alle loro caratteristiche. Vengono descritti e confrontati diversi modelli adottati per la soluzione delle condizioni al contorno di giunzione che includono il modello a pressione costante ei modelli di perdita di pressione. Il focus è poi centrato sui codici computazionali denominati subroutine, utilizzati per la soluzione di diversi tipi di giunzioni in base al modello teorico a pressione costante. L'applicazione ei risultati delle subroutine vengono analizzati per diverse configurazioni del motore. Alla fine, viene sviluppata una nuova subroutine generale in grado di fornire la soluzione di tutti i tipi di giunzione utilizzando un unico codice computazionale ed è più accurata e robusta. Il risultato della nuova subroutine viene convalidato sostituendo il vecchio codice di calcolo per ciascuna delle vecchie subroutine individualmente e quindi viene eseguita la sostituzione simultanea per convalidare finalmente la nuova subroutine. Lo sviluppo di una nuova subroutine generale ha avuto successo, il che è stato verificato dai risultati della sostituzione. Le nuove subroutine sono state ora incorporate con successo nel software Gasdyn al posto delle precedenti subroutine per diversi tipi di giunzione.

Parole chiave: Simulazione fluidodinamica 1-D, modello di giunzione a pressione costante, modello di perdita di pressione, sottoprogrammi, tipi di giunzione

List of Figures

List of Tables

1. Fundamental Equations

1.1 Introduction

Internal combustion engines have experienced a continuous evolution since their birth. Internal combustion engines experience a cyclic process for the replacement of charge. The general motion of flow gases in the duct system of an internal combustion engine can be highly unstable, the main reason for this being the rapid fluctuations in speed and pressure during the engine cycle along with continuous closing and opening of the engine cylinder valves. Inside the walls of engine cylinder and among the fluid there are friction forces present. The entropy and temperature within the fluid is not constant and gradients of these properties cannot be neglected. The fluid has considerable viscosity and compressibility. The unsteady phenomenon gives rise to complexities which led to the numerical code development that can be applied to model these complexities on the internal combustion engine.

Due to the complex phenomenon in the ducts of internal combustion engines, there has been vast research for the creation of models that are able to solve the inlet and outlet flow characteristics. Navier-Stokes system of differential equations can be used for the establishment of a procedure for the description of this type of phenomenon. These systems of equations are three-dimensional and often involve turbulent models. However, the nature of these 3D equations can be very complex such that the computing time and method can be very challenging and costly therefore it would require the need for a series of simplifications and assumptions, such that these simplifications would still ensure sufficient accuracy of gas dynamic processes. These simplifications would be strong but should allow for model to be of certain relevance with the actual and the objective of these simplifications should be to maintain a suitable compromise between complexity of calculations and accuracy of predictions.

One of the fundamental hypotheses that simplifies the procedure is of one-dimensional flow. This hypothesis is based on the fact that the longitudinal size of the ducts for internal combustion engines is prevalent in comparison to the transverse dimensions. Also, the radii of curvature are quite wide, and the section variation is contained. In order to simulate the fluid dynamics in the exhaust or intake of an internal combustion engines, the computational programs used are mostly one dimensional, this is due to the fact that multiple engine cycle are required to achieve a cyclic convergence. Although due to revolution in computing technology it is possible in this modern era to perform multidimensional simulations for unsteady flows. The 1-D approach remains a commonly used method due to the simplicity it adds such as it does not require the complex meshing of components and on top of that it has certainly high calculations times which allows the engineers to perform multiple tests of designs and configurations in a short interval.

This hypothesis of one-dimensional analysis permits us to analyze the fluid dynamic characteristics such as density, speed, pressure, and other properties to be a function of only the axial variable x and to be constant across the cross-section of the ducts. [1]

$$u = u(x,t) \tag{1.1}$$

$$p = p(x,t) \tag{1.2}$$

$$\rho = \rho(x,t) \tag{1.3}$$

1.2 One dimensional Model

As in the Gasdyn code the following hypothesis is adopted, and the motion is always considered as one dimensional unless stated otherwise. The following simplifications are adopted [2], [3]

- One dimensional motion
- Compressible fluid
- Non isentropic motion
- Ducts with variable cross section
- Non adiabatic process: The heat exchange will only be considered at the walls of the ducts

As already specified by *Eq (1.1-1.3)* the properties of the fluid will be considered only as a function of time and axial coordinate x.

Based on these hypotheses, the derivations for the conservations of mass, momentum and energy for an appropriate control volume will be performed.

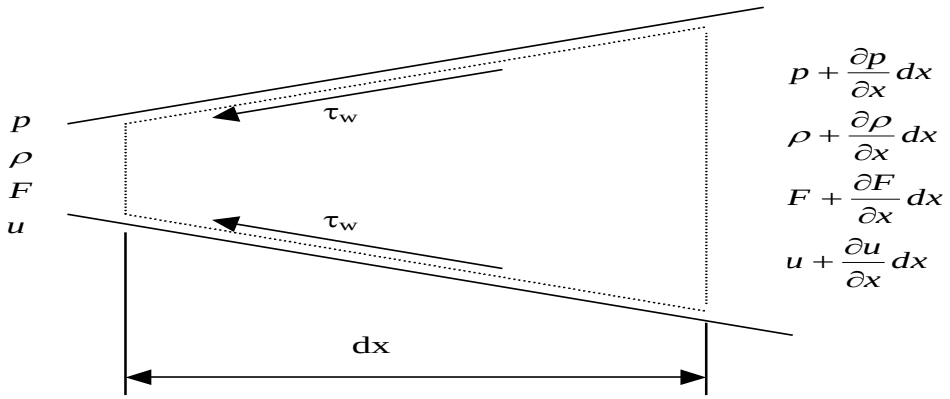

Figure 1.1: Control Volume for a mono dimensional scheme for 1-D analysis

Where:

- F represents the cross-section area
- u represents the velocity of the fluid
- ρ represents the density of fluid
- p represents the pressure of the fluid

1.2.1 Continuity Equation

The basic continuity equation for any control volume is given by:

$$\dot{m} = \rho_{in} u_{in} F_{in} = \rho_{out} u_{out} F_{out} \tag{1.4}$$

The hypothesis for the given control volume in *Figure 1.1* is that the walls are rigid and mass flows are not permeable through the walls. The area of cross section is a function of longitudinal direction x only

For the Continuity Equation, the flow coming out of the volume in consideration should be equal to the rate of change of mass inside the volume. If we consider the *Figure 1.1*, mass flow rate that enters the left surface is equal to

$$\rho U F \tag{1.5}$$

While the mass flow rate that leaves the right surface is given by:

$$\left(\rho + \frac{\partial \rho}{\partial x} dx\right)\left(u + \frac{\partial u}{\partial x}\partial x\right)\left(F + \frac{\partial F}{\partial x}\partial x\right) \tag{1.6}$$

Therefore, the rate at which the mass flow rate is decreasing inside the control volume is given as:

$$-\frac{\partial}{\partial t}(\rho F dx) \tag{1.7}$$

Hence the substitution of above equations into the continuity equation and then simplifying, following relation is obtained:

$$\frac{\partial \rho}{\partial t} + \frac{\partial(\rho u)}{\partial t} + \frac{\rho u}{F}.\frac{dF}{dx} = 0 \tag{1.8}$$

1.2.2 Conservation of momentum

The conservation equation states that for a control volume the sum of the forces due to pressure and the shear forces of walls must be equal to sum of the net rate of change of momentum within the control volume and the net efflux of momentum from the control surface.

The various contributions are then defined

$$pF - \left(p + \frac{\partial p}{\partial x}\partial x\right)\left(F + \frac{\partial F}{\partial x}\partial x\right) + p\frac{\partial F}{\partial x}\partial x \tag{1.9}$$

The above equation considers the pressure forces exerted along the longitudinal directions. The terminal section pressure is denoted with the first two terms while the third term denotes the pressure exerted by the lateral surface of the control volume on the fluid.

In order to predict the internal change in flow of fluid, friction is considered a source term while writing the equation for the conservation of momentum. This is because that approximation of one-dimensional flow does not allow to point the adherence condition of fluid flow to the duct walls. As shown in the *Figure 1.1*, the shear stress T_w on the control volume is because of the frictional force between the fluid and walls of the duct. The shear stress is given by:

$$\tau_w = f * \frac{1}{2} * \rho\, u^2 \tag{1.10}$$

Starting from the definition of the frictional force, it is possible to define the force applied to the opposite lateral surface due to friction

$$F_{fric} = -f\frac{1}{2}\,\rho\, u^2.\pi\, D\, dx \tag{1.11}$$

The value of friction coefficient f can be determined by the formulation proposed by Swamee and Jain given as below:

$$f = \frac{0.25}{\left[\log_{10}\left(\frac{k}{3.7D} + \frac{5.74}{Re^{0.9}}\right)\right]} \tag{1.12}$$

The net flow of momentum through the control volume is given by the *Eq (1.13)* and we obtain *Eq (1.14)* simplifying and considering only first order derivates :

$$\frac{\partial(\rho F dx.u)}{\partial t} \tag{1.13}$$

$$\left(\rho + \frac{\partial\rho}{\partial x}\partial x\right)\left(u + \frac{\partial u}{\partial x}\partial x\right)^2\left(F + \frac{\partial F}{\partial x}\partial x\right) - \rho F u^2 = \frac{\partial(\rho F u^2)}{\partial x}\partial x \tag{1.14}$$

Applying the definition of conservation of momentum to contributions already defined above, the following equation is obtained :

$$\frac{\partial(\rho u F)}{\partial t} + \frac{d(\rho u^2 + p)F}{dx} - \frac{p dF}{dx} + f.\frac{1}{2}\rho u^2.\pi D = 0 \tag{1.15}$$

Introducing the term G representing the effect of viscosity:

$$G = f\frac{u^2}{2}\frac{\mu}{|u|}\frac{4}{D} \tag{1.16}$$

It is now possible to write in simple form the final equation of conservation of momentum

$$\frac{\partial u}{\partial t} + u\frac{\partial u}{\partial x} + \frac{1}{\rho}\cdot\frac{\partial p}{\partial x} + G = 0 \tag{1.17}$$

1.2.3 Conservation of Energy

Based on the laws of conservation of energy and thermodynamics of the control volume in consideration Figure 1.1

$$\frac{\partial E_o}{\partial t} + \frac{\partial H_o}{\partial x}\partial x = \dot{Q} - \dot{L} \tag{1.18}$$

The first term of the above equation denotes the change of total internal energy per unit time which is followed by the net enthalpy flow across the surface. The sum of both internal energy and enthalpy change cannot be equal to the difference between the incoming thermal energy and the work done from the system. Highlighting the specific total energy, if we denote the total internal energy E_o in form of specific energy e_o and the total specific enthalpy H_o in form of specific enthalpy h_o, then we can rewrite the equation as below :

$$\frac{\partial(e_o \rho F \partial x)}{\partial t} + \frac{\partial(h_o \rho F u)}{\partial x} dx = \dot{q}\rho F dx + \Delta H_{react} F dx \tag{1.19}$$

Where

- e_o is the total specific energy and is given by $e_o = e + u^2/2$
- h_o is the total specific enthalpy and is given by $h_o = e_o + p/\rho$
- $\dot{q}$ is the amount of heat exchanged per unit time
- ΔH_{react} is the amount of heat released per unit time and unit volume due to chemical reactions that may occurs in the fluids

The term $\dot{q}$ which denotes the heat flux that occurs radially from the fluid to the pipes is expressed as follows:

$$\dot{q} = \frac{4h}{\rho D}(T_w - T_g) \tag{1.20}$$

Where:

T_w = Temperature of the surface walls

T_g = Temperature of gas

D = Duct diameter

h = convective heat transfer coefficient

The convective heat transfer coefficient is calculated as per the literature found from Churchill or Sider.

Since in the internal combustion engines, specifically the intake and exhaust ducts there is no mechanical work, therefore we have not considered mechanical work for the conservation of energy.

The *Eq (1.19)* represents a partial differential hyperbolic system that is non-linear in closed form, because there are four unknowns being pressure, density , specific internal energy, and velocity of fluid. The solution cannot be obtained with only the three available equations, and there should be another equation describing the behavior of fluid. As first approximation, it is possible to model the gas through hypothesis of perfect gas having constant specific heats. Since the specific heats of ideal gases varies directly with the temperature and inside the duct the temperature gradient is negligible, therefore this assumption would not produce any significant errors. Another hypothesis we adopt is to neglect the term $\Delta H_{react} F dx$ since we assume that there will be no chemical reactions occurring in the ducts or the amount of energy released will not be significant.

The perfect gas equation is written below *Eq (1.21)* and the internal energy for a perfect gas with constant specific heats is represented by *Eq (1.22)*

$$\frac{p}{\rho} = RT \tag{1.21}$$

$$e = C_v T \tag{1.22}$$

If the hypothesis is implemented, we can eliminate the fourth unknown and rewrite the energy conservation by substituting the internal energy from *Eq (1.22)*

$$\frac{\partial}{\partial t}\left[\rho F \partial x \,(c_v T + \frac{u^2}{2})\right] + \frac{\partial}{\partial x}\left[(\rho F \partial x)(c_v T + \frac{p}{\rho} + \frac{u^2}{2})\right] dx = \dot{q}\rho F dx \tag{1.23}$$

A subsequent recombination of the above equation with the conservation equations of mass and equation of the momentum leads to the non-conservative formulation of the equation of energy conservation:

$$\left(\frac{\partial p}{\partial t} + u\frac{\partial p}{\partial x}\right) - a^2\left(\frac{\partial p}{\partial t} + u\frac{\partial p}{\partial x}\right) - \rho(k-1)(q + \dot{u}G) = 0 \tag{1.24}$$

Where ‘a’ represents the speed of propagation of sound in a perfect gas and is given as

$$a = \sqrt{kRT} \tag{1.25}$$

And k is the ratio of gas specific heats at constant pressure and constant volume

$$k = \frac{c_p}{c_v} \tag{1.26}$$

The system of nonlinear hyperbolic system in non-conservative form is now constituted with the help of the final forms for the equations for conservation of energy, mass and momentum with additional relations that describe the gas model and were essential for closing the problem.

The system of equations in non-conservative form lends itself to a form which can be solved using different methods. One of these methods is a method of characteristics which is discussed later in this report. Method of Characteristics (MOC) was used as primary method for the study of intake and exhaust tuning phenomenon in internal combustion engines. Many computer programs which were used to predict the one-dimensional analysis of waves actions were based initially on this method. This method has a 1st order accuracy in space and time but also has a limiting feature in its detailed analysis because it is not able to capture micro-oscillations of the quantities and this effect is notable at higher operating frequencies. This imposes a limitation to the use of this method and another method was developed to cope with the limitation of capturing all oscillations regardless of the operating frequency.

Since the phenomenon that characterize the motion of the flow needs to be identified with precision this led to the development of a method along with the evolution of modern computational fluid dynamics , this method is called Shock Capturing Method. The shock capturing method is a second order numerical method that can describe with greater accuracy all sort of discontinuities in the flow being observed. [1]

But the methods described above as method of characteristics or the shock capturing method requires a conservative formulation of the nonlinear hyperbolic system. In order to write the conservative formulation of the system , first it becomes necessary to check which group of variables can be conserved at the time of collisions. Thus, first such groups are identified and then the equations are written again such that the group of variables identified are brought together in a common differential. The classical equation for the conservation of momentum is not used for this purpose, instead the impulse equation is used. The impulse equation is actually a combination of conservation of momentum and the continuity equation.

The system of conservation in conserved form is given as:

$$\frac{\partial(\rho F)}{\partial t} + \frac{\partial(\rho u F)}{\partial x} = 0$$

$$\frac{\partial(\rho u F)}{\partial t} + \frac{\partial(\rho u^2 F + pF)}{\partial x} - p\frac{dF}{dx} + \rho G F = 0$$

$$\frac{\partial(\rho e_o F)}{\partial t} + \frac{\partial(\rho u h_o)}{\partial x} - \rho \dot{F} = 0$$

The system of equations described above should be written in matrix form to make the shock capturing methods applicable such that four vectors are identified. Which are respectively W being vector of conserved variables, F being vector of fluxes , vector B contains the source terms related to pressure forces due to section variation. The vector B(x,W) is conservative because it is related to the dimensions of the duct. The vector C is a vector of source term that includes the effect of friction and heat exchange which is irreversible. The vector C is not conservative.

The four vectors are as follows :

- Vector of conserved variables:

$$W(x,t) = \begin{bmatrix} \rho F \\ \rho u F \\ \rho e_0 F \end{bmatrix} \tag{1.27}$$

- Flow vector of conserved variables

$$F(W) = \begin{bmatrix} \rho u F \\ (\rho u^2 + p)F \\ (\rho e_0 u + up)F \end{bmatrix} \tag{1.28}$$

- Vector for the source terms :

$$B(x,W) = \begin{bmatrix} 0 \\ -p\frac{\partial F}{\partial x} \\ 0 \end{bmatrix} \tag{1.29}$$

$$C(x,W) = \begin{bmatrix} 0 \\ -\rho G F \\ -\rho \dot{q} F \end{bmatrix} \tag{1.30}$$

The system written in matrix form results

$$\frac{\partial W(x,t)}{\partial t} + \frac{\partial F(W)}{\partial x} + B(x,W) + C(x,W) = 0 \tag{1.31}$$

Which can also be simplified as follows

$$W_t + F(W)_x = S(x, W) \tag{1.32}$$

Since it is discussed before, that without an additional hypothesis, that describe the behavior of the gas it is not possible to find the solution to the problem. This hypothesis to be adopted can be of a perfect gas with constant specific heat or could be a more general model that could describe a mixture of ideal gases.

2. Numerical Methods

The solution to the hyperbolic partial derivative equations developed in the previous chapter cannot be possibly determined in an analytical manner and there is need for a numerical approach so that the complex system of equations could be solved. This requires implementing a discretization of space and time domains so as to result in an algebraic formulation of the problem which can be utilized by a software program in order to produce a solution.

The formulation for solution of problems like these have been developed and improved continuously from decades, the first of these algorithms was developed by Riemann who called the method as Method of Characteristics. The method is simple and relies on reformulation of partial differential equations as ordinary differential equations. This method has been applied widely in modelling of fluid dynamic processes for internal combustion engines and was used for years for the study of compressible fluids. [4]

The method of characteristics although widely used for years was not very accurate, more accurate and robust methods were developed later

For the past decades, several methods have been developed in computational fluid dynamics, these methods are able to provide more accuracy compared to the previous methods. The methods developed include the Shock capturing method which provide second order accuracy and thus better results. These methods allow to measure any sort of discontinuity in the flow and are able to capture with accuracy any shock wave present in the flow path. The methods start from hyperbolic system's conservative solution determination and are more robust.

There can be two different classifications of these methods which are based on shock-capturing techniques.

- Upwind / Characteristic based: These methods orient the solution scheme based on the flow direction, the results obtained from these methods provide the results with extreme accuracy. However, the computational times required by this method are high. [1]

- Symmetrical methods: Also referred to as the non upwind method, as opposed to the upwind method, the symmetrical method is not sensitive to the direction of flow and apply the same finite difference scheme in order to express the terms of partial derivative at all nodes. Although the accuracy achieved is not in comparison with the upwind based method but is reliable. Despite being less accurate, they provide the advantage of having short computational times [5]

2.1 Method of characteristics

In 1858, Riemann introduced this method which was the first computational scheme to be utilized by a computer program. The method of characteristics as by the name suggests uses characteristic lines which are traceable in the field of flow, along these lines the partial differential equations are transformed into ordinary differential equations. [1] , [4]

The flow in the duct system of internal combustion engines is irreversible mostly because of heat transfer and friction with the duct walls. Henceforth, variation in entropy is evident and the flow is defined to be non-homentropic when entropy is not constant. Therefore, for solution of non-homentropic flow, we must take into account the energy equations along with the two compatibility equations driven from continuity and conservation of momentum.

As previously specified, the method applies to the hyperbolic system in its non-conservative formulation

$$\frac{\partial \rho}{\partial t} + \frac{\partial}{\partial x}(\rho u) + \frac{\rho u}{F}\frac{dF}{dx} = 0 \tag{2.1}$$

$$\frac{\partial(\rho uF)}{\partial t}+\frac{\partial(\rho u^2+p)F}{\partial x}-\frac{pdF}{dx}+f\frac{1}{2}u^2.\pi D=0 \tag{2.2}$$

$$\left(\frac{\partial p}{\partial t}+u\frac{\partial p}{\partial x}\right)-a^2\left(\frac{\partial p}{\partial t}+u\frac{\partial p}{\partial x}\right)-\rho(k-1)\left(\dot{q}-\frac{\Delta H_{react}}{\rho}+uG\right)=0 \tag{2.3}$$

It is possible to express the system in a form that puts in highlights the quantities (u + a), (u - a) and u:

$$\left(\frac{\partial p}{\partial t}+(u+a)\frac{\partial p}{\partial x}\right)+\rho a\left(\frac{\partial u}{\partial t}+(u+a)\frac{\partial u}{\partial x}\right)-(k-1)(\rho q\dot{}-\Delta H_{react}+\rho uG)+a^2\frac{\rho u}{F}\frac{dF}{dx}+\rho aG=0 \tag{2.4}$$

$$\left(\frac{\partial p}{\partial t}+(u-a)\frac{\partial p}{\partial x}\right)+\rho a\left(\frac{\partial u}{\partial t}+(u-a)\frac{\partial u}{\partial x}\right)-(k-1)(\rho q\dot{}-\Delta H_{react}+\rho uG)+a^2\frac{\rho u}{F}\frac{dF}{dx}-\rho aG=0 \tag{2.5}$$

$$\left(\frac{\partial p}{\partial t}+u\frac{\partial p}{\partial x}\right)+a^2\left(\frac{\partial \rho}{\partial t}+u\frac{\partial \rho}{\partial x}\right)-(\rho q\dot{}-\Delta H_{react}+\rho uG)=0 \tag{2.6}$$

In order to write the equations above in a simplified manner simplify the writing, we denote the terms in the above equations as below:

$$\Delta_1=-(k-1)(\rho q\dot{}-\Delta H_{react}+\rho uG) \tag{2.7}$$

$$\Delta_2=a^2\frac{\rho u}{F}\frac{dF}{dx} \tag{2.8}$$

$$\Delta_{3=}\rho aG \tag{2.9}$$

Where the terms Δ_j represents

Δ_1: irreversible heat transfer

Δ_2: change of section along the duct (reversible term)

Δ_3: friction with walls (irreversible term)

The terms Δ_1 and Δ_3 are dissipative in nature by considering the presence of friction and heat exchange with the wall respectively. In case of non-homentropic flow these

terms tend to be greater than zero. On the other hand, the term Δ_2 is conserved and depends on the of variation of the duct section.

$$\left(\frac{\partial p}{\partial t}+(u+a)\frac{\partial p}{\partial x}\right)+\rho a\left(\frac{\partial u}{\partial t}+(u+a)\frac{\partial u}{\partial x}\right)+\ \boldsymbol{\Delta_1}+\ \boldsymbol{\Delta_2}+\ \boldsymbol{\Delta_3}=\mathbf{0} \tag{2.10}$$

$$\left(\frac{\partial p}{\partial t}+(u-a)\frac{\partial p}{\partial x}\right)+\rho a\left(\frac{\partial u}{\partial t}+(u-a)\frac{\partial u}{\partial x}\right)-(k-1)+\ \boldsymbol{\Delta_1}+\ \boldsymbol{\Delta_2}-\ \boldsymbol{\Delta_3}=\mathbf{0} \tag{2.11}$$

$$\left(\frac{\partial p}{\partial t}+u\frac{\partial p}{\partial x}\right)+a^2\left(\frac{\partial \rho}{\partial t}+u\frac{\partial \rho}{\partial x}\right)+\boldsymbol{\Delta_1}=0 \tag{2.12}$$

The terms in the paranthesis of above system of equations represent the differentials of independent variables p, u and ρ along the characteristic curve. The slope of the characteristic curve depends on flow properties, similar to the pressure wave which propagates in the duct with speed u+a

$$\frac{dp(x(t),t)}{dt}=\frac{dp}{dt}+(u+a)\frac{dp}{dx} \tag{2.13}$$

It is possible to define the slope of the curves along which the transformation of partial differential equations to ordinary differential equations is performed:

$$\frac{dx}{dt}=u+a \tag{2.14}$$

$$\frac{dx}{dt}=u-a \tag{2.15}$$

$$\frac{dx}{dt}=u \tag{2.16}$$

Eq (2.14) & (Eq 2.15) represent the propagating nature of the required solutions with their slopes inducating the absolute velocity of the wave progagation inside the given duct. The *Eq (2.16)* is directly related to the velocity of fluid particles and provides information about the entropic flow level. The single characterstic line demarcates the seperation between two regions of the plane in which fluid dynamic quantities differ infinitesimally, thus representing for derived quantites such as velocity a boundary of disconitnuity. For the three curves that are identified by the *Eq (2.14 - 2.16*), with the help of the system of equations that allow us to transform partial derivatives to ordinary derivatives and the compatibility equations, the system of equation can be rewriten as follows:

$$\frac{\partial p}{\partial t} + \rho a \frac{\partial u}{\partial t} + \Delta_1 + \Delta_2 + \Delta_3 = 0 \tag{2.17}$$

$$\frac{\partial p}{\partial t} - \rho a \frac{\partial u}{\partial t} + \Delta_1 + \Delta_2 - \Delta_3 = 0 \tag{2.18}$$

$$\frac{\partial p}{\partial t} - a^2 \frac{\partial \rho}{\partial t} + \Delta_1 = \mathbf{0} \tag{2.19}$$

For the moment we consider the homoentropic flow, the hypothesis renders the source terms and the equation along the characterstic line would be transformed to the following for the homoentropic case:

$$\partial p + \rho a du = 0 \tag{2.20}$$

$$\partial p - \rho a du = 0 \tag{2.21}$$

$$\partial p - a^2 dp = 0 \tag{2.22}$$

Since the *Eq (2.22*), is a redundant equation only representing the speed of sound, which means that the system of equation is simplified with only two unkonwns remaining. The two unknowns being the sound velocity a and the fluid velocity u. Since the flow being considered is the homoentropic flow, therefore the isentropic relations are valid.

$$\frac{p}{\rho^k} = const \tag{2.23}$$

$$\frac{p}{a^{\frac{2}{k-1}}} = const \tag{2.24}$$

After differentiating the above isentropic relations and using in the compatibility equations we get:

$$du + \frac{2}{k-1} da = 0 \tag{2.25}$$

$$du - \frac{2}{k-1} da = 0 \tag{2.26}$$

The *Eq (2.25) & Eq (2.26)* can be represented on a planes (u,a) and (x,t) which are named as the state diagram and position diagram respectively.

In order to distinguish the curves associated with running waves from those associated with regressive waves, we introduce two families of curves λ and β [4]

$$\boldsymbol{\lambda}: \quad \frac{\mathrm{dx}}{\mathrm{dt}} = u + a \quad ; \quad \frac{da}{du} = -\frac{k-1}{2} \tag{2.27}$$

$$\boldsymbol{\beta}: \quad \frac{\mathrm{dx}}{\mathrm{dt}} = u - a \quad ; \quad \frac{da}{du} = +\frac{k-1}{2} \tag{2.28}$$

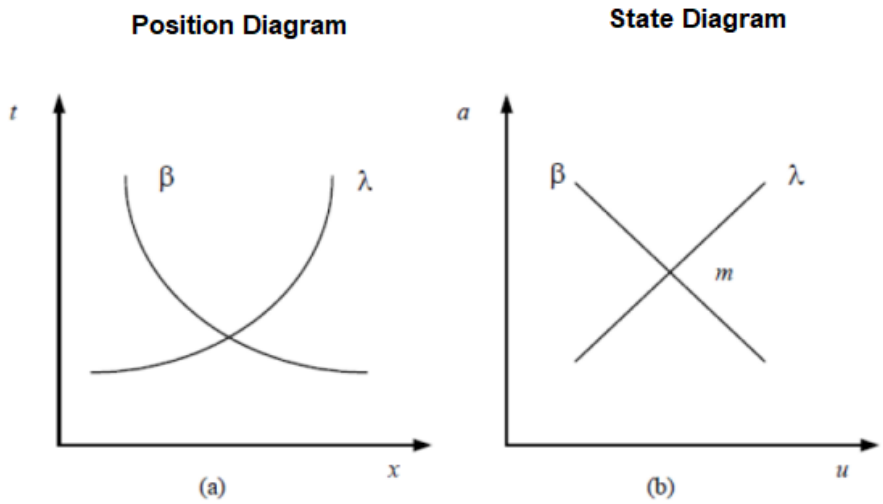

Figure 2.1 : Position and State diagram for the curves λ & β

It is possible to find the solution graphically, the point where the curves intersect is the solution point. For the case being considered it is possible to cancel the following differentials

$$d\left(u + \frac{2}{k-1}a\right) = 0 \tag{2.29}$$

$$d\left(u - \frac{2}{k-1}a\right) = 0 \tag{2.30}$$

Hence for the case under consideration, this is linked to the presence of some quantities which remain conserved along the characterstic curves, so we can define the Rieman invariants invariants $J+$ and $J-$ as follows:

$$J_+ = u + \frac{2}{k-1}a \tag{2.31}$$

$$J_- = u - \frac{2}{k-1}a \tag{2.32}$$

The Riemann invariant J+ and J- remain constant along the curves of λ & β respectively for the case of homoentropic flows

In the above scenario only homoentropic flow was considered and the source terms were neglected, which is not possible for the non-homoentropic flow. For the varying entropy field which is the case of non-homoentropic flow, we can not neglect the source terms. Therefore the Rieman invariants introduced in the previous section remain no longer constant for these cases and thus called Rieman variables. [4]

2.1.1 Introduction to dimensionless variables

As anticipated, the junctions define the boundary conditions for the calculation of the flow in the ducts that contribute to it, and the equations describing these conditions are derived by the method of characteristics.

Benson who first used this method in the field of fluid dynamics simulations of IC engines, modified the equations using instead of the usual thermodynamic variables, variables with the same meaning, but dimensionless, with the aim of streamlining the calculation procedure. [1]

With reference to the graph (*a-s*) of Figure 2.2 , a reference pressure p_{REF} and a speed of propagation of the reference sound are fixed a_{REF}. Remember that for a perfect gas $\left(\frac{c_p}{c_v} = cos\, t\right)$ the diagram a-s is equivalent to the diagram (*T-s*), and therefore fixing a_{REF} is the same as fixing a reference temperature T_{REF}. Similarly, a reference length should also be fixedx_{REF}.

The dimensioned variables are consequently defined as follows:

$$A = \frac{a}{a_{ref}}; \quad U = \frac{u}{a_{ref}}; \quad Z = \frac{a_{ref}\, t}{x_{ref}}; \quad X = \frac{x}{x_{ref}}; \tag{2.33}$$

For the homentropic flow it is not necessary to introduce any other variable because the entropy s does not appear in the cardinal equations for 1-D flows. In the non-homentropic flow it is necessary to use, in addition to eq. of continuity and eq. of the momentum., also the eq. of energy to take into account entropy variations due to dissipative effects or the simple mixing of gases under different conditions.

To this end, the concept of dimensionless variables with respect to an index of the instantaneous entropic level of the gas is introduced.

To define the index of the entropic level it is necessary to recall the isentropic transformation for a perfect gas:

$$\frac{p}{\rho^k} = cos\, t$$

Suppose the gas performs an isentropic compression, or expansion, from the initial state (p,s) to the final state (p_{ref},s). The value of sound speed a that reads on the ordinate axis at the point (p_{ref},s) is the index of the entropic level a_A for the gas under the initial conditions (p,s)

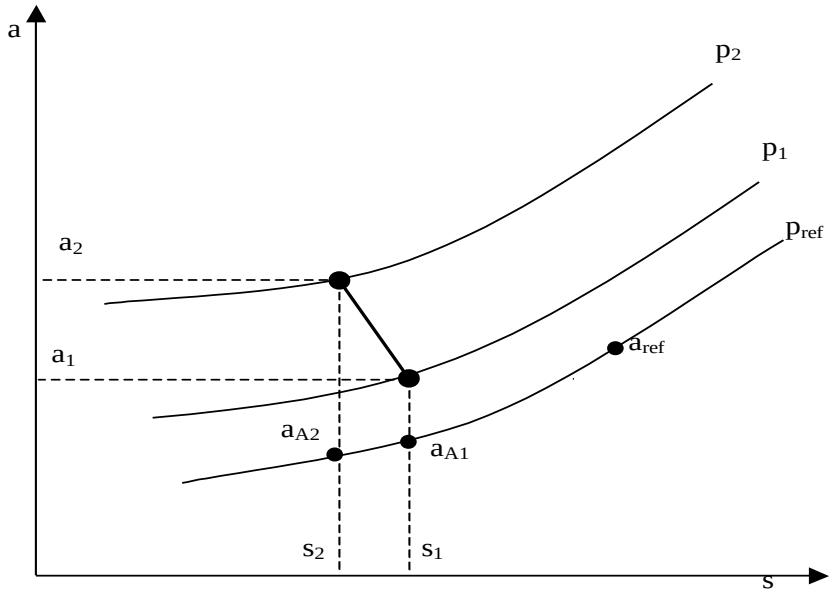

Figure 2.2 : Speed of sound-entropy diagram

On the graph it is possible to identify, starting from the local conditions of pressure p and density ρ, the local speed of sound a. Performing an isentropic transformation up to the reference conditions p_{ref} and a_{ref} goes back to the speed of sound a_A, corresponding to the local entropic state s.

In practice, all entropic levels are compared to the reference pressure:

$$\frac{\rho}{\rho_A} = \left(\frac{p}{p_{ref}}\right)^{\frac{1}{k}}$$

$$\frac{p}{p_{ref}} = \left(\frac{a}{a_A}\right)^{\frac{2k}{k-1}}$$

from which the dimensionless entropic level is obtained:

$$A_A = \frac{a_A}{a_{ref}} \tag{2.34}$$

In general, for a non-homentropic flow the value of the entropy s under the starting conditions p, a, ρ does not correspond to the reference value s_{ref}. For this reason, a_A differs from a_{ref}, which can be defined as the speed of sound corresponding to the isentropic state of reference. Therefore, the dimensionless quantity A_A is an indication of the entropic level of the gas with respect to the reference conditions.

So far it has not been clarified how to use the dimensionless variables for the description of the non-homentropic flow, to do so it is necessary to use dimensionless Riemann λ variables and β. The opportunity is used to introduce the nomenclature of Riemann variables used in the following discussions

$$\lambda = \lambda_{in} = A + \frac{k-1}{2}U \tag{2.35}$$

$$\beta = \lambda_{out} = A - \frac{k-1}{2}U \tag{2.36}$$

dividing the Eq (2.35) & Eq (2.36) by A_A you get the stared dimensionless variables *:*

$$A^* = \frac{A}{A_A}; \tag{2.37}$$

$$\lambda_{in}^* = \frac{\lambda_{in}}{A_A}; \tag{2.38}$$

$$\lambda_{out}^* = \frac{\lambda_{out}}{A_A}; \tag{2.39}$$

one can rewrite the Riemann variables in *star* terms:

$$\lambda_{in}^* = A^* + \frac{k-1}{2}U^* \tag{2.40}$$

$$\lambda_{out}^* = A^* - \frac{k-1}{2}U^* \tag{2.41}$$

The term A^* can be rewritten as:

$$A^* = \frac{a}{a_A} = \left(\frac{p}{p_{REF}}\right)^{\frac{k-1}{2k}} \tag{2.42}$$

and is therefore interpretable as a pressure level. This property is used to define pressure drops at duct joints.

The convenience of writing equations in star terms lies in the fact that the information about the entropic level of the gas is already contained in the Riemann variables λ_{in}^{*} and λ_{out}^{*}. These concepts will be clarified in the discussions of the junction modelling routines.

Associating now to the characteristic lines the respective compatibility equations, rewritten in terms of Riemann invariant, we have:

$$d\lambda = \frac{k-1}{2}\frac{T}{a}ds - \frac{k-1}{2\rho a}\,[\Delta_1 + \Delta_2 + \Delta_3]dt \tag{2.43}$$

$$d\beta = \frac{k-1}{2}\frac{T}{a}ds - \frac{k-1}{2\rho a}\,[\Delta_1 + \Delta_2 - \Delta_3]dt \tag{2.44}$$

For compatibility equations, note that the variation of Riemann variable depends on four fundamental terms namely [4]

- Change in duct section
- Wall friction
- Heat exchange through the walls
- Change in entropy

$$d(\lambda, \beta) = \delta_{area} + + \delta_{entropy} + \delta_{friction} + \delta_{heattransfer} \tag{2.45}$$

2.1.2 Physical meaning for method of Characteristics

Consider now the physical significance of the Method of Characteristics. Within a duct affected by the unsteady flow of a compressible fluid, the fluid dynamic quantities in a given section are influenced only by mass transport phenomena and pressure perturbations. The latter propagate through the moving fluid at the speed of sound.

The diagram of the procedure for calculating the mesh method of characteristics is shown in Figure 2.1 to which reference will be made for analytical treatment.

In order to apply the method for 1-D solution in the duct. It is required to mesh the duct that means set a step of division Δx of the average line of the duct. Moreover, it is necessary to fix the time Δt of calculation to obtain the grid in the plane (x,t) as shown in Figure 2.1 . It's worth keeping in mind that terms Δx and Δt are not independent of each other.

For the homentropic flow the relation applies:

$$\lambda_i^{n+1} = \lambda_L^n \tag{2.46}$$

$$\beta_R^{n+1} = \beta_R^n \tag{2.47}$$

The Riemann variables actually behave as constants for homentropic flows, while this is no longer true for the non-homentropic flows where it is necessary to take into account the corrective terms dλ *Eq (2.45)* that will modify the previous relations

$$\lambda_i^{n+1} = \lambda_L^n + d\lambda_L \tag{2.48}$$

$$\beta_R^{n+1} = \beta_R^n + d\beta_R \tag{2.49}$$

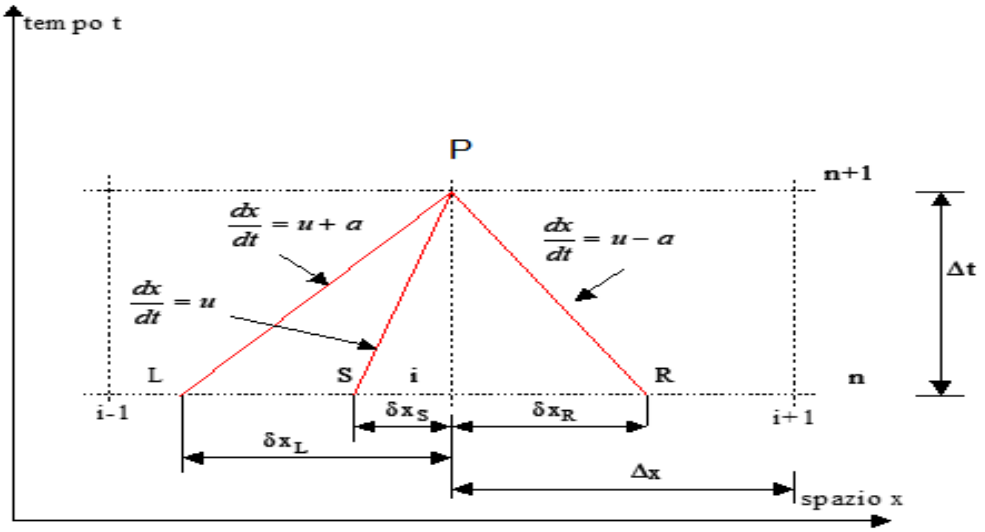

Figure 2.3 : Characteristic lines for non-homentropic flow in the x-t plane

The flow variables at the points P at the new time instant *(n+1)Δt* can be evaluated by the exploitation of the knowledge of flow properties at the adjacent mesh points (L,S and R) at the previous instant of time n*Δt*. The characteristic lines are represented by LP, RP & SP in the Figure 2.3. The slope of these characteristic lines directly depends on the sound speed. The Riemann variable at current time interval n*Δt* is written in analytical terms as in *Eq (2.50) & Eq (2.51).* The Riemann variable at these adjacent points (L & R) for time instant n*Δt* is used to calculate the Riemann variable at point P at the new time interval *(n+1)Δt.* [4]

$$\lambda_L^n = \lambda_i^n - \frac{\delta x_L}{\Delta x}(\lambda_i^n - \lambda_{i-1}^n) \tag{2.50}$$

$$\beta_R^n = \beta_i^n - \frac{\delta x_R}{\Delta x}(\beta_i^n - \beta_{i-1}^n) \tag{2.51}$$

2.1.3 Limitation of Method of Characteristics

The method of characteristics was an early method developed for the solution of conservation equations, however it has certain limitations due to which better models were developed later.

Following are some limitations of the method of characteristics:

- The method is not precisely accurate. It does not show good robustness in the modelling of discontinuity in the flow and is unable to capture the effect of shock waves.
- The interpolation performed is linear which means that the accuracy is of the first order in time and space. This feature would be highly limiting when very detailed analyses were required, as it would be impossible for the algorithms to grasp the small oscillations of the quantities at high frequencies
- It is based on the assumption of perfect gas with constant specific heat, so it is difficult to generalize the method to case of mixture of ideal gases to specific values dependent on the temperature. The transformation of conservation equations from partial differential to ordinary differential equations is based on the same hypothesis in this method
- The method is initiated from equations written in non-conservative form; this includes mass flow variation along the ducts.
- The speed and accuracy provided by this method is lower in comparison to other numerical methods used for the solution of conservation equations.

2.2 Shock capturing methods

In an internal combustion engine, there are contact discontinuities for the flow of fluid inside the ducts, these contact discontinuities can be due to various reasons that may include shock waves, or fluid portion with different chemical composition or fluid areas with different temperature. In gas dynamic calculations, one of the major difficulties that occurs in the numerical methods adopted is to take into account the presence of these flow discontinuities. The numerical methods that are able to solve complex discontinuities in the flow are called shock-capturing methods. These methods are able to calculate with high accuracy by applying directly the same numerical scheme in all calculation nodes.

As already seen, the application of Shock-Capturing methods is made possible by the conservative formulation of the system of fundamental equations of motion. In this formulation, the vector $\bar{W}$(x,t) fully characterizes the flow conditions:

$$\bar{W}(x,t) = \begin{bmatrix} \rho F \\ \rho v F \\ \rho e_o F \end{bmatrix}$$

The vector $\bar{W}$((x,t) must be replaced with the equivalent $\bar{W}_i^n(i\Delta x,\ n\Delta t)$, after the discretization of the space and time domains. Approximation to W_i^n(iΔx,nΔt), where the subscript i indicates the space coordinate and the superscript n the time coordinate. In this way a computational grid characterized by the steps Δx and Δt is obtained.

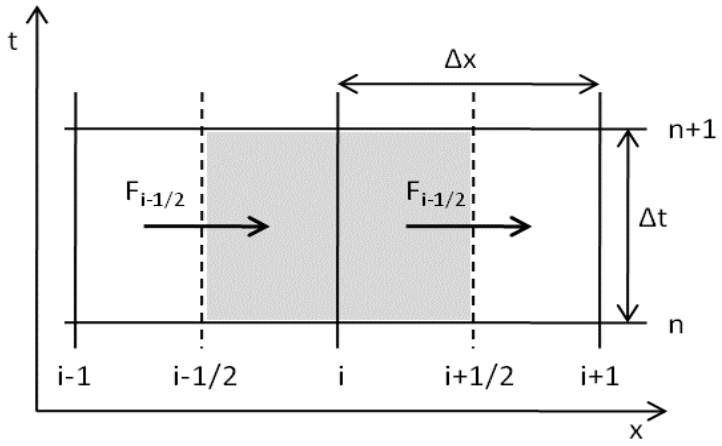

Figure 2.4: Representation of generalized computation grid

To proceed with the Euler's equation, obtained by canceling the vector of the source terms $\bar{B}$ ($\bar{W}$(x,t)) and $\bar{C}(\bar{W}$(x,t)), from the fundamental equations in the conservative form. Furthermore, describing the evolution of a homentropic flow in a duct, the hypothesis is easily removed in the more general case of non-homentropic flow. The matrix system in compact form is

$$\frac{\partial \bar{W}(x,T)}{\partial t} + \frac{\partial \bar{F}(\bar{W})}{\partial x} = 0 \qquad (2.52)$$

Where

$$\bar{F}(\bar{W}) = \begin{bmatrix} \rho u \\ \rho u^2 + p \\ \rho u h_o \end{bmatrix}$$

By applying Gauss's divergence theorem and integrating the system in space and time yields [6]

$$\int_{t}^{t+\Delta t}\int_{x}^{x+\Delta x}\left(\frac{\delta W(x,t)}{\delta t}+\frac{\delta F(W)}{\delta x}\right)dx.dt=0 \tag{2.53}$$

Introducing the equivalent numerical vectors and taking out of the integration sign we get:

$$(W_i^{n+1}+W_i^n)\Delta x+\left(F^n_{i+\frac{1}{2}}+F^n_{i-\frac{1}{2}}\right)\Delta t=0 \tag{2.54}$$

Where the terms $(\overline{W})$ and $\bar{F}$ are derived from the following expressions:

$$W_i=\frac{1}{\Delta x}\int_{x_{i+\frac{1}{2}}}^{x_{i+\frac{1}{2}}} W dx \tag{2.55}$$

$$F_{\,i\pm1/2}=\frac{1}{\Delta x}\int_{t^n}^{t^{n+1}} F dx \tag{2.56}$$

Even in the presence of discontinuities the *Eq (2.54)* has the advantage of being independent from the condition of derivability required by *Eq (2.53).* Hence without knowing the position of discontinuities in advance, it is possible to deal with the discontinuities. Furthermore, this formulation has the property of telescopicity that means the integral law continues to maintain the validity if it is applied to control volume that are adjacent to each other. This happens because the flows that cross the separation surface of the adjacent control volumes are equal and opposite therefore, cancelling themselves, they do not appear additional terms in *Eq (2.54).* [6]

Rearranging the equation (2.54) we have:

$$\frac{W_i^{n+1}-W_i^n}{\Delta t}+\frac{\left(F^{n+1}_{i+\frac{1}{2}}-F^n_{i-\frac{1}{2}}\right)}{\Delta t}=0 \tag{2.57}$$

This expression is the discretization of the continuum, by subdivision into meshes, both spatial and temporal, necessary to use the methods to finite differences. Summing up the differences along x throughout the field of definition yields:

$$\Delta x \sum_{i_{min}}^{i_{max}} W_i^{n+1} = \Delta x \sum_{i_{min}}^{i_{max}} W_i^{n+1} + \left(F^n_{i_{min}+\frac{1}{2}} - F^n_{i_{max}-\frac{1}{2}} \right) \Delta t = 0 \tag{2.58}$$

Where,

- The first term represents the total mass, the total momentum, and the total amount of energy at the new time instant
- The first term on the right represents mass, momentum and the total energy at instant in initial time instant.
- The second term at the right represents the flow of conserved quantities at the extreme section of duct.

In case of constant duct area, the equations applied to the flow of fluid will result into cancellation of internal fluxes and will preserve for the governing equations the integral property such as mass conservation. The method described is based on finite difference method or conservative methods, the application of these methods are Lax Wendroff and MacCormack schemes. [7], [8]

The equations thus defined constitute a conservative discretization scheme, a characteristic that guarantees the validity of the integral properties of differential equations. Methods operating according to this scheme are explicit methods and have second-order accuracy in the space-time domain. However, an accuracy of a higher order than the first can lead to some problems of spurious oscillations in the solution, it is therefore essential to equip the calculation program with accessory algorithms aimed at mitigating this phenomenon.

2.2.1 Corberàn-Gascòn method

In several problems of practical interests, we come across Euler equations with the inclusion of the source terms that represent some geometric characteristics. An example can be considered here is the case of 1-D flow in ducts having varying cross sectional area. The source term inclusion in the hyperbolic system of equations in one dimension has been described earlier. In order to solve the non-homogeneous set of equations, several approaches have been adopted. The conservative finite difference method was most adopted by several authors, due to some spurious oscillations the effect of source term was added into the homogenous system which served as the correction of conservation procedure. This method was found to be inefficient at particular conditions. Such conditions include the instances of source terms having strong influence on the solution leading to inaccurate solutions and errors, thus the

accuracy of the procedure was compromised and at times this also resulted into non convergence of the solution. [9]

For non-homogeneous conservation laws, a typical technique utilized for the prediction of solution is the fractional splitting method along with system of ordinary differential equations which are as below:

$$W_t + F(W)_x = 0 \tag{2.59}$$

$$W_t = S(x, W) \tag{2.60}$$

To solve the homogenous system of equations , this method utilizes existing computational methods along with implementation of TVD scheme. These methods are not always successful in particular cases specially when a steady state is near to the solution where the gradient of flux and source terms requires consideration. The reason of the failure of these methods is the fact that they don't consider the steady state equation which is :

$$F(W)_x = S(x, W) \tag{2.61}$$

If we consider the steady state solution related to the problem, then *Eq (2.59)* is written as:

$$W_t + F(W)_x = S(x) \tag{2.62}$$

The source term S(x) is considered to be independent of the variable W. Upon the integration of the associated stationary equation that respect the condition

$$F(W)_x = S(x) \tag{2.63}$$

Then the flux vector can be written as:

$$F(W) = K + \int_0^x S(y)dy \tag{2.64}$$

Where K is a constant. The equation above represents the proper discretization of the stationary equation related to the conservation laws of non-homogenous system. The method is properly described as to consider for the fluxes and the source terms the same criteria. Which means that when the fluxes are being utilized by central discretization the source terms must also be utilizing the central discretization and the source terms should always be directly linked to the fluxes. Or in case of upwind physical flows the source term should also be considered up winded. The inclusion of the source terms in the computation methods being used will be in the form below:

$$G(x,W) = F(W) - \int_0^x S(y)dy \tag{2.65}$$

So, the original *Eq (2.62)* can be transformed and rewritten as:

$$W_t + G(x,W)_x = 0 \tag{2.66}$$

By the combination of the source term and physical flux function, the new flux , $G(x,W)_x$ is formed represented in the *Eq (2.66)*

After the transformation it is possible to apply to the system TVD with the help of an appropriate technique as described above as the source terms are included in the form of divergence terms and the method is able to recognize the steady state solution. [10]

Integrating *Eq (2.65)* on the rectangle in Figure 2.4, along the coordinates $\left[x_{i-\frac{1}{2}}, x_{i+\frac{1}{2}}\right], [t_n, t_{n+1}]$, we obtain:

$$W_i^{n+1} = W_i^n - \frac{1}{\Delta x}\int_{t_n}^{t_{n+1}} (F(W(x_{i+1/2}, t)) - F(W(x_{i-1/2}, t)))dt + \frac{1}{\Delta x}\int_{t_n}^{t_{n+1}} \int_{x_{i-1/2}}^{x_{i+1/2}} S\big(x, W(x,t)\big)dxdt \tag{2.67}$$

In the above equation the average values for the variables W_i^n and W_i^{n+1} should substitute the exact integrals for the numerical cell being considered, and for the time instant due to unique characteristic of the problem. Thus:

$$W_i^n = \frac{1}{\Delta x}\int_{x_{i-\frac{1}{2}}}^{x_{i+\frac{1}{2}}} W(x, t_n)dx \tag{2.68}$$

With the help of the definition of the new flux $G(x,W)_x$ we can thus rewrite the *(Eq 2.67)*

$$W_i^{n+1} = W_i^n - \frac{1}{\Delta x}\int_{t_n}^{t_{n+1}} (G(x_{i+\frac{1}{2}}, W(x_{i+\frac{1}{2}}, t)) - G(x_{i-\frac{1}{2}}, W(x_{i-\frac{1}{2}}, t)))dt \tag{2.69}$$

Where

$$G(x,W) = F(W) - \int_0^x S\big(y, W(y,t)\big)dy \tag{2.70}$$

(2k+1) explicit schemes written in conservation form are used to obtain the numerical approximation for the solution of Eq (2.65)

$$W_i^{n+1} = W_i^n - \lambda \left[\bar{G}^n_{i+\frac{1}{2}} - \bar{G}^n_{i-\frac{1}{2}} \right] \tag{2.71}$$

Where $\lambda = \frac{\Delta t}{\Delta x}$ and

$$\bar{G}^n_{i+\frac{1}{2}} = \bar{G}(x_{i-k+1} \dots \dots x_{i+k}, W^n_{i-k+1} \dots \dots W^n_{i+k}) \tag{2.72}$$

For consistency:

$$\bar{G}(x \dots \dots x, W \dots \dots W) = G(x, W) \tag{2.73}$$

The above property is valid in the cases when the numerical flux $\bar{G}$ is directly linked with the physical flow $F(W)$ with the additional condition that the discretization corresponding to the source terms will converge at the point when Δt and Δx tend to 0.

The following discretized equation is used in addition to find an appropriate approximation to the steady state solutions

$$\bar{G}^n_{i+\frac{1}{2}} - \bar{G}^n_{i-\frac{1}{2}} = 0 \tag{2.74}$$

The above relation should approximate a second order approximation to the stationary equation:

$$F(W)_x = S(x, W) \tag{2.75}$$

This is due to the fact that if W_i^n provides the approximation of the stationary equation to level n, this will result in $W_i^{n+1}$and W_i^n to be equal and the method will adopt stationary solution with accuracy of second order.

The developments of explicit finite difference scheme of the second order were provided by Corberan and Gascon which is actually an extension of the Lax-Wendroff scheme applied to a non-homogeneous scalar conservation law. Corberan and Gascon concluded that the Lax Wendroff scheme does not block the total variation of numerical approximations from increasing. Because of this fact, Corberan and Gascon also observed certain conditions which should be sufficient for the implementation of TVD schemes of the second order for non-homogenous conservation law in scalar form. [10]

2.2.2 TVD Scheme

TVD (Total variation Diminishing) was developed by Corberan-Gascon in order to solve the problem of spurious oscillations which were not avoidable around the shock. Oscillations like these should be removed and mathematical specific algorithms are used for this purpose. These schemes maintain an appropriate balance at steady state between flux and the source terms, and can be used for the computation of solutions for non-homogenous conservation laws. An artificial value of viscosity is predicted at all points of the constructed mesh with accuracy by the introduction of a term which is nonlinear in nature. The conservative methods are reformed, and the solutions are modified in this manner. [10]

The TVD scheme can be of two different types:

- Post processing schemes: This type of numerical computational method involves the evaluation of the selected numerical method which is then later modified or post processed to satisfy the TVD criteria of shock being dependent on the solution vector W.
- Pre-processing schemes, as opposed to the post processing schemes, these methods modify the data before the implantation of the solution.

The flux limiters and the Flux Corrected Transport are example of TVD schemes.

We discussed in this chapter the method developed by Corberan-Gascon which is capable of recognizing the stationary solutions for conservation laws including the source terms with second order terms limitation. [10]

Gudnov's theorem [10] provides an explanation as to how second order method failed to capture the discontinuities present and generated the oscillations. The theorem indicates that all second order numerical scheme take the general form as below:

$$W_i^{n+1} = \sum_k c_k W_{i+k}^n \tag{2.76}$$

The oscillations related to the discontinuity of the solution is represented by c_k. To avoid presence of the spurious oscillations related to the solution, a criteria indicated the basic condition needed that if we define for the vector W at the new time instant, the total variation as below:

$$TV(W^n) = \sum \left| W_i^{n+1} - W_i^n \right| \tag{2.77}$$

In case for the solution, the total variation does not increase across the successive time steps:

$$TV(W^{n+1}) \leq TV(W^n) \tag{2.78}$$

The TVD scheme has an advantage that the accuracy is in the second order and the solution is free of the oscillation along the discontinuities. The data obtained is said to be TVD (Total variation Diminishing). It should be noted that the basic condition for any method to be a TVD is that the finite difference scheme should be non-linear, which means that the oscillation coefficient related to the discontinuity c_k should be a function of W^n. So, in case of constant c_k the method cannot be declared as TVD, and in order to make any computational scheme to be TVD, one should make the coefficient c_k to be a function of the solution vector. [10]

3. Constant pressure Junction Model

3.1 Introduction

The modelling of pressure waves across the junctions of exhaust and intake system with the one-dimensional simulation is a complex task because the wave propagation across the junction can be multidimensional phenomenon. The reason for this problem of modelling a multi-dimensional phenomenon with a one-dimensional approach is that the junction geometry cannot be represented in a 1-D model, but it could have a significant impact on the flow. The models that are being used to predict the behavior of flow in the intake and exhaust systems of an internal combustion engine are actually variation of two different type of models. The basic models are based on the approach of hypothesis that the flows that enter the junction and the flows leaving the junction are one dimensional. These models are constant pressure junction model and pressure loss junction model. These models adopt another hypothesis and assume that the overall dimension of the network of ducts is significantly larger than the size of the junction such that the junction size can be neglected. Constant pressure junction model is the simpler among the models in consideration which states that for a given junction of n ducts the pressure at the junction end for all ducts is the same. If the numbers 1,2,3,…n represent the duct forming the junction, then according to the constant pressure junction model as proposed by Benson:

$$p_1 = p_2 = p_3 = p_n \tag{3.1}$$

The assumption of constant pressure junction relies on some finding as observed by List and Reyl [11] who concluded that the pressure drop across the junctions is negligible for small waves. The advantage of using this model is that no steady flow

loss data is required to define the characteristic of the junction and that the junction characteristics can be defined only by the duct cross sectional areas forming the junction. Thus, this theory also does not take into account the angular relationship between the ducts and neglects the effects of angle between the ducts for the solution procedure. Bingham and Blair in their research also considered the angular relationship between the ducts for their model which is explained later in detail. The constant pressure model is a simple model, and it does not need any experimental data which may be required by other models that are adopted. This makes the constant pressure model approach to be very cost effective since the geometry of the end sections of the duct are used to completely characterize the junction without any need to perform tests or need of any sort of additional information of the elements of the junction. Also, another important aspect of this model is that it can be applied to any number of ducts in consideration that make up the junction without any detailed complications. This makes the constant pressure junction model a handy tool for design specially in early stages where there is not a requirement of too much accuracy for the simulation results. [11], [9]

3.2 Application and development of Constant Pressure Model

There are many different applications of the constant pressure junction model, one of which is proposed by Benson. It was assumed that the junction volume is negligible with respect to the volume of the ducts, and the element can be treated in possibly a quasi-static manner. The model by Benson was first developed in such a way that it would deal with homentropic flows, which was further extended to also deal with the non-homentropic flows. Below we will develop the basic constant pressure model for non-homentropic flow. We will use starred Riemann variables in order to consider the fact that the flow is in a variable entropy field. [12]

We can write the relationship between the pressure at the junction for duct n and the speed of sound in dimensionless form An

$$A_N = \left(\frac{p}{p_{ref}}\right)^{\frac{k-1}{2k}} = constant \tag{3.2}$$

The suffix n represents the duct end at the junction. Among the connected ducts, it is also necessary to make further distinction which is as follows: The subscript NJ (J: Joining) is going to be used for the ducts where the flow is towards the junction

whereas for the ducts where the flow is away from the junction the subscript NS (S: separating) is going to be used. Also, we should remember the sign convention for positive and negative flows. If the flow in the duct is towards the junction it is considered a positive flow whereas if the flow in the duct is away from the junction it is considered a negative flow. By that we can also write again the equation for the conservation of mass flow rate:

$$\sum \rho_n u_n F_n = 0 \tag{3.3}$$

In terms of Riemann variables, *Eq (3.3)* can be written as follows:

$$\sum \left\{ (A_N^*)^{\frac{2}{k-1}} \frac{(\lambda_{\mathrm{inN}}^* - \mathrm{A_N^*})}{\mathrm{A_{A_N}}} \mathrm{F_N} \right\} = 0 \tag{3.4}$$

Multiplying and rearranging the above equation:

$$\sum \left(\frac{\lambda_{\mathrm{inN}}^*}{\mathrm{A_{A_N}}} \mathrm{F_N} \, (A_N^*)^{\frac{2}{k-1}} \right) = \sum \left(\frac{A_N^*}{A_{A_N}} \mathrm{F_N} (A_N^*)^{\frac{2}{k-1}} \right) \tag{3.5}$$

Since A_N^* is a constant, therefore we can remove it form the Summation sign and take it outside the bracket as a common term.

$$(A_N^*)^{\frac{2}{k-1}} \sum \left(\frac{\lambda_{\mathrm{inN}}^*}{\mathrm{A_{A_N}}} F_N \right) = A_N^* (A_N^*)^{\frac{2}{k-1}} \sum \left(\frac{F_N}{\mathrm{A_{A_N}}} \right) \tag{3.6}$$

This can be further simplified to write the expression for A_N^* :

$$A_N^* = \frac{\Sigma \left(\frac{\lambda_{\mathrm{inN}}^*}{\mathrm{A_{A_N}}} F_N \right)}{\Sigma \left(\frac{F_N}{\mathrm{A_{A_N}}} \right)} = \left(\frac{p}{p_{ref}} \right)^{\frac{k-1}{2k}} \tag{3.7}$$

For the *Eq (3.7)* , the summation is to be performed for all the ducts that meet at the junction, and the expression can be used to find the pressure at the junction. For the pressure calculation of boundary, it is necessary to know in all the sections the entropy levels , hence it is important to identify the flow directions and distinguish the ducts on the basis of the flow direction with respect to the junction.

In order to obtain the entropy levels for all the duct ends, following assumption has been adopted according to Benson's model:

- For the duct ends where the flow is positive or towards the junction ($U_N^* > 0$), the entropy levels remain unchanged and $(A_{AN})_{NJ}$ is equal to the previous value of A_{AN}

- For the duct ends where the flow is negative or away from junction ($U_N^* < 0$), the entropy levels does not remain the same and is calculated as the weighted average of the entropy levels of the joining flows.

Thus, summarizing both above points :

$$U_N^* = \frac{2}{k-1}(\lambda_{\text{inN}}^* - A_N^*) \tag{3.8}$$

For positive Flows (When $U_N^* > 0$)

$$AA_{N\,(N=Nj)} = AA_N \tag{3.9}$$

For negative Flows (When $U_N^* < 0$)

$$AA_{N\,(N=NS)} = \frac{\sum(U_N F_N A_{A_N}^*)}{\sum(U_N F_N)} \tag{3.10}$$

So, each duct in which the flow is negative (flow away from the junction) will have same entropy level which is calculated from *Eq (3.10)*.

For the ducts with flow direction away from the junction in which the entropy level is varied, the Riemann variable is also corrected due to the change in entropy level and the corrected Riemann variable is given by *Eq (3.11)*.

$$\lambda_{\text{inNc}}^* = \lambda_{\text{inNn}}^* + \frac{A_N}{A_{A_{N_C}}}(A_{A_{N_C}} - A_{A_{N_n}}) \tag{3.11}$$

The above *Eq (3.11)* can also be written in the form of starred Riemann variables as follows:

$$\lambda_{\text{inNc}}^* = \frac{\lambda_{\text{inNc}}}{A_{A_{N_C}}} \tag{3.12}$$

or

$$\lambda^*_{\mathrm{inNc}} = \lambda_{\frac{\mathrm{inNn}}{A_{A_{N_C}}}} + A^*_N \left(1 - \frac{A_{A_{N_n}}}{A_{A_{N_c}}}\right) \tag{3.13}$$

or

$$\lambda^*_{\mathrm{inNc}} = \mathrm{A}^*_{\mathrm{N}} + \frac{A_{A_{N_n}}}{A_{A_{N_c}}} (\lambda^*_{\mathrm{inNn}} - \mathrm{A}^*_{\mathrm{N}}) \tag{3.14}$$

Similarly, the Riemann variable $\lambda^*_{\mathrm{outN}}$ can be written as

$$\lambda_{\mathrm{outN}} = A_{A_{N_c}} (2\,\mathrm{A}^*_{\mathrm{N}} - \lambda^*_{\mathrm{inNc}}) \tag{3.15}$$

The procedure will be adopted iteratively until the solution reaches a convergence such that the two successive values of A_N are within a tolerance limit difference.

3.3 Flow Chart for Constant pressure Model by Benson

As per the general Benson Model for the solution of constant pressure type junctions, the calculation is started from the program receiving some inputs which in this case are the values of Riemann variable, number of ducts at the junction and the entropy level at the junction for each duct. The number & type of inputs can vary depending on the computational code and the junction types which are discussed later in the following chapters. Initially the error E is set to be zero for the first iteration and is set to be equal to the previous value of A_N* for the following iterations. The first step is to calculate the starred Riemann variables for each duct from the input parameters. Then using *Eq (3.7)*, $\mathrm{A}^*_{\mathrm{N}}$ is calculated. The flow is checked for each duct to be either positive (towards the junction) or negative (away from the junction) and accordingly the entropy levels are updated according to what was explained in the Benson's Model. The corrected starred Riemann variable is then calculated with respect to updated entropy levels. The $\mathrm{A}^*_{\mathrm{N}}$ value is compared with the result from previous iteration , and if the difference is between the tolerance limit that was set, the solution is converged and ended otherwise the procedure is repeated until convergence is achieved.

The constant pressure junction model takes various forms and can be applied for the junctions with the help of computational programs based on the flow chart represented in this chapter by Figure 3.1. There are several computer program

subroutines that are used for the solution of different junction types. Most of the subroutines for the calculation across the junctions are based on this constant pressure model. The common subroutine based on constant pressure model by Benson are used and applied for the following junction types:

- Junction of n-ducts
- Catalyst junction
- Intercooler Junction
- Perforates
- Filters

The subroutines for the above-mentioned junction types based on the Benson's model for the constant pressure junctions are presented in the report later. The general scheme for all the subroutine is based on the flow chart as illustrated by the Figure 3.1

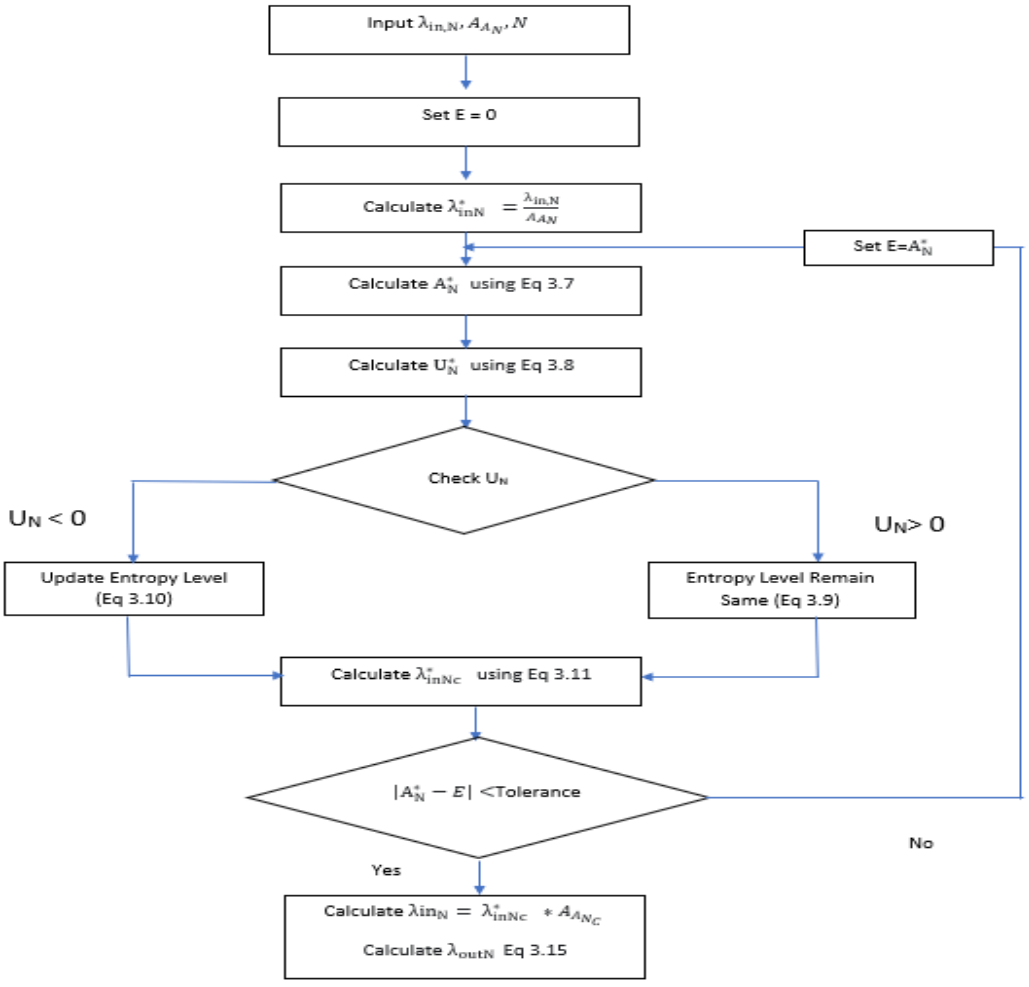

Figure 3.1: General Flow chart for the constant Pressure Model

3.4 Validation of Constant Pressure Model

Benson also performed experiments in order to check the validity of the results obtained from the constant pressure model and observed that the constant pressure model provided reasonable results and with accuracy which can be acceptable in most cases.

Benson performed these observations for Constant pressure model on a 4-way junction. The results were compared with the experimental results and with the pressure loss model. The pressure curve thus obtained was plotted against crank angle for the three curves and is shown below in the Figure 3.2 [1]

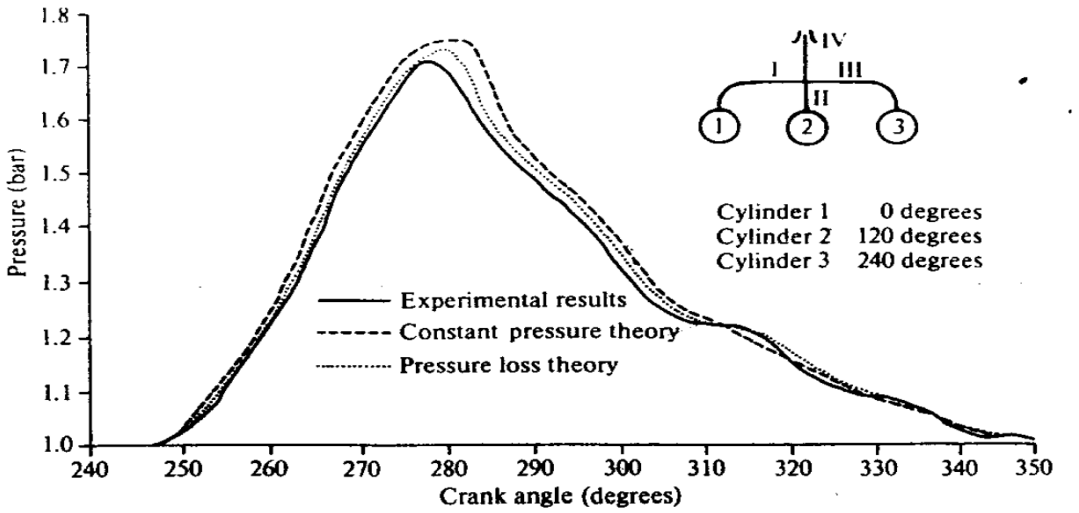

Figure 3.2: Pressure curve obtained for a 3-cylinder engine using constant pressure and pressure loss models

The results thus obtained with the constant pressure model were in close proximity with both the experimental results and the pressure loss model.

In order to validate the authenticity of constant pressure model, another experimental verification was performed by Benson and the result obtained with the help of constant pressure model were compared with the measured data. The experiment was performed on the engine intake and exhaust duct.

The test was performed on following operating conditions.

N= 612 RPM

p_a = 15.1 lb/in^2 gauge

pcr = 48.0 lbf/in^2 gauge

Tcr = 142 ^{o}F

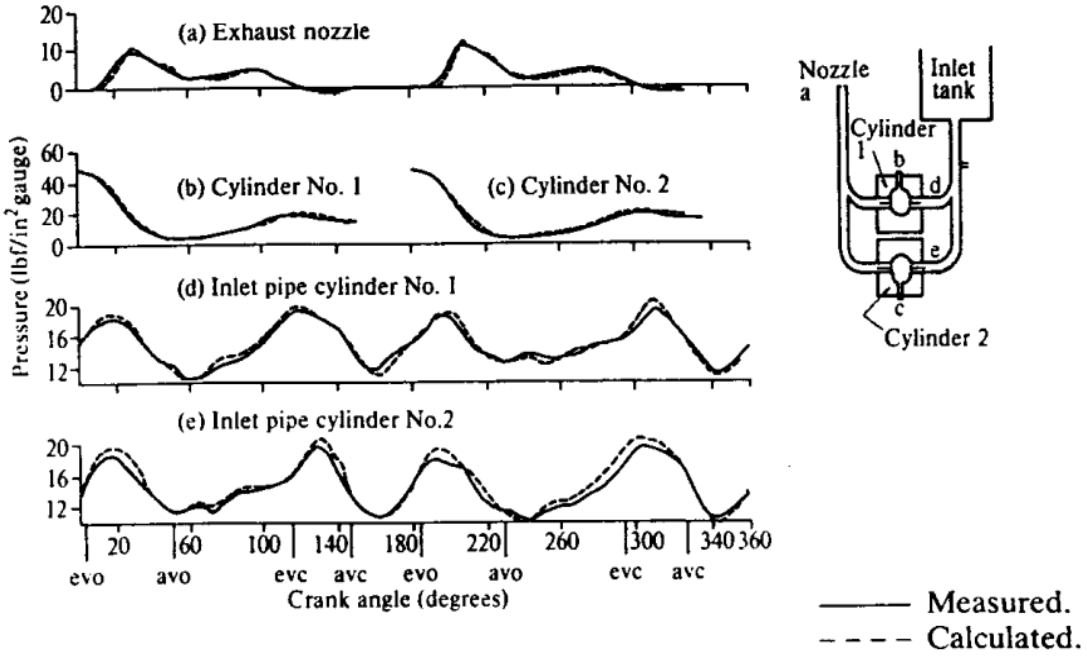

Figure 3.3: Comparison of measured pressure with the predicted pressure using the constant pressure model

The pressure vs crank angle curve was drawn for the two cylinders for both intake and exhaust valves, The results thus obtained in Figure 3.2 & Figure 3.3 showed that the constant pressure model gave results with good accuracy in comparison to the measure pressure.

When the velocity of flow is not too high and the angle between the ducts are not too large, the constant pressure model will give results with acceptable accuracy. Benson further recommended the use of constant pressure model in case of unavailability of loss data of duct junctions. [1]

4. Pressure Loss Models

4.1 Pressure Loss model for three-duct junctions

Several routines are utilized by GASDYN code for the solution at the junction, these routines can be as simple as the constant pressure model which was proposed by Benson or can be complex as well like the pressure loss models.
In the intake or exhaust ducts of an internal combustion engine, there could be pressure drops that may change the average level of pressure and could also change the response to pressure disturbances on the junction. The pressure drops across the junction for both intake and exhaust systems are very important for the accurate prediction of pressure waves.
As explained in the previous chapter, the constant pressure model is rather a simpler model, that is based on the hypothesis that all the joining ducts at the junction have the same static pressure and it does not take into account any pressure drop that may occur in the junction. This model is described by the geometry of the joining ducts and does not require any additional data in order to predict the pressure waves. Because of the reason that the model provides so much simplicity, it results into a consequence that the junction schematization is not affected by the directionality of the flow which means it does not consider the pressure waves coming from various branches that may arise due to valve opening/closing or any other reason.
Therefore, in order to take into account also the effect of directionality, there became a need to develop a different model that does take into account directionality and its effects that fall in the limits imposed by the schematization of the model in 1-D system. Certain geometric junctions with their configurations have been implemented in Gasdyn routines which were developed on the basis of results as obtained from flushing tests.

4.1.1 Junction Types

In the first section of this chapter we will discuss in detail about how to model a junction involving three pipes with all possible configurations. The work is divided into two segments where one model works for a T-type junction and the other for the Y-type junction. The T-type junction is the one with the lateral duct of any section and angle of inclination with respect to the generic main duct, while the Y-type junction being the one with the central duct of generic section splitting into two branches with an angle between the two side branches. The two generic junctions are represented by Figure 4.1.

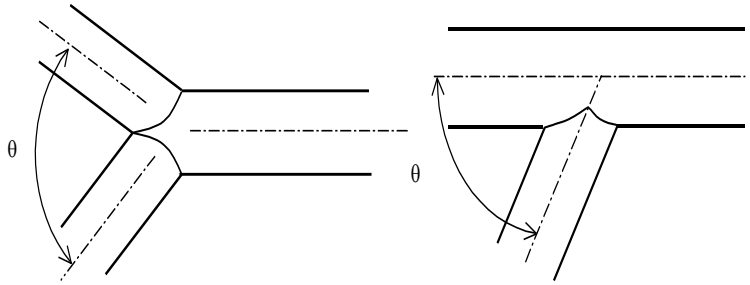

Figure 4.1 : A general Y-Type (left) and T-Type Junction (right)

The junction models are treated numerically with the reference to the Winter bone-Bassett [3]

4.1.2 Loss coefficients

We can define for any moment in time the flows for a three-pipe junction, there can be six different possible cases which are shown in the Figure 4.2-Figure 4.5. The type of flow that can be recognized is based on the direction of velocities for each pipe that is connected to the junction. The configurations can be easily identified and can be recognized as either joining type in which the flow joins or the separating type in which the flow separates. Two flow coefficients can be associated with each flow type, which are also represented by the figure below, thus a total of 12 distinct loss coefficients can be adopted. We have adopted the same flow types which were adopted by Nichols and have numbered it in the same manner from 1 to 6 and thus for six flow types a total of 12 loss coefficients are numbers from 1 to 12. [13]

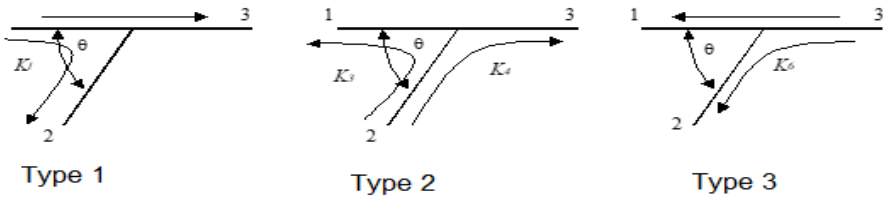

Figure 4.2: Separating flows for a T-type Junction

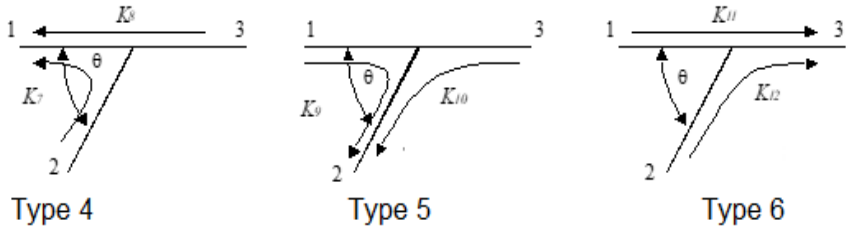

Figure 4.3: Joining flows for a T-type Junction

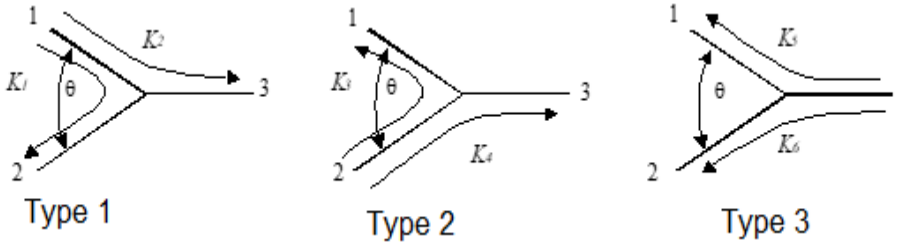

Figure 4.4: Separating flows for a Y-type Junction

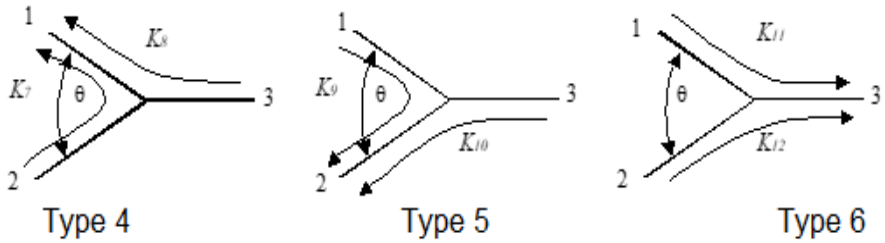

Figure 4.5: Joining flows for a Y-type Junction

The numbering of ducts which is necessary for depicting the flow type and the losses that are related to these flow types are also represented by the Figure 4.2-Figure 4.5

Daneshar & Pearson also depicted a model for the calculation of pressure loss for a three-pipe junction, but the model had 14 different configurations for the flow types

instead of six configurations used here by the Winterbone's model which is a simpler approach comparatively. [14]

The adopted hypothesis for the given model is to use loss coefficients which are calculated for a stationary type of flow and then applied for a flow that is unsteady with the same conditions instantly as of the stationary flow. This is the same hypothesis on which the flush tests are also based.

It is not possible to prove the validity of such a hypothesis because the pressure losses which occur in the pipes at the junction are usually related to the flow deviation and the development of separation bubbles. The separation bubbles that are formed can vary in position and size and is greatly dependent on the unsteady flow which can advance as well as delay the flow vein detachment from the junction wall, which means that a pressure wave can vary with a great impact the loss regime of a junction.

It will be discovered how the use of stationary flow loss coefficient hypothesis will produce accurate results even when there are inconsistencies in velocities of flow.

By the definition of the static pressure loss coefficient, as the difference in pressure (static) between the 2 branches of a junction with respect to the pressure (static) in the branch of the junction having the entire mass flow referred to as the common branch.

The loss coefficient is mathematically expressed as Li:

$$L_i = \frac{p_{upstream} - p_{downstream}}{p_{common}} = \frac{p_{us} - p_{ds}}{p_{com}} \tag{4.1}$$

Where p_{us}-p_{ds} is the drop in static pressure in the positive mass flow direction (from upstream to downstream) and p_{com} refers to the pressure in the common branch in which the entire mass flows that is the same as the entire mass flow rate that flows across the junction.

For every type of flow, there are two static pressure loss co-efficients defined for a pair of duct, The common branch is not fixed and will depend on the type of flow in consideration. The definition of static pressure loss co-efficient is commonly used by other authors as well for engine simulations however stagnation pressure loss coefficient or total pressure loss coefficient is a term that is more widely adopted which describes the loss as reduction in the stagnation pressure. This wide adoption of the total pressure loss coefficient instead of the static pressure loss coefficient is due to several reason. As a general rule in any machine or equipment the total energy of a fluid can only increase if work is done on the fluid, while the total energy is decreased in the opposite case (where work is extracted or done by the fluid). The

total pressure loss along a duct which is isolated is due to the entropy production within the fluid which means that for an isolated duct the total pressure should only decrease. While studying a 3 ducts junction, if we examine the total pressure for two ducts it will be observed that the total pressure in two ducts is increased since the third duct is contributing to the mass flow. This third duct contribution to mass flow will affect the kinetic energy and the total pressure. There will be a strong reduction in the total pressure between the common duct and the branch due to this reason except for the cases where the third duct is responsible for removing the mass from the junction.

The total or stagnation pressure loss coefficient Ki is defined as in *Eq (4.2)* for a three-pipe junction

$$K_i = \frac{(p_{us} + \frac{1}{2}\rho u_{us}^2) - (p_{ds} + \frac{1}{2}\rho u_{ds}^2)}{\frac{1}{2}\rho u_{com}^2} \tag{4.2}$$

To write the above equation, a hypothesis of incompressible fluid is adopted which means that it is assumed that the fluid has constant density. The hypothesis is valid for up to a certain limitation of relatively low Mach numbers. It is difficult to remove the hypothesis of incompressible fluids while preforming the calculations for the theoretical pressure loss co-efficient associated with the flow type, since to derive the theoretical loss coefficients Bernoulli's' equation will be necessarily used. However, in some cases it will be simpler to consider variable density fluid.

The *Eq (4.1)* & *Eq (4.2)* can be rearranged to give a simple expression that relates the total and the static pressure loss coefficients:

$$K_i = \frac{p_{com}}{\frac{1}{2}\rho u_{com}^2} L_i + \frac{u_{us}^2}{u_{com}^2} - \frac{u_{ds}^2}{u_{com}^2} \tag{4.3}$$

or this can be rearranged to be written as

$$L_i = \frac{\frac{1}{2}\rho u_{com}^2}{P_{com}} \left[K_i + \frac{u_{ds}^2}{u_{com}^2} - \frac{u_{us}^2}{u_{com}^2} \right] \tag{4.4}$$

It was observed by Chan that the pressure loss coefficients thus obtained are dependent on the speed of sound and can be related to the Mach number in the common duct, Chan also observed that the relation is such that the loss coefficient was proportional to the Mach number square. [14]

We can also write the above *Eq (4.4)* in form of Mach Number M

$$L_i = \frac{1}{2} k M_{com}^2 \left[K_i + \frac{u_{ds}^2}{u_{com}^2} - \frac{u_{us}^2}{u_{com}^2} \right] \tag{4.5}$$

If we define the mass flow ratio q as the ratio between the mass of the given duct to the mass of common duct (the duct which contains the total mass that passes through the junction).

$$q = \frac{\dot{m}}{\dot{m_{com}}} \tag{4.6}$$

The q which is the mass flow ratios is depicted in the *Table 4.1* below for all types of flow configuratoins. If the assumption of the flow to be incompressible remains, the relation for the total pressure loss coefficient, Ki given by *Eq (4.2)* is independent of the Mach number of the common duct.

It was observed by Dixon and Abou-Haider that the hypothesis of air to be incompressible is valid for low values of Mach numbers, specifically if the Mach number of the fluid is less than 0.2, then the hypothesis is perfectly valid. [15]

Decorte and Deprez observed the relation between the static pressure loss coefficient L and common branch Mach number, the results taken from there observation are represented in Figure 4.6, They obtained the static pressure loss coefficient for flow type 3 for a 90° branch, the working fluid used was air. [16]

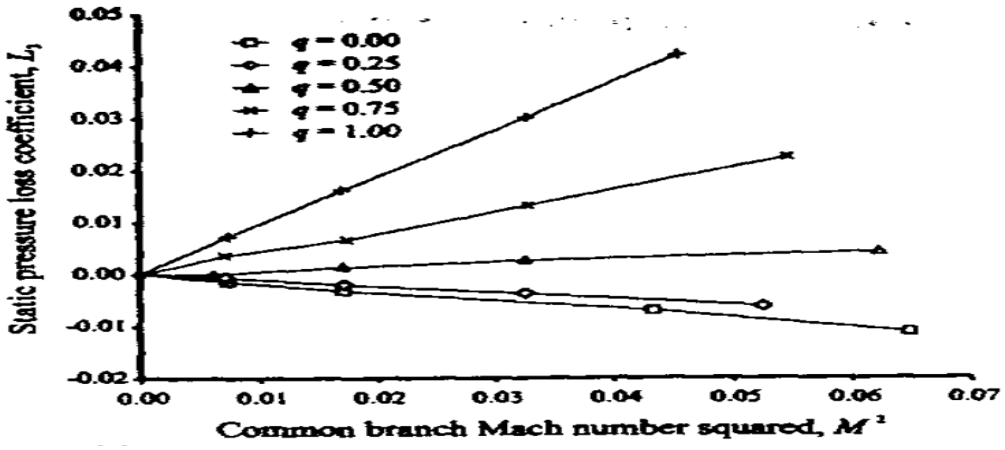

Figure 4.6: Static pressure loss coefficients for a 90° T-Junction for flow type 3. (Experimental results from Decorte & Deprez)

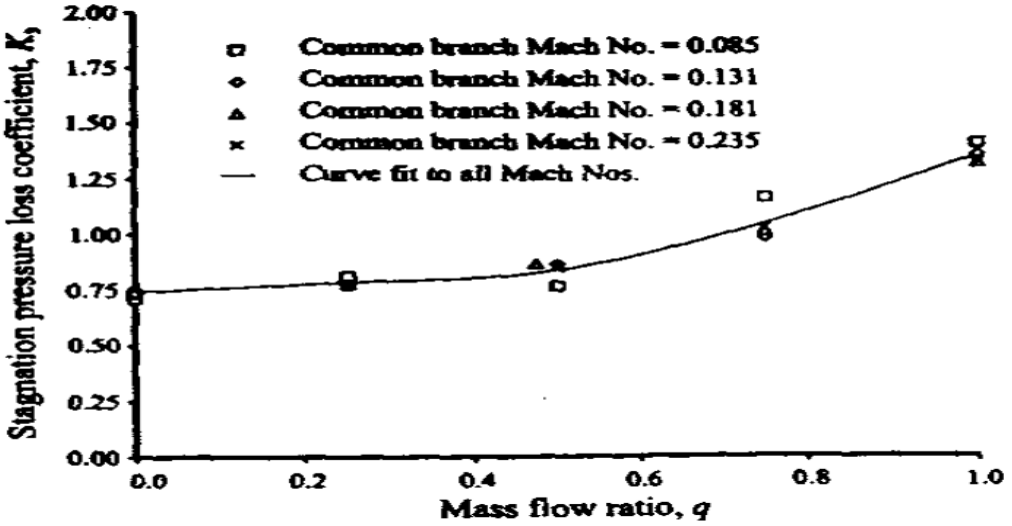

Figure 4.7: Total Pressure loss coefficients K with 90° T-Junction for flow type 3 (Experimental results from Decorte & Deprez)

Similar observations were performed with total pressure loss coefficient K with the help of *Eq (4.3)* using the relation between K and L. As also described above in that the total pressure loss coefficient is a more compact and reliable method of displaying the loss data which can also be verified from the results thus obtained in Figure 4.6 & Figure 4.7.

	Flow Type	**K_i**	**L_i**	**q**
Separating Flows	1	$K_1 = \frac{(p_1 + 1/2\,\rho u_1^2) - (p_2 + 1/2\,\rho u_2^2)}{1/2\,\rho u_1^2}$	$L_1 = \frac{p_1 - p_2}{p_1}$	$q = \frac{\dot{m}_{II}}{\dot{m}_I}$
		$K_2 = \frac{(p_1 + {}^1/_2\,\rho u_1^2) - (p_3 + {}^1/_2\,\rho u_3^2)}{{}^1/_2\,\rho u_1^2}$	$L_2 = \frac{p_1 - p_3}{p_1}$	$q = \frac{\dot{m}_{III}}{\dot{m}_I}$
	2	$K_3 = \frac{(p_2 + {}^1/_2\,\rho u_2^2) - (p_1 + {}^1/_2\,\rho u_1^2)}{{}^1/_2\,\rho u_2^2}$	$L_3 = \frac{p_2 - p_1}{p_2}$	$q = \frac{\dot{m}_I}{\dot{m}_{III}}$
		$K_4 = \frac{(p_2 + {}^1/_2\,\rho u_2^2) - (p_3 + {}^1/_2\,\rho u_3^2)}{{}^1/_2\,\rho u_2^2}$	$L_4 = \frac{p_2 - p_3}{p_2}$	$q = \frac{\dot{m}_{III}}{\dot{m}_{II}}$
	3	$K_5 = \frac{(p_3 + {}^1/_2\,\rho u_3^2) - (p_1 + {}^1/_2\,\rho u_1^2)}{{}^1/_2\,\rho u_3^2}$	$L_5 = \frac{p_3 - p_1}{p_3}$	$q = \frac{\dot{m}_I}{\dot{m}_{III}}$
		$K_6 = \frac{(p_3 + {}^1/_2\,\rho u_3^2) - (p_2 + {}^1/_2\,\rho u_2^2)}{{}^1/_2\,\rho u_3^2}$	$L_6 = \frac{p_3 - p_2}{p_3}$	$q = \frac{\dot{m}_{II}}{\dot{m}_{III}}$

Joining Flows	4	$K_7 = \frac{(p_2 + {}^1/_2\,\rho u_2^2) - (p_1 + {}^1/_2\,\rho u_1^2)}{{}^1/_2\,\rho u_1^2}$	$L_7 = \frac{p_2 - p_1}{p_2}$	$q = \frac{\dot{m}_{II}}{\dot{m}_I}$
		$K_8 = \frac{(p_3 + {}^1/_2\,\rho u_3^2) - (p_1 + {}^1/_2\,\rho u_1^2)}{{}^1/_2\,\rho u_1^2}$	$L_8 = \frac{p_3 - p_1}{p_2}$	$q = \frac{\dot{m}_{III}}{\dot{m}_I}$
	5	$K_9 = \frac{(p_1 + {}^1/_2\,\rho u_1^2) - (p_2 + {}^1/_2\,\rho u_2^2)}{{}^1/_2\,\rho u_2^2}$	$L_9 = \frac{p_1 - p_2}{p_2}$	$q = \frac{\dot{m}_I}{\dot{m}_{II}}$
		$K_{10} = \frac{(p_{31} + {}^1/_2\,\rho u_3^2) - (p_2 + {}^1/_2\,\rho u_2^2)}{{}^1/_2\,\rho u_2^2}$	$L_{10} = \frac{p_3 - p_2}{p_2}$	$q = \frac{\dot{m}_{III}}{\dot{m}_{II}}$
	6	$K_{11} = \frac{(p_1 + {}^1/_2\,\rho u_1^2) - (p_3 + {}^1/_2\,\rho u_3^2)}{{}^1/_2\,\rho u_3^2}$	$L_{11} = \frac{p_1 - p_3}{p_3}$	$q = \frac{\dot{m}_I}{\dot{m}_{III}}$
		$K_{12} = \frac{(p_2 + {}^1/_2\,\rho u_2^2) - (p_3 + {}^1/_2\,\rho u_3^2)}{{}^1/_2\,\rho u_3^2}$	$L_{12} = \frac{p_2 - p_3}{p_3}$	$q = \frac{\dot{m}_{II}}{\dot{m}_{III}}$

Table 4.1: Static and total loss pressure coefficients along with mass flow ratio q for a junction of three ducts.

Table 4.1 defines both type of loss coefficients i.e., static and stagnation pressure loss coefficients along with the mass flow ratio q for all type of flow configurations as described in the beginning of this chapter.

4.1.3 Conservation Equations for 3 ducts junctions

The conservation equations for mass, energy and momentum must be written in order to implement the boundary conditions that is provided by a junction of 3 ducts. Dissipations are also considered in this model, and thus pressure loss coefficients are introduced to the conservation equations.

Mass Conservation:

For the Mass conservation, we can write the following in general for a junction of three pipes:

$$\sum_{j=1}^{3} \dot{m}_j = 0 \tag{4.7}$$

By using the definition of the mass flow rate, *Eq (4.7)* can be rewritten as:

$$\sum_{j=1}^{3} \rho_j u_j F_j = 0 \tag{4.8}$$

or we can expand the relation :

$$\rho_1 u_1 F_1 + \rho_2 u_1 F_1 + \rho_1 u_1 F_1 = 0 \tag{4.9}$$

By the definition of Starred variable for the varying entropy field as defined before

$$A_j^* = \frac{a_j}{a_{Aj}} = \left(\frac{p_j}{p_{ref}}\right)^{\frac{k-1}{2k}} \tag{4.10}$$

$$A_A = \frac{a_{Aj}}{a_{ref}} \tag{4.11}$$

$$U_j^* = \frac{u_j}{a_{Aj}} \tag{4.12}$$

Using the basic relations for the density and isentropic expansion ratio and rearranging, we can write the expression of mass conservation in Starred variables

$$\sum_{j=1}^{3} (A_j^*)^{\frac{2}{k-1}} U_j^* \frac{F_j}{A_{Aj}} = 0 \tag{4.13}$$

The Riemann variable is defined as:

$$\lambda_{in,j} = A_j^* + \frac{k-1}{2} U_j^* \tag{4.14}$$

Thus, we can also write the velocity of fluid in starred form:

$$U_j^* = \frac{2}{k-1} (\lambda_{in,j} - A_j^*) \tag{4.15}$$

Substituting in Equation 4.10

$$\sum_{j=1}^{3} (A_j^*)^{\frac{2}{k-1}} (\lambda_{in,j} - A_j^*) \frac{F_j}{A_{Aj}} = 0 \tag{4.16}$$

If Δ represent the difference in properties for a pipe with reference to the datum duct, then we can define Δ as follows:

$$A_j^* = A_{ref}^* - \Delta_j^* \tag{4.17}$$

The Δ_j^* in the equation 4.14 considers the pressure drop with respect to the datum duct for all ducts.

We can write for j=1,2,3

$$\Delta_j^* = A_{ref}^* - A_j^* \tag{4.18}$$

Therefore, on the substitution, we obtain the final expression for the mass conservation equation that includes the pressure loss for a junction connecting 3 ducts

$$\sum_{j=1}^{3} (A_1^* - \Delta_j^*)^{\frac{2}{k-1}} [\lambda_{in,j} - (A_{ref}^* - \Delta_j^*)] \frac{F_j}{A_{Aj}} = 0 \tag{4.19}$$

The above equation 4.16, should be solved for the unknown A_{ref}^* with the help of an iterative procedure.

Energy Conservation:

The energy conservation equation can be written in two ways, one for the joining flows and the other for the separating flows. On the control volume that is made up of the junction, the energy conservation equation is applied for the joining flows, which states that the total enthalpy into the control volume must be equal to the total enthalpy that goes out of the control volume. For the separating flows the energy conservation equation assumes that the enthalpy level of the single fluid vein remains constant in the redistribution process and the total specific enthalpy of the all the ducts are same and equal to the total specific enthalpy that enters the junction.

- Energy Equation for joining flows

The joining flows which are designated by the type 4,5,6 have the flow in such a way that two ducts have incoming flow and the entire mass flow rate then goes into the third duct whose direction of flow is away from the junction. We will write the conservation of total energy for the joining flow:

$$\sum_{j=1}^{3} \dot{m}_j h_{0j} = \sum_{j=1}^{3} \dot{m}_j (C_p T + \frac{u^2}{2}) = 0 \tag{4.20}$$

Since the flow is in a non-homentropic region, we will use the stared variables to express the above equation. Recalling the dimensionless variables defined before.

$$h_0 = \frac{a_0^2}{k-1} = \frac{A_0^2}{k-1} a_{ref}^2 \tag{4.21}$$

$$A_0^2 = (A^2 + \frac{k-1}{2} U^2) \tag{4.22}$$

So

$$h_0 = \frac{a_{ref}^2}{k-1} (A^2 + \frac{k-1}{2} U^2) \tag{4.23}$$

In stared variables form:

$$h_0 = \frac{a_{ref}^2}{k-1} A_A^2 \left[(A^*)^2 + \frac{k-1}{2} (U^*)^2 \right] \tag{4.24}$$

With the help of mass conservation and the above relation, we can simplify the conservation of total energy as follows:

$$\sum_{j=1}^{3} \left\{ A_{Aj} (A_j^*)^{\frac{2}{k-1}} U_j^* \left[(A_j^*)^2 + \frac{k-1}{2} (U_j^*)^2 \right] F_j \right\} = 0 \tag{4.25}$$

We should solve the above equation with respect to the term A_{Aj}, where j will be used to identify duct with flow direction away from the junction and those ducts with flow towards the junction will not be considered for the correction purpose because the fluid does not undergo mixing for those ducts.

- Energy Equation for separating flows

The separating flows which are designated by the types 1,2,3 are characterized by one duct having flow towards the junction while the two ducts having flow away from the junction. Corberan proposed a hypothesis that the total specific enthalpy for the ducts in separating flow is same for all the three ducts involved. [9]

$$h_{0i} = constant \qquad \text{for i=1,2,3}$$

Therefore, we can rewrite the *Eq (4.24)* for this case in stared variable as:

$$A_{A1}^2 [(A_1^*)^2 + \frac{k-1}{2} (U_1^*)^2] = A_{A2}^2 [(A_2^*)^2 + \frac{k-1}{2} (U_2^*)^2] = A_{A3}^2 [(A_3^*)^2 + \frac{k-1}{2} (U_3^*)^2] \tag{4.26}$$

Apart from A_{Aj}, other variable are known from the last step of the basic iteration. As far as the variable A_{Aj} is concerned, this needs to be calculated for the two ducts having flow in direction away from the junction.

For the incoming duct, the term A_A will not need to be corrected, hence

$$A_{A1c} = A_{A1in} \tag{4.27}$$

For the two ducts having outgoing flow, the corrected values are determined with reference to the first duct with incoming flow rate.

$$A_{A2c} = A_{A1in}\sqrt{\left(\frac{[(A_1^*)^2 + \frac{k-1}{2}(U_1^*)^2]}{[(A_2^*)^2 + \frac{k-1}{2}(U_2^*)^2]}\right)} \tag{4.28}$$

$$A_{A3c} = A_{A1in}\sqrt{\left(\frac{[(A_1^*)^2 + \frac{k-1}{2}(U_1^*)^2]}{[(A_3^*)^2 + \frac{k-1}{2}(U_3^*)^2]}\right)} \tag{4.29}$$

Where the subscript 'in' represents the initial values and subscript 'c' represents the corrected values for the given ducts.

4.1.4 Pressure drop term

In order to complete the set of equation, the remaining equation is that for the conservation of momentum which will allow us to calculate the loss of pressure for each duct with respect to the reference ducts. Thus, we will be able to find the term Δ_j^* , which indicates the level of loss in static pressure for each duct. The Δ_j^* are function of static pressure loss coefficients L_i which can be calculated from the flushing tests. While for the model being considered Li is calculated theoretically.

We can define the static pressure loss coefficient for a duct as the relative pressure difference between the duct and the reference duct, mathematically this can be written as:

$$L_i = \frac{p_{us} - p_{ds}}{p_{com}} \tag{4.30}$$

p_{us}: represents the static pressure of the upstream duct

p_{ds}: represents the static pressure of the downstream duct

p_{com}: represents the static pressure of the common duct that carries the entire mass flow rate

We know the basic relations:

$$\frac{p}{p_{ref}} = (A^*)^{\frac{2k}{k-1}}$$

$$A^* = \frac{a}{a_A} = \frac{A}{A_A}$$

With the definition of the common variables, *Eq (4.30)* can be simplified and rewritten as:

$$(A^*_{us})^{\frac{2k}{k-1}} - (A^*_{ds})^{\frac{2k}{k-1}} = L_i(A^*_{com})^{\frac{2k}{k-1}} \tag{4.31}$$

The *Eq (4.31)* can be written for all types of flows with their associated loss coefficients, remember that there are two loss coefficients associated with all flow types thus making 12 loss coefficients for the 6 flow types being studied

We discuss here the method for the derivation of loss coefficients for the flow type 1, which will help to identify that the procedure is the same for the other flow types involved and thus the procedure for the other flow types will not be derived here but the final result will be presented in the tabular form for all the flow types.

Let us denote the common terms in the exponent of the equation *Eq (4.31)* by some variable so as to simplify the equation:

Let $\xi = \frac{2k}{k-1}$ & $\eta = \frac{k-1}{2k}$

Eq (4.31) can be written in simple form:

$$(A^*_1)^{\xi} - (A^*_3)^{\xi} = L_2(A^*_1)^{\xi} \tag{4.32}$$

The pressure ratios be :

$$x^*_2 = \frac{A^*_2}{A^*_1}; \quad ; \quad x^*_3 = \frac{A^*_3}{A^*_1}$$

We can rewrite *Eq (4.31)* as:

$$A^*_2 = A^*_1(1 - L_1)^{\eta} \tag{4.33}$$

$$A_3^* = A_1^*(1 - L_2)^\eta \tag{4.34}$$

Using the pressure ratio defined,

$$x_2^* = (1 - L_1)^\eta$$
$$x_3^* = (1 - L_2)^\eta$$

Hence the method considers for each type of flow, the derivation of two pressure ratios which are here represented by x_2, x_3 as a function of two loss coefficients associated with the flow type.

With the help of above derivation, we can conclude that for any type of flow:

$$\Delta_1^* = 0$$
$$\Delta_2^* = A_1^*(1 - x_2^*)$$
$$\Delta_3^* = A_1^*(1 - x_3^*)$$

It is essential to indicate the flow type based on the flow direction and thus calculate based on flow type the associated loss coefficients Li.

The results extended as per the above derivation for flow type 1 to all the other flows type are indicated in the table below.

Category	**Flow Type configuration**	$x_2^* = \frac{A_2^*}{A_1^*}$	$x_3^* = \frac{A_3^*}{A_1^*}$
Flow separating	Type 1	$x_2^* = (1 - L_1)^\eta$	$x_3^* = (1 - L_2)^\eta$
	Type 2	$x_2^* = (1 - L_3)^{-\eta}$	$x_3^* = \frac{(1 - L_4)^\eta}{(1 - L_3)^\eta}$
	Type 3	$x_2^* = \frac{(1 - L_6)^\eta}{(1 - L_5)^\eta}$	$x_3^* = (1 - L_5)^{-\eta}$
Joining Flows	Type 4	$x_2^* = (1 + L_7)^\eta$	$x_3^* = (1 - L_8)^\eta$
	Type 5	$x_2^* = (1 + L_9)^{-\eta}$	$x_3^* = \frac{(1 + L_{10})^\eta}{(1 + L_9)^\eta}$
	Type 6	$x_2^* = \frac{(1 + L_{12})^\eta}{(1 + L_{11})^\eta}$	$x_3^* = (1 + L_{11})^{-\eta}$

Table 4.2: Pressure ratios for all flow configurations for a three- duct junction

4.1.5 Loss Coefficient Calculation

As in the beginning of the chapter, the relation between the static pressure loss coefficient and the total pressure loss coefficient has been derived, recalling *Eq (4.5)*

$$L_i = \frac{1}{2} k M_{com}^2 \left[K_i + \frac{u_{ds}^2}{u_{com}^2} - \frac{u_{us}^2}{u_{com}^2} \right] \tag{4.35}$$

We will develop a method to calculate the total pressure loss coefficients K, for the two types of flow which are type 3 and type 6. These types are selected because they refer to different categories, as type 3 is a separating flow configuration while type 6 is a joining flow configuration. Moreover, different hypothesis will be adopted for the separating flow types and the joining flow types. As mentioned before that with each flow configuration there are always two loss coefficients associated, we will derive the expression for one of these in detail and will report the results of the other in the tabular form. The junction here being considered is the T-type junction

The flush tests used to derive the loss coefficient are utilized by the simulation software for the modelling of junctions. We here present the model that will not rely on the flush tests rather we create the loss coefficients theoretically thus leaving the dependence on the flush tests.

For the joining Flows:

For the joining flows, we consider the hypothesis of assuming that the two ducts that have the incoming flows are at the same static pressure, with reference to the Figure 4.8, it is also assumed that the cross-sectional area of the main duct is constant.

Such that:

$$p_1 = p_3 \qquad ; F_1 = F_3$$

Based on the definition of the total pressure loss coefficients, we can write the total pressure loss coefficient between the first and the second duct K_{12} as below:

$$K_{12} = \frac{(p_2 + \frac{1}{2}\rho u_2^2) - (p_3 + \frac{1}{2}\rho u_3^2)}{\frac{1}{2}\rho u_3^2}$$

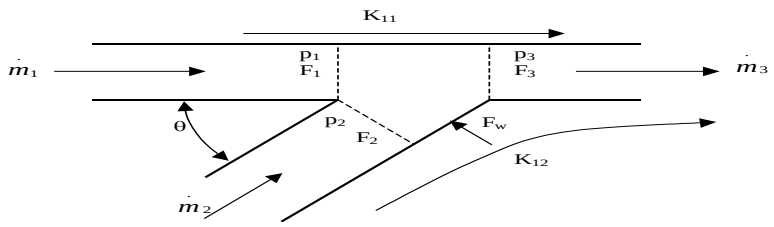

Figure 4.8: Generic joining flows scheme for calculation for

pressure loss coefficient for joining flow

We write the equation for the conservation of momentum for the control volume as marked in the Figure 4.8, considering that there is no friction.

$$p_1F_1 + p_2F_2\cos\theta - p_3F_3 - R_{Wx} = -\dot{m}_1u_1 - \dot{m}_2u_2\cos\theta + \dot{m}_3u_3 \tag{4.36}$$

The reaction component to the wall depends on the pressure variation and the angle between the connecting duct with the main duct, for simplicity we adopt the hypothesis that the pressure variation is linear from section 2 to 3, therefore we can write the reaction component R as:

$$R_{Wx} = \left(\frac{p_2 + p_3}{2}\right)F_2\cos\theta \tag{4.37}$$

It is possible to write the continuity equation as below:

$$u_1F_1 + u_2F_2 = u_3F_3 \tag{4.38}$$

The above equation of continuity is written assuming that the density is constant along the duct and across the junction.

Now we also introduce the mass flow ratio :

$$q = \frac{\dot{m}_{pipe}}{\dot{m}_{com}} \tag{4.39}$$

The mass flow ratio for the concerned loss coefficient is :

$$q = \frac{\dot{m}_2}{\dot{m}_3}$$

Therefore, we can express the velocity of fluid in terms of area ratios and mass flow ratios as below:

$$u_1 = (1-q)u_3 \quad ; \quad u_2 = q\frac{F_3}{F_2}u_3 \tag{4.40}$$

We substitute the expression of fluid velocity obtained in terms of mass flow ratio and area ratio in the conservation of momentum equation:

$$\frac{p_3 - p_2}{\rho u_3^2} = \frac{F_3}{F_3 + \frac{1}{2}F_2\cos\theta}\left[(1-q)^2 - 1 + q^2\frac{F_3}{F_2}\cos\theta\right] \tag{4.41}$$

We again write the loss coefficient K_{12} in the form of:

$$K_{12} = \frac{p_2 - p_3}{\frac{1}{2}\rho u_3^2} + \frac{u_2^2}{u_3^2} - 1 \tag{4.42}$$

Thus, on combination of *Eq (4.41 - 4.43)* we can obtain a relation to express the total loss coefficient in terms of function of the mass ratios and the cross-sectional area and the angle between the ducts which are all known. Therefore, we conclude the below expression for the total loss coefficient

$$K_{12} = \frac{2F_3}{F_3 + \frac{1}{2}F_2 \cos\theta}\left[1 - (1-q)^2 - q^2\frac{F_3}{F_2}\cos\theta\right] + q^2\frac{F_3}{F_2} - 1 \tag{4.43}$$

We can extend the same derivation for other flow configurations, the derivation will not be performed for each of the loss coefficient, since the same procedure is to be adopted for all. The results are reported in tabular form in Table 4.3 for all the loss coefficients thus obtained

The model thus developed here, have following difference from the model proposed by Blair [17]:

- The angle between the main duct and the branches do not belong to a discrete set and can vary continuously between 0 and 180 degrees.

- Flushing tests and the associated data are no longer needed due to the development of simple theoretical functions related to the loss coefficients

- The ducts area can vary, and this it is not necessary that the ducts be of the same cross section to calculate the loss coefficients.

For the separating Flows:

Since now we deal with the separating flows, we cannot have the condition for the same pressure in the branches. Hence, we require a new hypothesis on the flow characteristic. The hypothesis by Hagar [12] is to be adopted on the maximum deviation of flow. [17]

We can observe the similarity in flow of type 1 to the type 3 flow defined before, thus the coefficients K_2 and K_5 tends to be equal and therefore we only derive the relation for K_5.

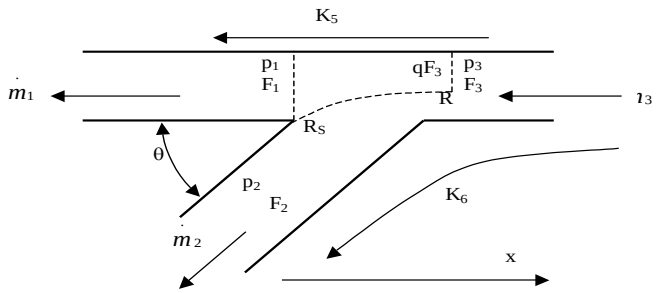

Figure 4.9 : Generic joining flows scheme for calculation for

pressure loss coefficient for separating flow

We write the equation for the conservation of momentum for the control volume as shown in above Figure 4.9 for separating flows

$$p_3 q F_3 - p_1 F_1 + p_3(1-q)F_3 = \dot{m}_1 u_1 - q\dot{m}_3 u_3 \tag{4.44}$$

Where the average pressure along the flow line R-R′ is represented by p_3

$$p_3^* = \left(\frac{p_3 + p_{03}}{2}\right) = p_3 + {}^1\!/_4\,\rho u_3^2 \tag{4.45}$$

While the total pressure loss coefficient K_5 by its definition is written as:

$$K_5 = \frac{(p_3 + {}^1\!/_2\,\rho u_3^2) - (p_1 + {}^1\!/_2\,\rho u_1^2)}{{}^1\!/_2\,\rho u_3^2} \tag{4.46}$$

Thus, upon simplifications and substitution of relations in the momentum conservation equations and using the hypothesis of the model $F_1 = F_3$ we can conclude the total pressure loss coefficient K_5 to be only a function of the mass flow rates and obtain a simple relation for the loss coefficient of the separating flow here being considered

$$K_5 = q^2 - \frac{3}{2}q^2 + \frac{1}{2} \tag{4.47}$$

Based on the derivation of the loss coefficients for the separating and joining flows for the two basic flow configurations, we extend the derivation so as to obtain all loss coefficients related to the flow types defined for 3-duct junctions in the Table 4.3:

Category flow	**Flow Type**	K_{iT}
Flow separating	Type 1	$K_1 = q^2\Psi_T^2 + 1 - 2q\Psi_T \cos(\frac{3}{4}(\pi - \theta))$
		$K_2 = q^2 - \frac{3}{2}q + \frac{1}{2}$
	Type 2	$K_3 = 1 + \frac{q^2}{\Psi_T^2} - \frac{2q}{\Psi_T}\cos(\frac{3}{4}(\pi - \theta))$
		$K_4 = 1 + \frac{q^2}{\Psi_T^2} - \frac{2q}{\Psi_T}\cos(\frac{3}{4}\theta)$
	Type 3	$K_5 = q^2 - \frac{3}{2}q + \frac{1}{2}$
		$K_6 = q^2\Psi_T^2 + 1 - 2q\Psi_T \cos(\frac{3}{4}\theta)$
Flow that joins	Type 4	$K_7 = 4q - 1 + q^2(\Psi_T^2 - 2 + 2\Psi_T \cos\theta)$
		$K_8 = 1 - q^2 + 2(1 - q^2)\Psi_T \cos\theta$
	Type 5	$K_9 = 1 + \frac{2(2q-1)}{\Psi_T}\cos\theta + \frac{q^2}{\Psi_T^2}$
		$K_{10} = 1 + \frac{2(1-2q)}{\Psi_T}\cos\theta + \frac{q^2}{\Psi_T^2}$
	Type 6	$K_{11} = \frac{2\Psi_T}{\Psi_T + \frac{1}{2}\cos\theta}\left\{1 - q^2 - (1 - q^2)\Psi_T \cos\theta\right\} + q^2 - 1$
		$K_{12} = \frac{2\Psi_T}{\Psi_T + \frac{1}{2}\cos\theta}\left\{1 - (1 - q^2) - q^2\Psi_T \cos\theta\right\} + q^2\Psi_T^2 - 1$

Table 4.3: Total pressure loss coefficients for separating and joining flow configurations for three-duct junctions

4.2 Pressure loss model for multipipe junction

4.2.1 Introduction

We derived relation for the pressure loss model and corresponding static and total pressure loss coefficients for a three-pipe junction with all possible configurations. The number of possible configurations for a three-pipe junction in total was six and hence twelve loss coefficients were calculated. In case of number of pipes being 4 or more the number of possible configurations will increase, and we cannot define and derive each type of configuration, therefore we need a model that in its general form calculates the loss coefficients and the predict the behavior of the pressure waves for any number of pipes without specifying the exact configuration of the flow type.

For a multipipe junction with complex geometry, the pressure drop can be significant. This was observed by Winterbone in an experiment, the graphical representation in Figure 4.10, where a complex junction for a racing engine with five into one exhaust is compared. Both the pressure loss model and constant pressure model were applied to theoretically predict the behavior of the engine and compared with the measured actual exhaust pressure. It was noted that the constant pressure model predicts high pressure peaks as it was not taking into account the pressure drops across the junction and the results thus produced with the constant pressure model are significantly different from the actual results. [19]

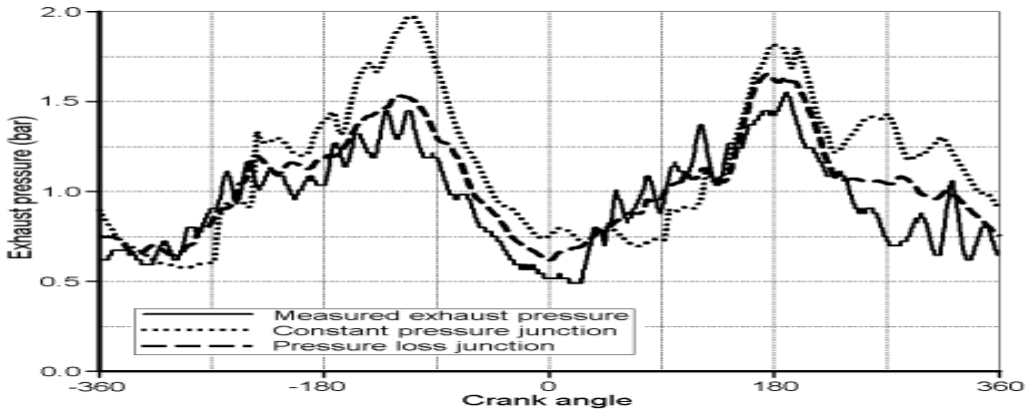

Figure 4.10: The pressure curve for a racing engine with a 5 into 1 exhaust at 7000 rpm

Also, in the Figure 4.11 below, the exhaust pressure was predicted for the same engine at 13000 rpm and again it was observed that constant pressure model predicted higher peak pressures. Thus, it can be concluded that the constant pressure model is

not always accurate when dealing with complex junctions involving a greater number of ducts.

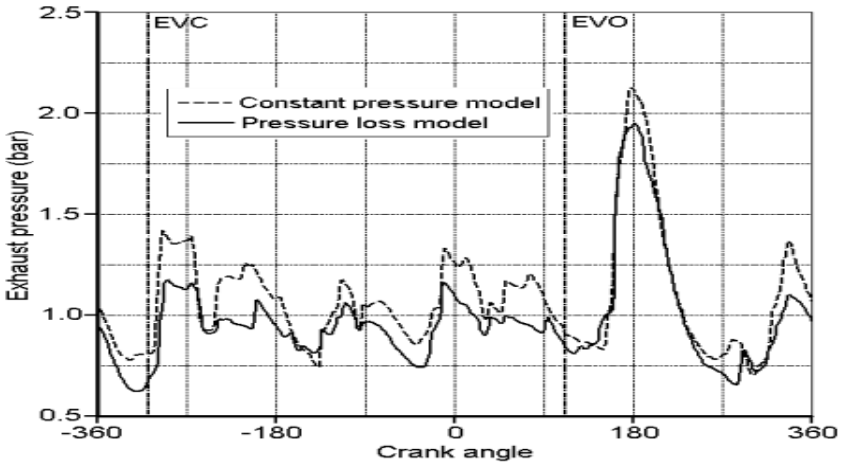

Figure 4.11: Exhaust pressure prediction at 13000 rpm

It should be noted that the constant pressure model proposed by Benson was a good approximation for cases where the angle between the ducts were not very large and the geometrical characteristics of the ducts were similar. In case of complex junctions with high relative angles and extremely different mass flow rates and area ratios, the constant pressure model was not a good approximation and did not provide accurate results. This was also observed by Winterbone [18]

In this chapter we are going to discuss the pressure loss model for a generic N number of pipes. In the Figure 4.12, we see how the multipipe junction can be selected in the Gasdyn code.

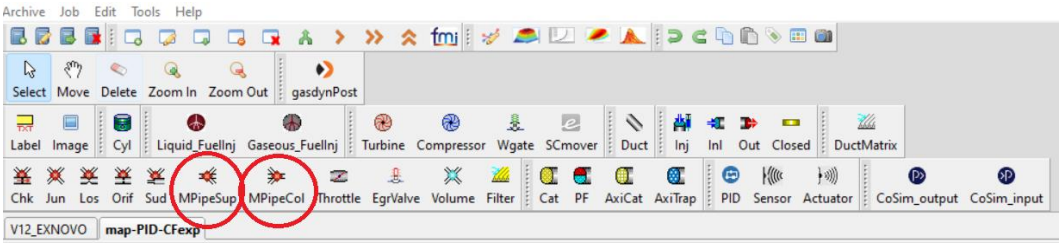

Figure 4.12: The Supplier and Collector type multipipe junction in Gasdyn

4.2.2 Junction Classifications

The multipipe junctions for this purpose can be distinguished into two types:

- **Supplier type:** This type of junction has a main duct from which the flow is supplied to the remaining ducts, also represented by Figure 4.13**.** This can be

found on usually the intake manifold. In this junction the first duct which is the primary duct is the supplier in which flow is towards the junction , while in the other ducts the flow is away from the junction

- **Collector type**: This type of junction has a particular configuration where main duct collects the flow from the other ducts. This can be found on an exhaust manifold. In this junction the main duct which is the primary duct is the collector in which flow is away the junction , while in the other ducts the flow is towards from the junction. A typical example of this is shown in the Figure 4.14

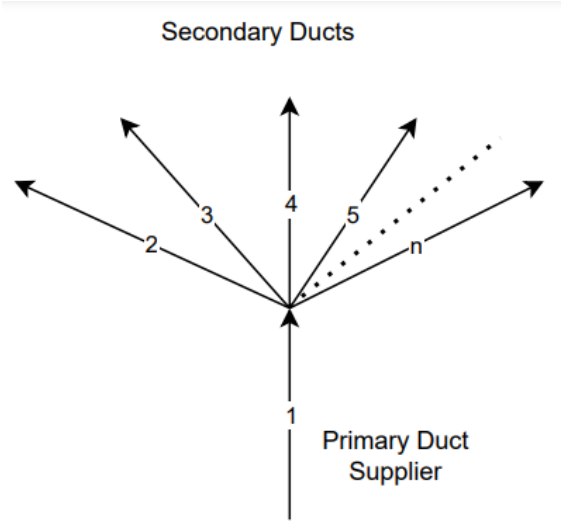

Figure 4.13: A generic Supplier type junction

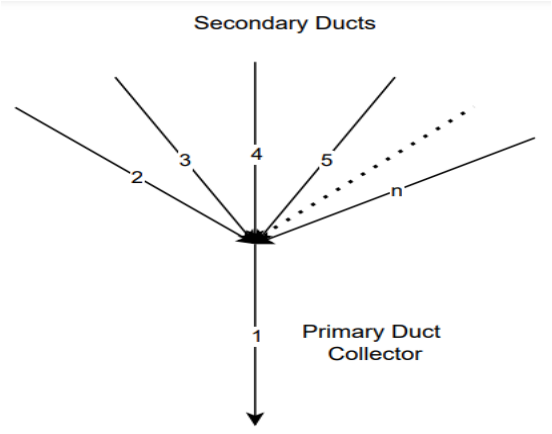

Figure 4.14: A generic collector type junction

In general, for the prediction of the pressure losses experimental data is required, which can be obtained from the flush tests. The flush tests are performed for various geometric configurations. The results from these types of tests are usually interpolated to be applied for the use in computational codes. Also, the test is not performed for large operating points and interpolation is involved so as not to have too much of data. However, the application of this model is in fact limited because of the interpolation which is usually dependent on the geometrical characteristics of the duct.

The multipipe junction model for the prediction of pressure loss for N pipes was studied by Winter bone. The method by Winterbone-Bassett is very flexible because of the reason that it is dependent on the theoretical strategy for the prediction of pressure drops. The method provides a theoretical way of predicting the static pressure loss coefficients. Due to this reason, it is better than the results being used from the flush test experimental method because it does not depend on the interpolation and shows better accuracy than the experimental flush tests. [18]

To predict the behavior of the pressure waves, we adopt the same procedure as adopted in the previous section and apply the equations of conservation.

4.2.3 Conservation of Mass

With reference to the mass conservation applied in the previous section for three pipe ducts, The equation for the conservation of mass is modified as per the scenario of multipipe junctions which means that the limit for the number of ducts will be changed from 3 to N. We can write the equation for the conservation of mass flow rate as below:

$$\sum_{j=1}^{N} (A_j^*)^{\frac{2}{k-1}} (\lambda_{in,j} - A_j^*) \frac{F_j}{A_{Aj}} = 0 \tag{4.48}$$

We again have to consider one duct as the reference duct to proceed with the numerical computation in a simple manner. The term datum ('dat') will be used to denote the reference duct and will be used to determine the pressure level in the other ducts as well. In this model by Winterbone-Bassett the reference duct is the one that have the greatest mass flow rate with the positive direction (with flow direction towards the junction). The A* for the other ducts will be based on this reference duct and will be written as below. [19]

By definition of Δ_j^*

$$\Delta_j^* = A_{dat}^* - A_j^* \tag{4.49}$$

or

$$A_j^* = A_{dat}^* - \Delta_j^*$$

By using the above relation in the equation for the conservation of momentum we can write the equation below, which will be solved with iteration for A_{dat}^*:

$$\sum_{j=1}^{N} (A_{dat}^* - \Delta_j^*)^{\frac{2}{k-1}} [\lambda_{in,j} - (A_{dat}^* - \Delta_j^*)] \frac{F_j}{A_{Aj}} = 0 \tag{4.50}$$

4.2.4 Conservation of Energy

Corberan's approach is adopted for applying the conservation of energy to the given junction. Corbreran's approach is based on the hypothesis that the ducts with incoming flow towards the junction does not face any change in the entropy, this is due to the fact that the flow does not get affected because of the mixing that occurs in the junction volume. Another hypothesis to be adopted is that of the perfect mixing of gases which means that the total specific enthalpy of outgoing flow is equal to the total specific enthalpy of the incoming flow, if we denote the total number of ducts with incoming flow by NJ, and the total number of ducts with outgoing flow by NS, *Eq (4.51)* represents the enthalpy balance. [9]

$$\sum_{j=1}^{NJ} (\dot{m}_j h_{0j})_J = \sum_{j=1}^{NS} (\dot{m}_j h_{0j})_S \tag{4.51}$$

In the above equations the terms $(h_{0j})_J$ are known for all the ducts, therefore the equation must be solved for $(h_{0j})_S$, which can be written as:

$$(h_{oj})_S = \frac{\sum_{j=1}^{NJ} (\dot{m}_j h_{0j})_J}{\sum_{j=1}^{NJ} \dot{m}_j} \tag{4.52}$$

And it is obvious that the total mass flow rate towards the junction is equal to the total mass flow rate outgoing from the junction

$$\sum_{j=1}^{NJ} \dot{m}_j = \sum_{j=1}^{NS} \dot{m}_j \tag{4.53}$$

As we derived in the previous chapter the expression of total enthalpy and mass flow rate in stared variables. Rewriting them here:

$$h_{0j} = \frac{a_{ref}^2}{k-1} A_{Aj}^2 [(A_j^*)^2 + \frac{k-1}{2}(U_j^*)^2] \tag{4.54}$$

$$\dot{m}_j = \frac{k p_{ref}}{a_{ref}} (A_j^*)^{\frac{2}{k-1}} U_j^* \frac{F_j}{A_{Aj}} \tag{4.55}$$

Therefore, we can write the *Eq (4.54)* again in stared variable form:

$$h_{0j} = \frac{a_{ref}^2}{k-1} \frac{\sum_{j=1}^{NJ} \left\{ (A_j^*)^{\frac{2}{k-1}} U_j^* F_j A_{Aj} \left[(A_j^*)^2 + \frac{k-1}{2}(U_j^*)^2 \right] \right\}}{\sum_{j=1}^{NJ} \left[\frac{(A_j^*)^{\frac{2}{k-1}} U_j^* F_j}{A_{Aj}} \right]} \tag{4.56}$$

For the incoming flows we already defined that the entropy level will not vary ,while for the outgoing flow it will vary because of the mixing, we can write the expression for the outgoing flow entropy level now for ducts with flow away from the junction:

$$A_{Aj} = \sqrt{\frac{h_{oj} \left[\frac{k-1}{a_{ref}^2} \right]}{\left[(A_j^*)^2 + \frac{k-1}{2}(U_j^*)^2 \right]}} \tag{4.57}$$

Hence the Riemann variables can now be computed for all the ducts, where the subscript ‘c’ is used for the corrected property and the subscript ‘un’ is used for the unchanged or initial value of the property :

For ducts with incoming flows:

$$\lambda_{in,c}^* = \lambda_{in,un}^* \tag{4.58}$$

For ducts with outgoing flows:

$$\lambda_{in,c}^* = \lambda_{in,un}^* \left[\frac{A_{A,un}}{A_{A,c}} \right] + A^* \left[\frac{1 - A_{A,un}}{A_{A,c}} \right] \tag{4.59}$$

4.2.5 Pressure drop Term

For the constant pressure model the term Δ_j^* was zero, but for the case in consideration it is an unknown which is yet not determined. The above equations of conservations

were written assuming that the term Δ_j^* is known. In this model the equation of momentum becomes a necessity for the solution of the system of equations.

We defined the total pressure loss coefficient in the previous chapter, lets recall the definition of the total pressure loss coefficient which is defined as the relative difference between the total pressure of the duct with respect to the reference duct.

For the model under consideration, we also define the ratio of cross-sectional area and the ratios of mass flow rates and represent them by ψ & q respectively

$$\psi_j = \frac{F_{dat}}{F_j} \tag{4.60}$$

$$q_j = \frac{\dot{m}_j}{\dot{m}_{dat}} \tag{4.61}$$

The total pressure loss coefficient is represented by K and is mathematically written as:

$$K_j = \frac{\left(\rho_{dat} + \frac{1}{2}\rho u_{dat}^2\right) - \left(\rho_j + \frac{1}{2}\rho u_j^2\right)}{\frac{1}{2}\rho u_{dat}^2} \tag{4.62}$$

We can rearrange the above equation so as to write the difference of pressure between any given duct and the reference duct to be a function of the total pressure loss coefficient K:

$$p_{dat} - p_j = \frac{1}{2}\rho u_j^2 \left\{\frac{K_j}{q_j^2\psi_j^2} - \frac{1}{q_j^2\psi_j^2} + 1\right\} \tag{4.63}$$

We introduce another loss coefficient C based on the above equation and write the above equation in a more simplified way as below:

$$p_{dat} - p_j = C_{j(}\rho u_j^2) \tag{4.64}$$

Where C_j is the other loss coefficient which is a function of the total pressure loss coefficient, the area ratio, and the mass flow ratio

$$C_j = C_j\left(K_j, q_j, \psi_j^2\right) = \frac{1}{2}\left\{\frac{K_j}{q_j^2\psi_j^2} - \frac{1}{q_j^2\psi_j^2} + 1\right\} \tag{4.65}$$

The loss prediction model for multipipe junction can be summarized by the *Eq (4.64)*, which expresses that the pressure of any duct can be predicted with reference to the

datum duct as a function of the loss coefficient C which itself is directly related to the area ratio, mass flow ratio and the total pressure loss coefficient for the ducts.

Rewriting the basic equation for the starred variables:

$$\frac{p_j}{p_{ref}} = \left(A_j^*\right)^{\frac{2k}{k-1}}$$

$$U_j^* = \frac{u_j}{A_{Aj} a_{ref}} \quad ; \qquad \rho_j = k \frac{\left(A_j^*\right)^{\frac{2}{k-1}}}{A_{Aj}^2} \frac{p_{ref}}{a_{ref}}$$

With the help of above relations, we can rewrite equation *Eq (4.64)*, as below:

$$\left(A_{dat}^*\right)^{\frac{2k}{k-1}} - \left(A_j^*\right)^{\frac{2k}{k-1}} = k C_i \left(A_j^*\right)^{\frac{2k}{k-1}} \left(U_j^*\right)^2 \tag{4.66}$$

This can be further simplified to give the expression for A_{dat}^*

$$A_{dat}^* = A_j^* \left\{ 1 + k C_j \left(\frac{U_j^*}{A_j^*} \right)^2 \right\}^{\frac{k-1}{2k}} \tag{4.67}$$

Since the term Δ_j^* by its definition is given by:

$$\Delta_j^* = A_{dat}^* - A_j^*$$

Therefore, we can write the relation for Δ_j^* as below:

$$\Delta_j^* = A_j^* \left\{ \left[1 + k C_j \left(\frac{U_j^*}{A_j^*} \right)^2 \right]^{\frac{k-1}{2k}} - 1 \right\} \tag{4.68}$$

4.2.6 Loss Coefficient

For the *Eq (4.68),* the unknown that remain in the calculation of Δ_j^* is the Cj. There are different loss prediction models proposed for the calculation of of this loss coefficient. These models can predict the value of the loss coefficient by adopting different approaches and hypothesis.

4.2.6.1 Bingham-Blair Model:

One model used for the prediction of loss coefficients C is the Bingham and Blair model, which requires the mandatory classification of the junction prior to the calculation of the loss coefficient as ‘supplier’ or collector’ . The classification was

explained in the beginning of this chapter. However, the Winterbone model provides an advantage to the Bingham and Blair model and does not need the classification of the junction in this manner and hence do not require the need to know the average direction of flow. [19]

The Bingham-Blair model sets the reference duct the one in which has the flow with the highest speed among the incoming flow ducts. For each time step this duct with the highest speed is set as the reference duct and the pressure loss between the reference ducts and the other ducts are calculated. Here the classification of the junction plays a significant role which is as follows. [19]

- **Collector Type junction:**

For the collector type junction classification, the loss is between the secondary duct upstream and the main duct downstream of the junction

- **Supplier Type junction:**

For the collector type junction classification, the loss is between the primary duct upstream and the branch duct downstream of the junction

While for the ducts with incoming flows the hypothesis adopted is of the equal pressure at the junction to allow for proper mixing of the gas. The same loss is fixed for all the ducts with incoming flows in the collector type junction and is set equal to the loss between the reference duct and the duct with greatest velocity towards the collector and the collector duct so as to respect the hypothesis of constant pressure for all incoming ducts. The problem with the model is that it is unable to capture effects of directionality of the flow.

Bingham-Blair on the basis of the results obtained from the flow tests, proposed the following linear equation for the calculation of the loss coefficient to simplify and generalize the calculation of the loss coefficient between any two branches of the junction:

$$C_j = 1.6 - \theta_d \frac{1.6}{167} \tag{4.69}$$

Where the angle between the two branches where the loss coefficient is to be determined is denoted by θ_d and is used in degrees. It was also stated that if the angle between the two branches of a junction is greater than 167 degrees then the loss coefficient would be neglected and C=0. [19]

Figure 4.15 represents graphically, the summarized results for Bingham and Blair's Model for joining and separating flows as well as for the general relation *Eq (4.69)* presented by the Model.

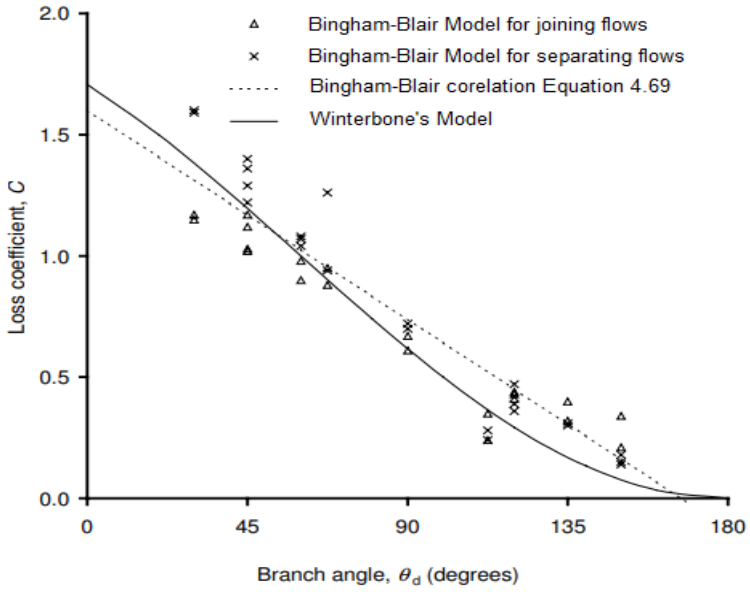

Figure 4.15: Variation of Loss coefficient with branch angle

4.2.6.2 Winterbone-Bassett Model:

The Winterbone model here presented does not need the determination of the junction type as supplier or collector as required by the previously described model by Bingham-Blair. This is because in the Winterbone-Bassett model the solution is entirely managed by the same equations. The basic scheme is to identify for each time step the reference duct which in this case is defined as the duct with positive flow towards the junction and having the greatest mass flow rate. Below we are going to determine the loss coefficient Cj so that the system of equations can be closed and proceeded to the iterative procedure for the solution.

As previously stated, that the models used for the prediction of pressure losses work on the hypothesis that the ducts having flow towards the junction are at the same static pressure. Now since the reference duct is the one with greatest mass flow towards the junction thus all the ducts with incoming flow will have the same pressure as of the reference duct. This leads to a simplification that the Δ_j^* for all the ducts with incoming flow will be zero.

Therefore, only for the branches with the flow away from the junction, there is need for the determination of Δ_j^* and the loss coefficient Cj. Hence for all the branches with negative flows, loss is calculated with respect to the datum duct.

As shown in the Figure 4.16, we demonstrate a N-duct junction in general to simplify the elaboration of the model being presented. At all instants, one can identify the

datum duct which is the duct with greatest mass flow rate towards the junction. If we consider any duct 'j' having negative flow (away from the junction), also represented in the Figure 4.16 below with its mass $\dot{m}_j$ and cross-sectional area F_j.

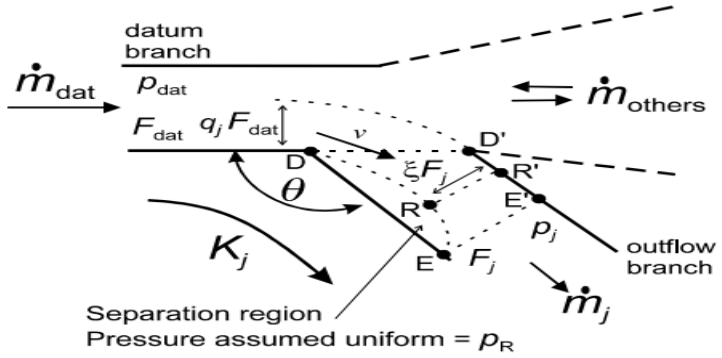

Figure 4.16: Flow pattern representation for N-duct junctions

This model here presented will be used to calculate the loss coefficient for a generic branch only and can be applied in the same way to all the branches using the same generic equations which will be developed. The mass flow rate of the other branches is denoted by $m_{j_{others}}$. There are two control volumes used for the calculation of the loss coefficients. The two control volumes are presented in the Figure 4.16 by the point R'-R-D'-D and E-E-R'-R. It can be assumed that pressure at point D' is equal to the datum branch's total pressure due to the isentropic transformation. [20]

We observe a separation zone or separation bubble when the flow enters the side from the datum branch as represented in the Figure 4.16. Due to this separation bubble the flow is disturbed in the lateral branch duct. If we represent the coefficient of restriction by the ξ which actually denotes the reduction in the cross section of the branch for the fluid flow. The pressure is constant in this separation zone, and it is considered that the pressure at the separation zone is the same as that on the section R-R'.

Hagar made a hypothesis based on the experimental results for a junction of three ducts having same cross-sectional area that the flow from the main duct to the secondary branched duct is in the following way: [17]

- The flow deviates when it enters from the main duct to the branched duct
- The deviation of flow is by an angle of $\theta/4$
- The flow after deviation has the same speed

It was shown that even though the above hypothesis by Hagar was for same cross-sectional area ducts but was still valid if the branched duct was different in cross section from the main duct. Therefore, based on this hypothesis we can say that the flow is deviated as it moves from the main duct to the branched duct j and the velocity in section D-D' is uniform and equal to u_{dat}. [17]

We assume that the entire loss occurs in the region after the contracted section that was affected by the separation bubble since due to Hagar's hypothesis, we say that the total pressure remains constant as long as the flow accelerates in the convergent region D'-R'-R-D

We define the ratio of mass flow rates and the coefficient of restriction as below and using the above hypothesis:

$$q_j = \frac{\dot{m}_j}{\dot{m}_{dat}}$$
$$\dot{m}_j = \dot{m}_R$$
$$\xi = \frac{F_R}{F_j}$$

Therefore, using the above relations, we get

$$u_j = q_j \, \psi_j \, u_{dat} \tag{4.70a}$$

$$u_R = q_j \psi_j \frac{u_{dat}}{\xi} \tag{4.70b}$$

Now we can apply the conservation of momentum equation to the control volume D'-R'-R-D:

$$\bar{p}_{dat} F_j - p_R F_j = \dot{m}_j u_R - \dot{m}_j u_{dat} \, cos\left[\frac{3}{4}(\pi - \theta)\right] \tag{4.71}$$

Where the term $\bar{p}_{dat}$ represents along the line D-D' the average pressure. The pressure at the point D' represents the total pressure of the datum duct.

$$\bar{p}_{dat} = \frac{p_{dat} + p_{0dat}}{2} \tag{4.72}$$

Which can also be written as

$$\bar{p}_{dat} = p_{dat} + \frac{1}{4}\rho u_{dat}^2$$

The pressure at point R can be written relations in *(Eq 4.70)* as:

$$p_R = p_{dat} + \frac{1}{2}\rho u_{dat}^2 \left\{\frac{3}{2} - q_j^2 \left(\frac{\psi_j}{\xi}\right)^2\right\} \tag{4.73}$$

Upon simplifying and solving for ξ

$$\frac{1}{\xi} = 1 + \sqrt{\left\{1 + \frac{1}{\left(q_j \psi_j\right)^2} - \frac{2\cos\left[\frac{3}{4}(\pi - \theta)\right]}{q_j \psi_j}\right\}} \tag{4.74}$$

Hence the coefficient of restriction, which represents the contraction of the fluid vein is a function of the angle between the ducts, the ratio of cross-sectional areas of the ducts and the ratio of mass flow rates of the given duct with the datum duct.

Now we apply the Bernoulli's equation on the control volume E-E-R'-R

$$\Delta p = p_j + {}^1/_2\,\rho u_j^2 - \left(p_R + {}^1/_2\,\rho u_R^2\right) \tag{4.75}$$

The conservation of momentum for the given control volume can be written:

$$p_R F_j - p_j F_j = \dot{m}_j u_j - \dot{m}_j u_R \tag{4.76}$$

Writing the expression for K_j & Δp and in terms of q_j & ψ_j

$$\Delta p = \frac{1}{2}\rho\, u_{dat}^2\, q_j^2\, \psi_j^2 \left\{1 - \frac{1}{\xi}\right\}^2 \tag{4.77}$$

$$K_j = \frac{\Delta p}{{}^1/_2\,\rho u_{dat}^2} = q_j^2 \psi_j^2 \left\{1 - \frac{1}{\xi}\right\}^2 \tag{4.78}$$

From the above expression of K_j we can eliminate ξ using the *Eq (4.74)*, therefore:

$$K_j = \left(q_j \psi_j\right)^2 + 1 - 2 q_j \psi_j \cos\left[\frac{3}{4}(\pi - \theta)\right] \tag{4.79}$$

We already established a relation between the total pressure loss coefficient K_j & loss coefficient Cj (*Eq 4.65)*, Hence

$$C_j = 1 - \frac{1}{q_j \psi_j}\cos\left[\frac{3}{4}(\pi - \theta)\right] \tag{4.80}$$

Therefore, we can write the final relation of the difference of pressure between the reference duct and the generic duct 'j' under consideration and express a general relation that can be used to predict the pressure loss for any branch in a multipipe junction using *Eq (4.64) & Eq (4.80)* as below:

$$p_{dat} - p_j = C_{j(}\rho u_j^2) = \rho\, u_j^2 - \rho\, u_{dat}\, u_j\, \cos\left[\frac{3}{4}(\pi - \theta)\right] \tag{4.81}$$

Hence the pressure difference between the different branches of the junction of N ducts depends on the fluid velocity & loss coefficient which in turn depends on the cross-sectional area, mass flow ratios and the angle between the ducts.

- **Geometric data to Gasdyn:**

The Gasdyn simulation software is based on the Gasdynpre which is the preprocessor for the Gasdyn simulation codes. The preprocessor has an interface where the engine scheme can be presented and seen graphically in a two-dimensional window, with all the elements of engine included that can be selected, modified and their characteristics and parameters can be defined.

The pressure loss junction as opposed to the constant pressure junction requires some additional information in GasdynPre. The additional information includes inserting the angles for the branches. For the multipipe junctions, there are two distinct options in Gasdyn for the representation of these junctions. These were already described and represented by the Figure 4.12. The two separate junction types called the supplier or collector are the requirement for the Bingham-Blair model. However, the Winterbone-Bassett model does not need such requirements but still these two distinct configurations were included in the Gasdynpre.

Figure 4.17 is the sample of how we can select the relative geometric angles of the branched ducts in GasdynPre. So, we have to compile a junction in such a way that the relative angle for the branches must be inserted.

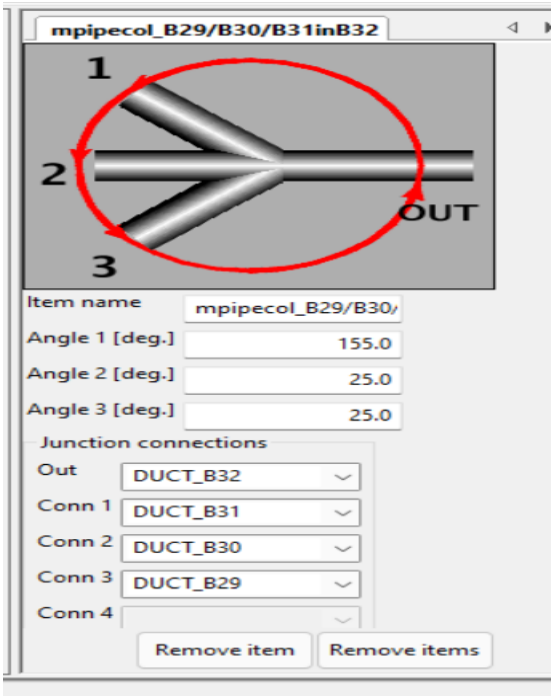

Figure 4.17: Sample for the selection of geometric angle in GasdynPre for collector junction

For a junction based on the configuration of supplier type junction where main branch splits the flow in lateral branches, the 2-D planar configuration is adopted and the junction is seen to be a flat junction, while for a junction based on the configuration of collector which means it joins several branches to the main branch, the junction is not realized in the planar form but in a cone with the main duct at the vertex. The branched ducts see the main duct at certain angle which is equal to the half of the opening angle of the cone θ_{cono} while the angle between them is given by θ_{delta}. The development of the cone is made with two input angles which are also required by the subroutines that solves the junction boundary conditions. The Figure 4.18 below elaborates how the angles are defined for the collector type junction forming a cone

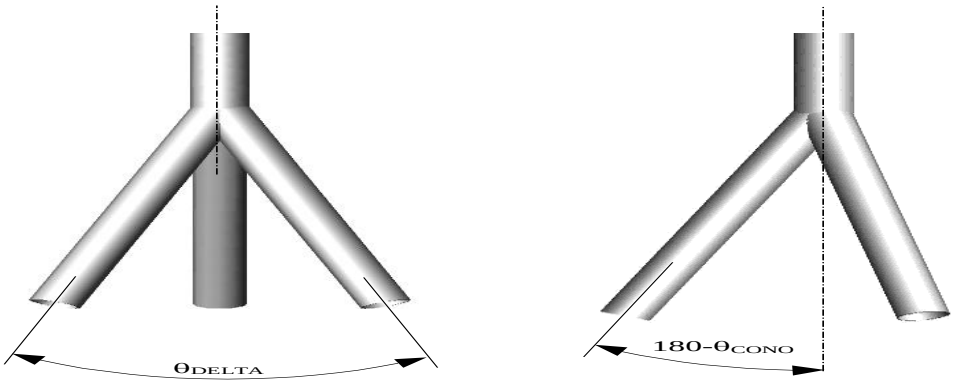

Figure 4.18: Reference angle for collector junctions for Gasdyn Pre

4.2.7 Comparison with the constant pressure model

The pressure loss model is obviously more robust and accurate for solving junction type which are rather geometrically complex which include having wide variation in cross sectional areas and mass flow ratios as well as having large angle between the ducts. In this section we compare the simulation results for two different engine scheme having complex junctions. The graphical results of the instantaneous properties against crank angle are plotted with the application of pressure loss model and constant pressure model-based subroutines on the same junctions. This analysis will provide a clear picture of the difference between the results obtained with both the models.

The first Gasdyn project for the comparison of results is a Lamborghini V-10 engine, whose configuration is represented by Figure 4.19.

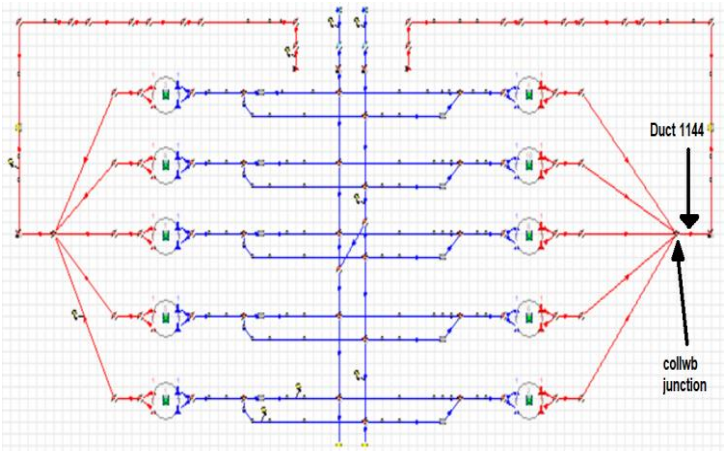

Figure 4.19: Gasdyn configuration of Lamborghini V-10 engine

The engine configuration has a 'collwb' type junction which is basically a collector junction where the supply from five ducts is collected into one duct, the duct that collects all other flows (the collector duct) is duct-1144. Both the collwb junction and the collector duct are highlighted in the Figure 4.19 on engine configuration.

The simulation is performed at operating point of 2500 rpm & 100 % Load, and the results of the characteristic properties are obtained on the collector duct which are represented graphically in this section below.

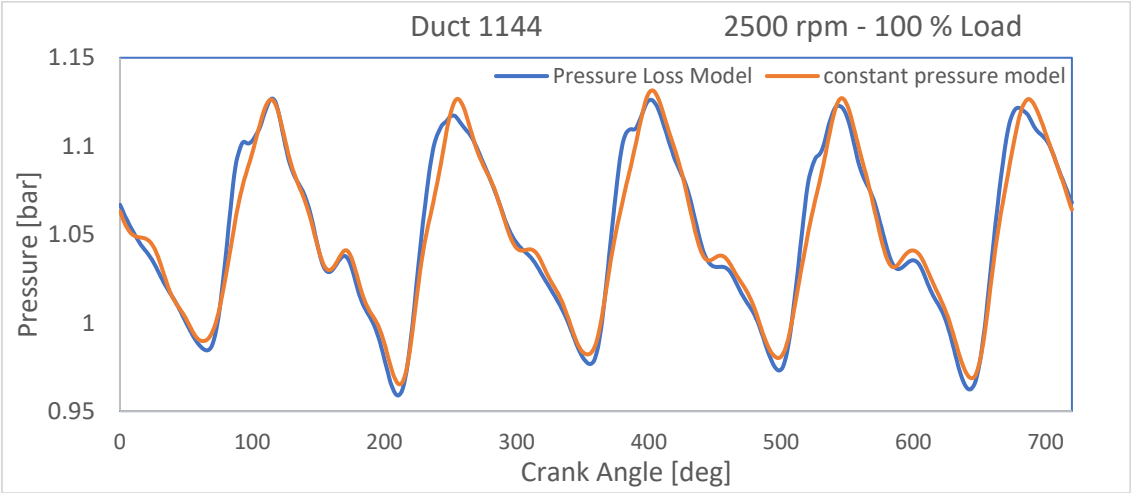

Figure 4.20: Pressure curves for Lamborghini V-10 engine using the constant pressure and pressure Loss model

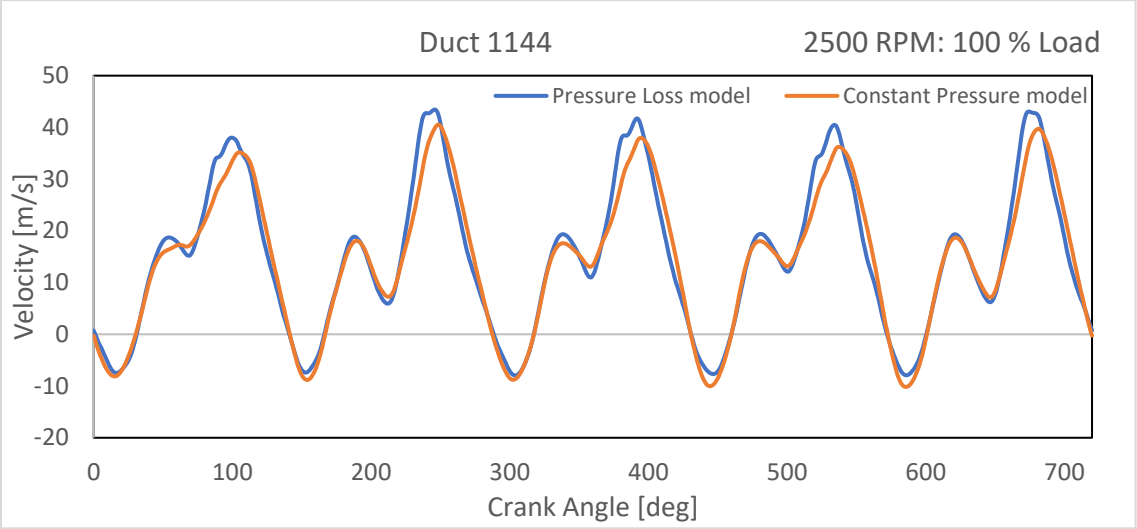

Figure 4.21: Velocity curves for Lamborghini V-10 engine using the constant pressure and pressure Loss model

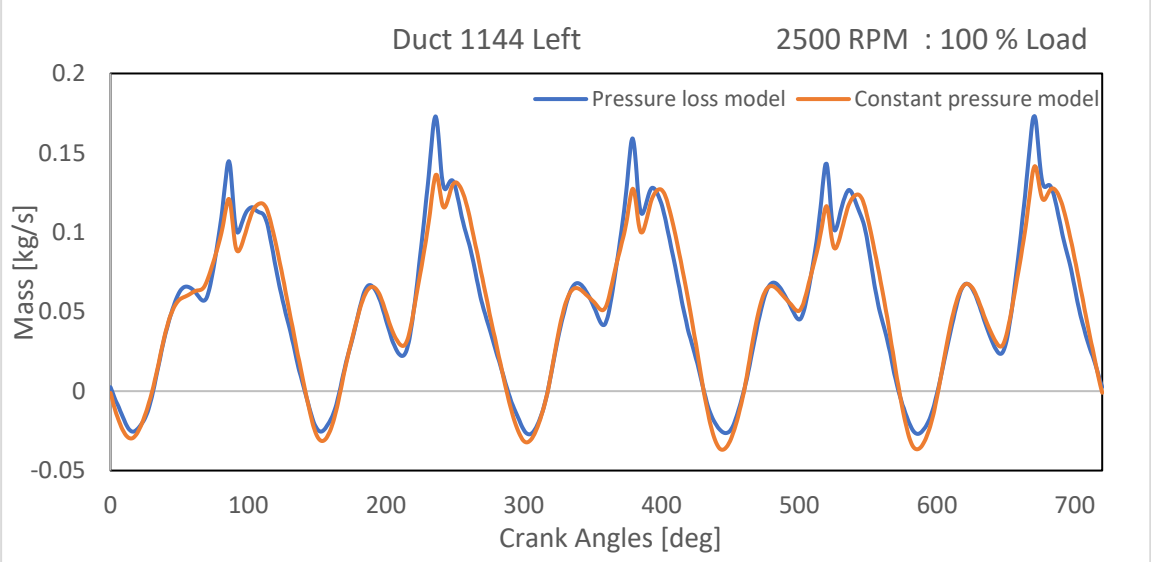

Figure 4.22: Mass flow rate curves for Lamborghini V-10 engine using the constant pressure and pressure Loss model

The next project to be investigated is another Lamborghini engine with 12 cylinders and more complex geometry of junctions. The engine configuration as on Gasdyn is represent by Figure 4.23. The complex junction which is also highlighted can be clearly seen in the engine scheme. The collwb type junction is present with 3 into 1 exhaust. The collector duct is named B-32 on which results are plotted.

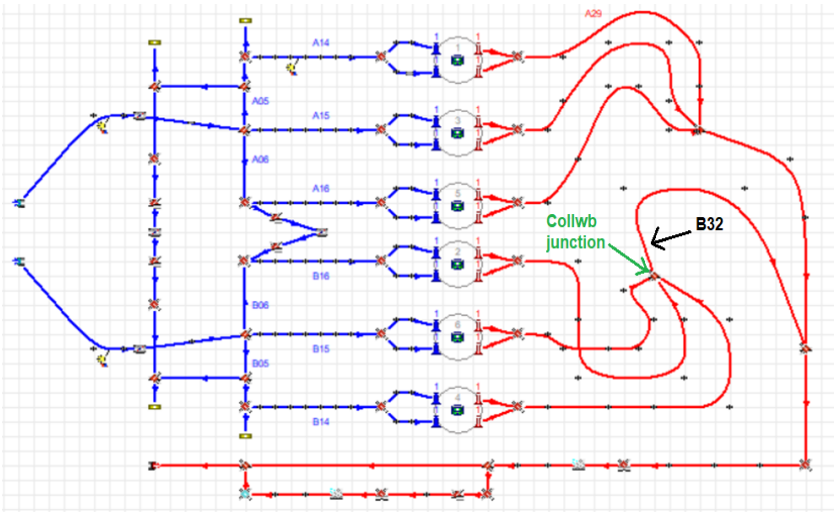

Figure 4.23: Gasdyn configuration of Lamborghini V-12 engine

The engine simulation for this project Lamborghini V-12 is performed at 2000 rpm & 100 % load. The simulation results as obtained for the collector duct using the model for pressure loss and the constant pressure model is represented by the graphs below.

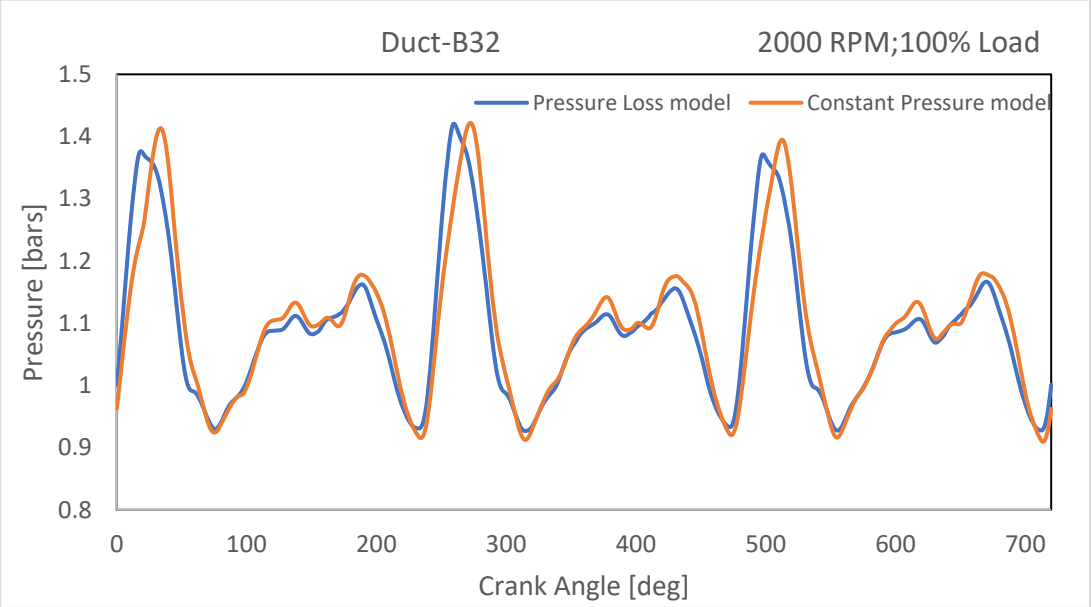

Figure 4.24: Pressure curves for Lamborghini V-12 engine using the constant pressure and pressure Loss model

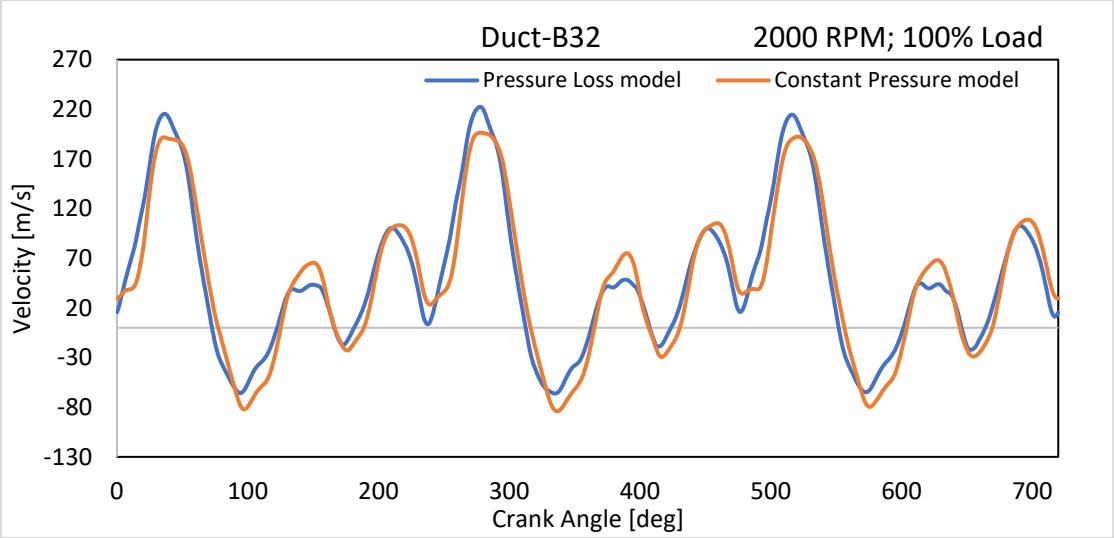

Figure 4.25: Velocity curves for Lamborghini V-12 engine using the constant pressure and pressure Loss model

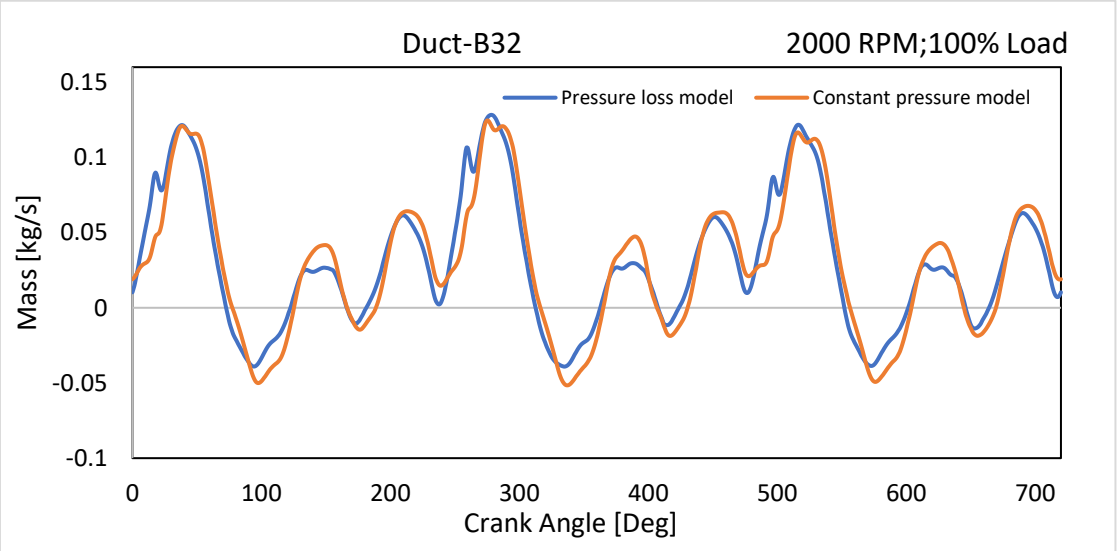

Figure 4.26: Mass flow rate curves for Lamborghini V-12 engine using the constant pressure and pressure Loss model

The above analysis on the Gasdyn Projects Lamborghini V-10 & V-12 engines depicts the comparison of results as produced from the pressure loss model against the constant pressure model. If we look at the pressure curves, we observe that the instantaneous pressure as predicted by the pressure loss model have a lower peak value compared to that predicted by the constant pressure model, this is expected since the pressure loss model takes into account the pressure drops across the junction, while

the constant pressure model assumes that there is zero pressure drop. The velocity of flow and the mass flow rate on the other hand shows a slightly higher peak for the pressure loss model, this is in accordance with the Bernoulli's theorem given that if the pressure is low the velocity is higher, hence the graphical representation for these complex junctions depicts accurately how the different models are applied to the junction solution. One notable outcome from these graphical representations is that even for the so complex junctions the difference of results as produced from both the models is not so large. The graphs from both the models follow the same trend and overlaps at certain points. Although for accuracy the difference cannot be neglected in such cases, but we can say that for junctions which are simpler than the ones being discussed, we may have overlapping curves and same results should be obtained for the characteristic properties. This is the reason that for junctions with not many complexities, the constant pressure model is a good approximation, while in case we have complex geometries of the ducts connected to the junction and accuracy is priority we should prefer pressure loss model

5 Subroutines for different junction types

Gasdyn software utilizes several routines for the computation of the physical properties for the ducts. These subroutines are based on different models used for the computational solution of the conservation equation. The numerical schemes are implemented with these subroutines in the Gasdyn software.

In this chapter we are going to discuss the different subroutines for the pipe junction solutions. The numerical code for the solution of the junctions based on constant pressure model is written in Fortran.

5.1 Introduction to Fortran

One of the computer languages which was developed in 20th century and is still in use is Fortran. The word Fortran is used in short for formula translation. It is regarded as a high-level computer language that is utilized by engineers, scientists, researchers for complex and lengthy calculations. Fortran was originally developed in 1950s by John Backus as a common purpose programming language that could be well adopted for scientific or numerical computation. Fortran has libraries and compilers that helps the codes to run faster. Efficient codes can be generated with the Fortran program. It is relatively easy to use and learn. The language helps you in writing the code in the manner that is preferable

The language is adaptable and numerous updated versions have been developed since its birth in order to cater the modern era of computation

The numerical methods adopted in order to solve the conversational equations require extensive calculations which are possible but probably too lengthy for manual calculations. Hence a computational program is always a better option for the complex and lengthy calculations. These programs can do extensive calculations in milliseconds and with greater accuracy and can store large amount of data in their library.

The computational program or codes which are used by the Gasdyn software are written and tested on Fortran. These codes are referred to as subroutines.

There are numerous subroutines which together make possible to predict the complete behavior of the engine at different operating points. With the help of these subroutines,

we can analyze any type of engine schemes and can predict at each time step or at all crank angles the characteristic or properties of the engine cycle.

GasdynPre software allows us to develop engine scheme according to our requirements as well as modify the existing engine models using the interface. We can select components and their characteristics in Gasdyn and design the engine accordingly. It is also possible to perform different engine design for tests using Gasdyn Pre. It has a user-friendly interface where we can add the components to the engine configuration or build an engine, define the parameters and type of components in detail. After the configuration of the engine is finalized, we can generate the input files for the desired operating points in order to run the engine solution using the Fortran program's computational codes or subroutines. The input parameters required by the code is present in the compiled input file as generated by GasdynPre.

5.2 Subroutines

As mentioned before that there are multiple subroutines used for the engine simulation by Gasdyn, for several purposes including combustion calculation, turbocharging, cylinder pressure, mass flow rates, velocities, temperatures at different time steps etc. However, the scope of this thesis is to consider and discuss the subroutines used by Gasdyn for the solution around the duct junctions. Hence, we will discuss computational codes used for solving different duct junction types.

As defined in the previous chapters, the solution criteria for the junctions in the engine scheme are categorized mainly by two different type of procedures that use different approaches to produce a solution. Hence the subroutines for junction type are also based on the two approaches and can be classified into following two types:

- Subroutines for constant pressure junction models
- Subroutine for junction pressure loss models

The first type of subroutines is based on Benson's theory and modelling of constant pressure junction and solves the junction boundaries assuming that the static pressure at the ends of the ducts connected to the junction are equal such that:

$$p_1 = p_2 = p_3 = \cdots = p_n$$

These types of subroutines are applied to those junctions where the geometrical characteristics are not very complex with minor angle between the ducts and low difference in cross sectional areas as specified by the Benson's model in his hypothesis.

The subroutines based on the constant pressure junction approach can be used for the solution of the following junction types:

- Multipipe junction
- Catalyst Junction
- Intercooler Junction
- Perforates Junction

For each of the junction types there was a separate subroutine that Gasdyn utilizes for the solution. Following are the subroutines written in Fortran being utilized by Gasdyn for the engine simulation

1) CPMBEN (Subroutine for n-pipes)
2) CPMCAT (Subroutine for catalyst junction)
3) CPMDUC (Subroutine for Intercooler junction)
4) CPMFOR (Subroutine for Perforates)

However, as the most important part of this thesis work, the development of a subroutine which alone is sufficient to solve each of the above junctions was performed. This subroutine which can be said a general subroutine for all the junction types based on Benson's constant pressure model is named subroutine bccpmben. We will discuss later in the chapter in detail, about how the subroutine 'bccpmben' was created and how it is implemented on different engine schemes and compare the results of this subroutine with the previously used subroutines to verify the accuracy of the new subroutine. Let us first discuss the old subroutine being used in Gasdyn software.

5.2.1 Subroutine CPMBEN for N-ducts junction

The first type of subroutine which is used for the solution of n number of ducts connected to the junction with no pressure drop is the CPMBEN, it is based on the Benson's model and the simplest of all routines. This subroutine is implemented and called when certain number of ducts are connected to a junction and the geometrical characteristics of the ducts are not very different from each other. In simple words this subroutine is used for the not so complex junction types. For the complex junctions, Gasdyn has a separate junction type and corresponding subroutine which solves the boundary condition for those type of junctions including the pressure drop across the junction

Since we are talking about the subroutine CPMBEN, we should discuss how it is applied to the junction.

In the Figure 5.1, the type of junction to be selected for use in the subroutine under discussion is highlighted

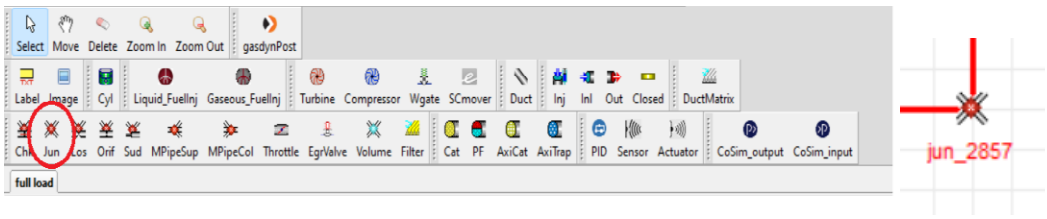

Figure 5.1: The Junction type for subroutine CPMBEN in GasdynPre

The subroutine CPMBEN when called in the main program for the solution of this type of junction requires some prerequisites calculation. Hence some variables are needed to be calculated before calling of this subroutine. These variables are calculated in the main program and used as input variables for the subroutine CPMBEN. The variables to be called before the implementation of CPMBEN are the Riemann variables for each duct, the entropy levels, cross sectional area of the ducts and number of ducts.

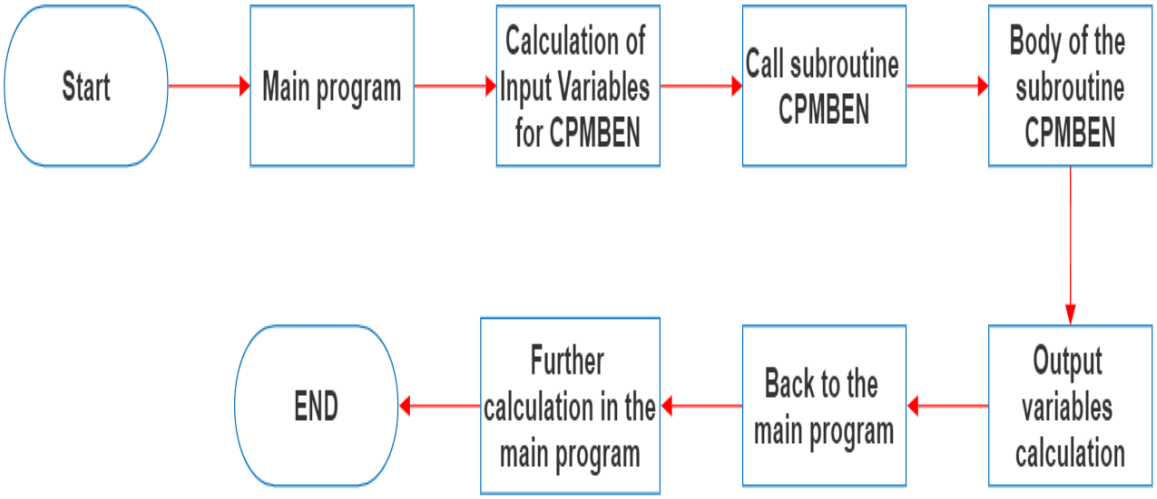

Figure 5.2: Process flow diagram for the implementation of the subroutine CPMBEN

A generalized description of the pattern on how the subroutine CPMBEN works is mentioned in the above process flow as shown in Figure 5.2. As the first step the subroutine takes these inputs, perform calculations inside the body of the subroutine which include iterative convergence of A* and then update the input variables to

supply as the output to the main program where further calculations are performed with those variables. Thus, the subroutine is dependent on the main program not only for the calculation of input variables but also after producing the output variables. This is not the case with the subroutine bccpmben that was developed during the thesis work as it does all the calculations for input and output variables inside the body of the subroutine itself. A dedicated and detailed section explaining the new developed subroutine is discussed later in this chapter.

The generalized flow chart of the subroutine as used in the Gasdyn simulation is presented in the Figure 5.3

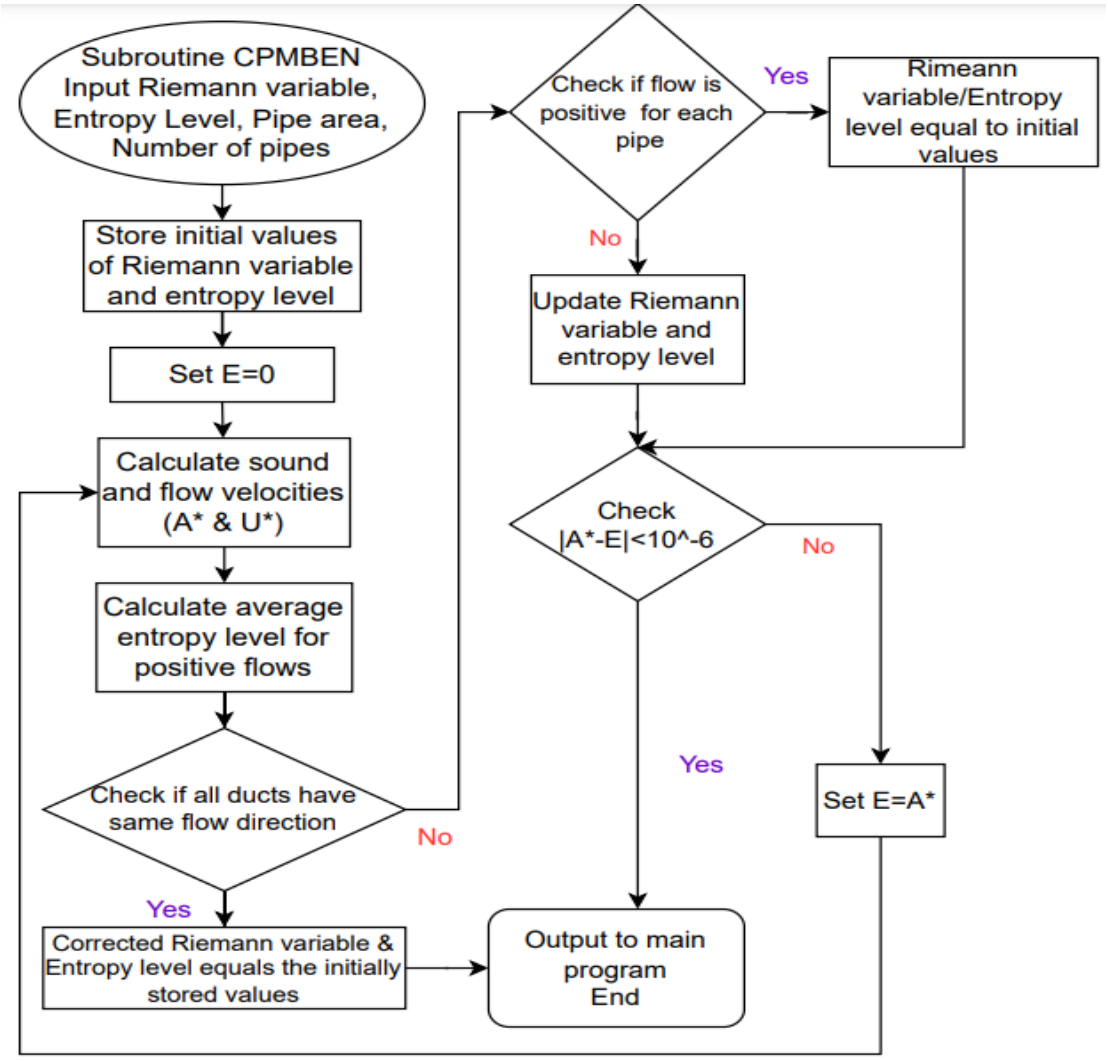

Figure 5.3: Generalized Flow chart for subroutine CPMBEN

An example of the results produced by this subroutine CPMBEN is shown in Figure 5.4, where a six-cylinder turbocharged engine was studied. The engine scheme is summarized below:

General Data of the Project

33 exhaust pipes

30 intake pipes

45 junctions

23 CPMBEN type junction

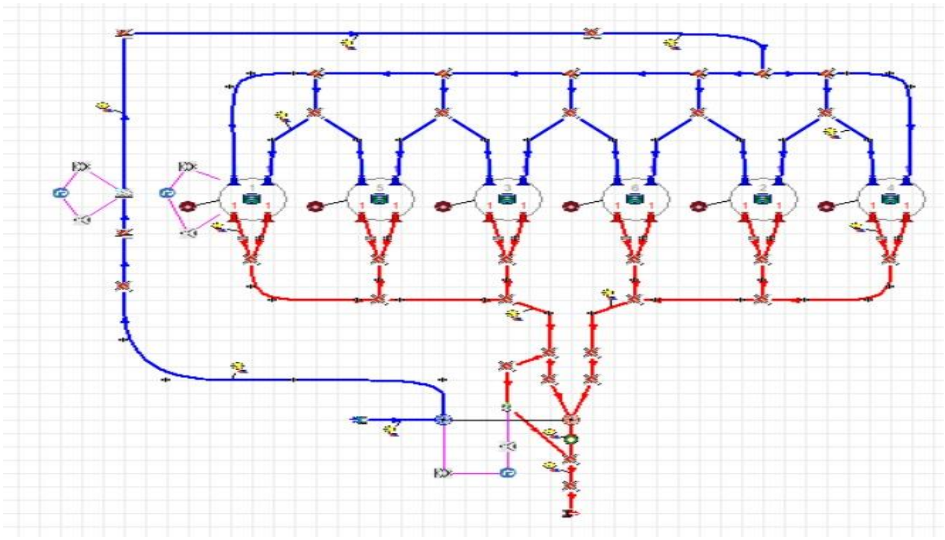

Figure 5.4: Engine configuration with CPMBEN Junctions – Project six-cylinder turbocharged engine

Since the scheme contains many junctions of the type being discussed therefore the project is a good test for the subroutine CPMBEN, we analyzed results on the several ducts in order to predict the behavior of engine with the help of simulation and observed the instantaneous properties of the ducts at various points.

The results for the engine instantaneous properties for the exhaust duct throughout the engine cycle of the first cylinder is represented in the graphs in Figure 5.5-Figure 5.7. The engine operating point for the graph plotting of instantaneous properties is selected as 2500 rpm & 100 % Load.

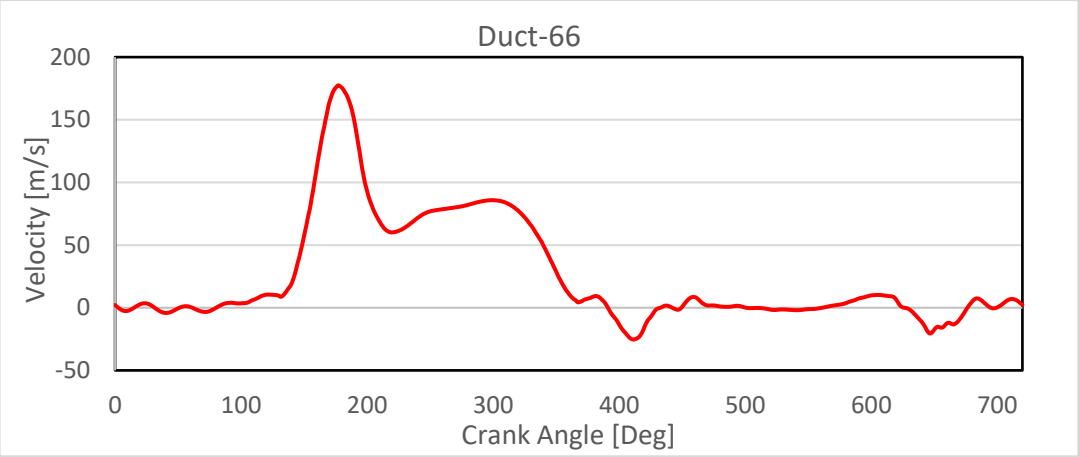

Figure 5.5: Instantaneous velocity for a duct using subroutine CPMBEN

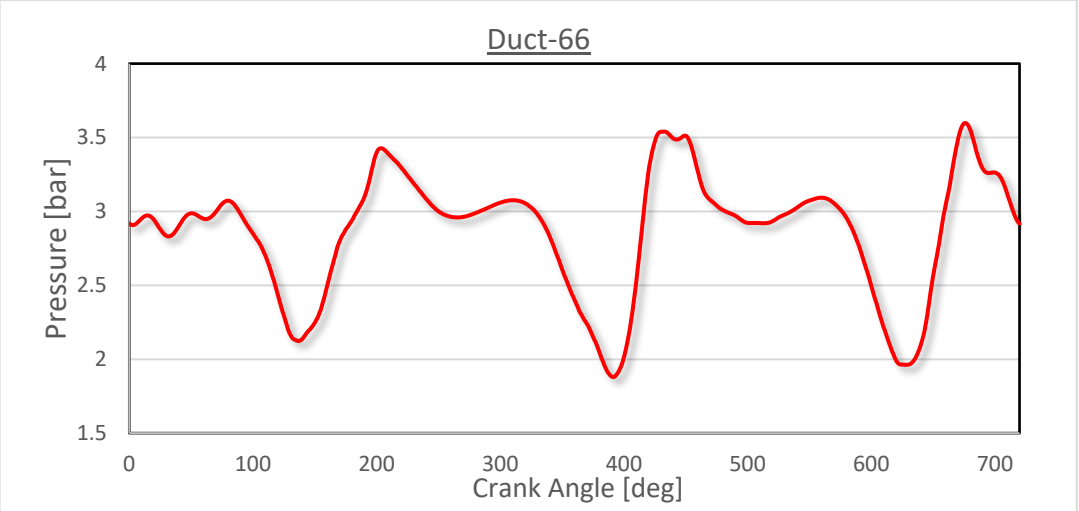

Figure 5.6 : Instantaneous pressure for a duct using subroutine CPMBEN

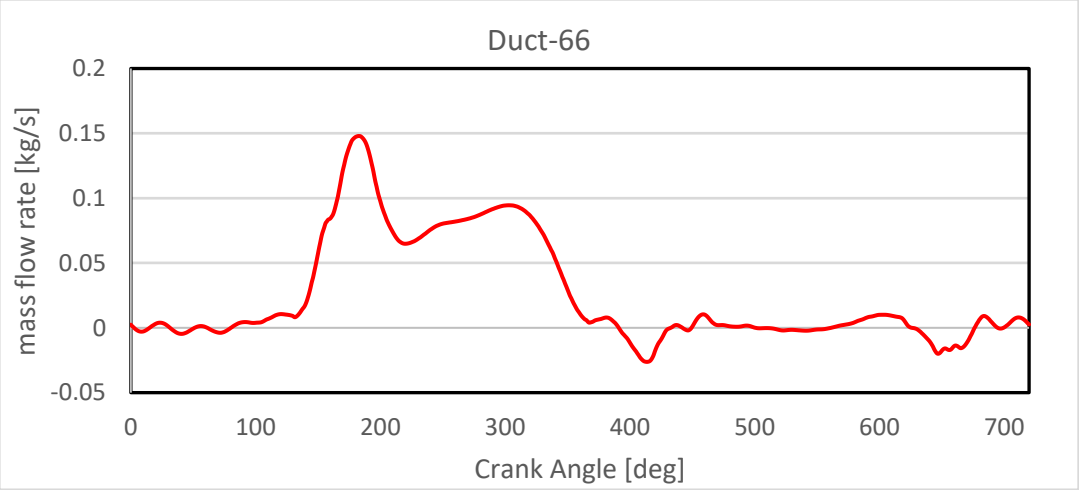

Figure 5.7 : Instantaneous mass flow rate for a duct using subroutine CPMBEN

5.2.2 Subroutine CPMCAT for Catalyst Junction

The second type of subroutine based on the constant pressure junction model by Benson is the subroutine CPMCAT. This subroutine is used when we have a catalyst connected to one end of the junction.

Figure 5.8 below highlights the tab used to select the catalyst option in the GasdynPre software.

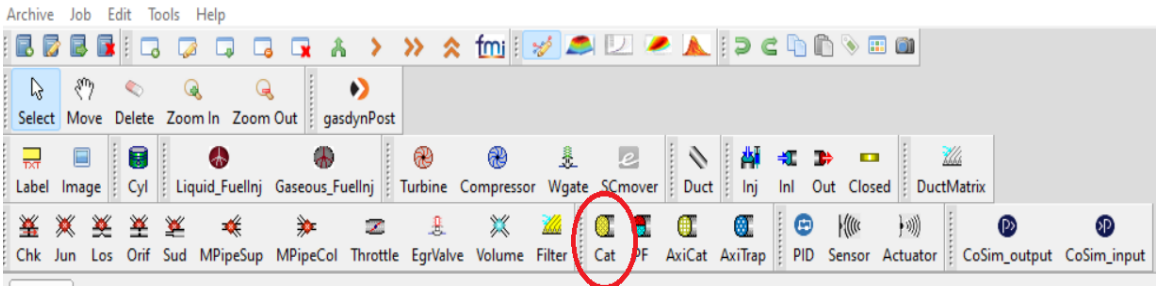

Figure 5.8: Selection of Catalyst in Gasdyn Pre

After the catalyst has been added in the exhaust portion of the engine configuration, Gasdyn pre allows us to completely define the characteristics of the catalyst including the geometric data, roughness, wash coat and substrate data in detail as per the required engine scheme.

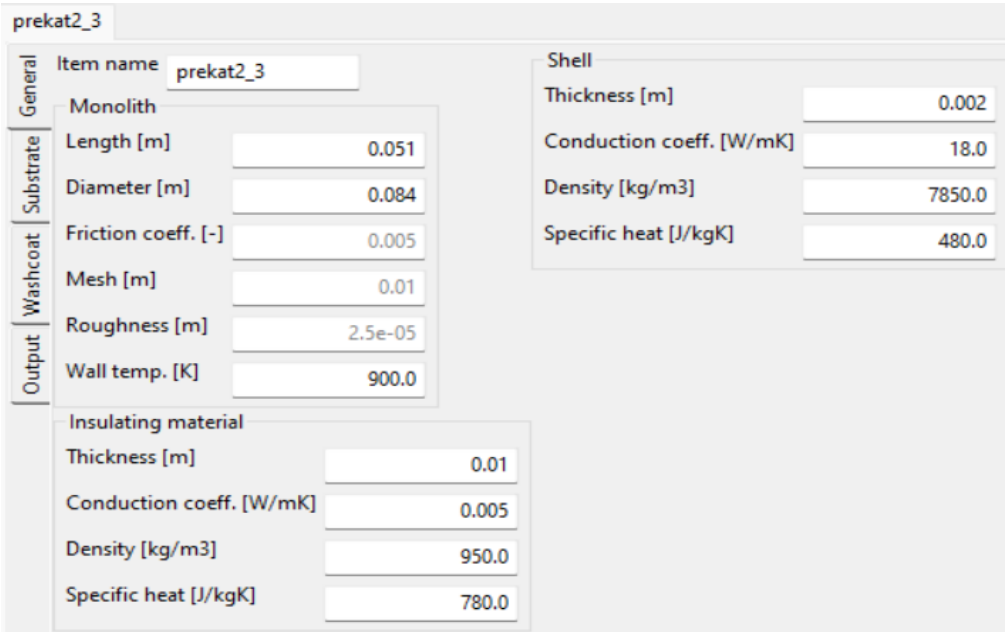

Figure 5.9: Catalyst Properties as inserted in GasdynPre

Similar to the CPMBEN subroutine, the CPMCAT also works in the same process, that means it is called in the main program and requires some input parameters to be calculated before the calling of the subroutine, once the required parameters are calculated in the main program the subroutine CPMCAT is called with the parameters as input variables, does the calculation of A*, Riemann variables and the entropy levels within the body of the subroutine and return these values corrected to the main program where further calculations are performed. So, the process flow diagram of this subroutine is the same as the process flow diagram of CPMBEN with the difference that the subroutine CPMCAT is used to solve a junction connected with two pipes, one of which is a catalyst mesh with multiple pipes in parallel

The general flow diagram of the subroutine is shown by the Figure 5.10

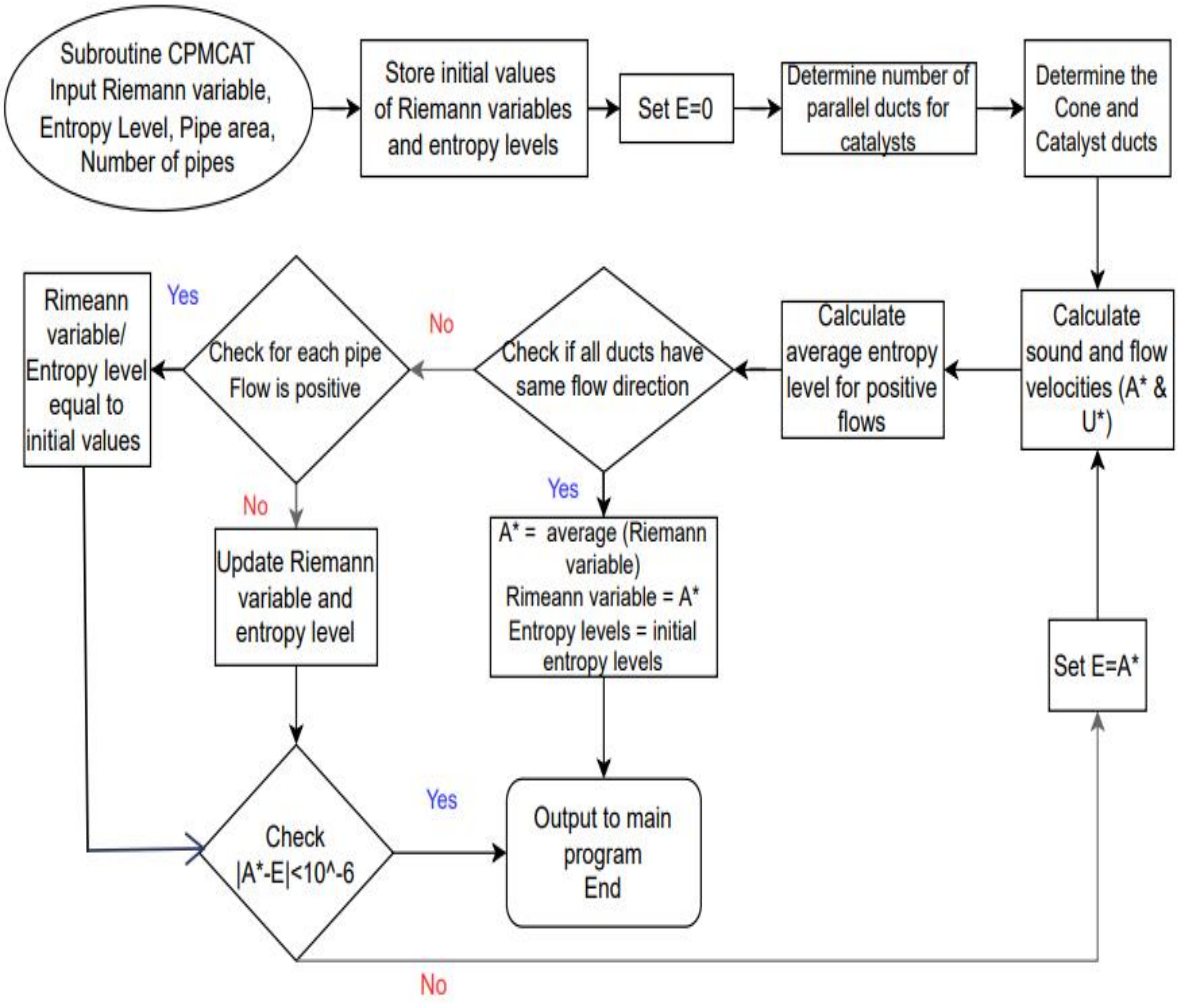

Figure 5.10: Generalized Flow chart for subroutine CPMCAT

An example of the project with a catalyst junction where the subroutine CPMCAT is applied for the solution of boundary conditions is represented by configuration in Figure 5.11. The engine scheme for the project named HRR10DDTG is summarized as below:

23 exhaust pipes
33 intake pipes
48 junctions
01 Catalyst Junction
01 Air Intercooler

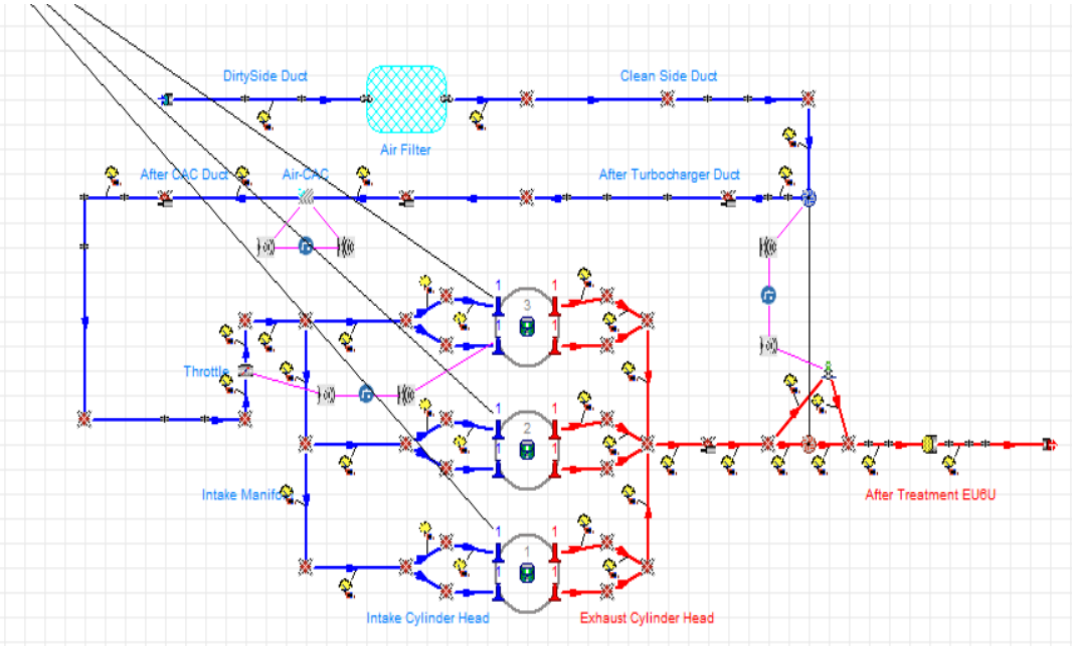

Figure 5.11: Engine configuration with Junction CPMCAT –Project: HR10DDTG

The results after the engine simulation were performed implementing the subroutine are represented by the graphs in Figure 5.12 - Figure 5.14. The instantaneous values of the characteristic properties are plotted against the crank angles for the duct connected to the catalyst junction.

The engine operating point for the graph plotting of instantaneous properties is selected as 2000 rpm & 100 % Load

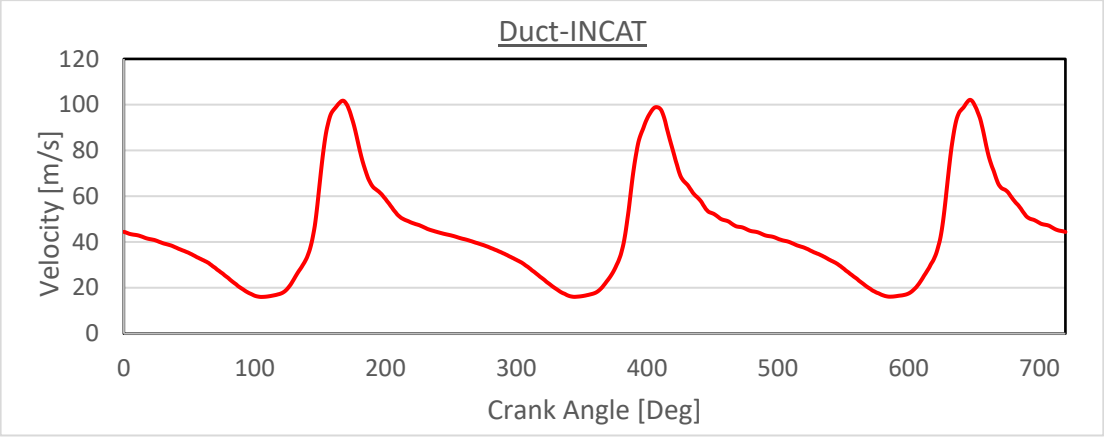

Figure 5.12: Instantaneous velocity for duct inlet-catalyst using subroutine CPMCAT

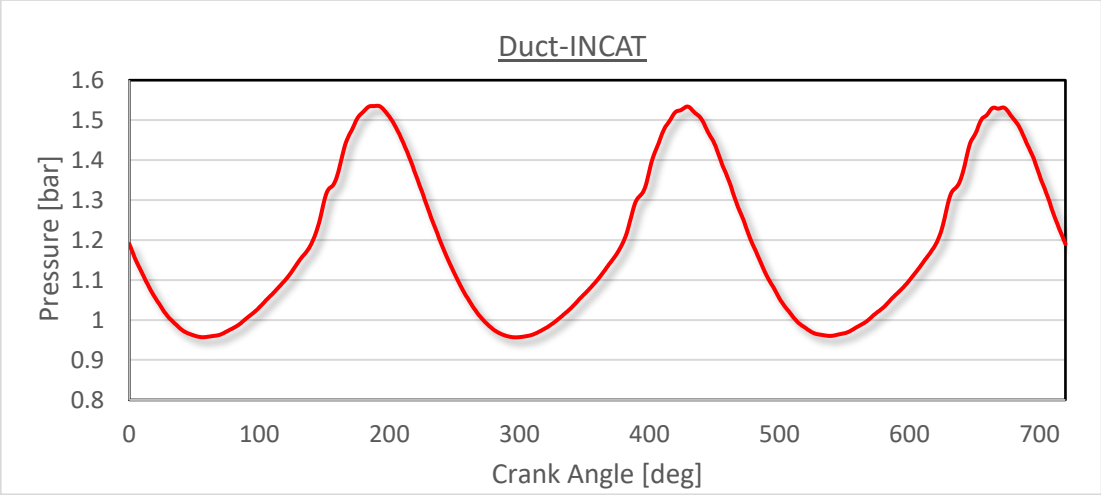

Figure 5.13 Instantaneous pressure for duct inlet-catalyst using subroutine CPMCAT

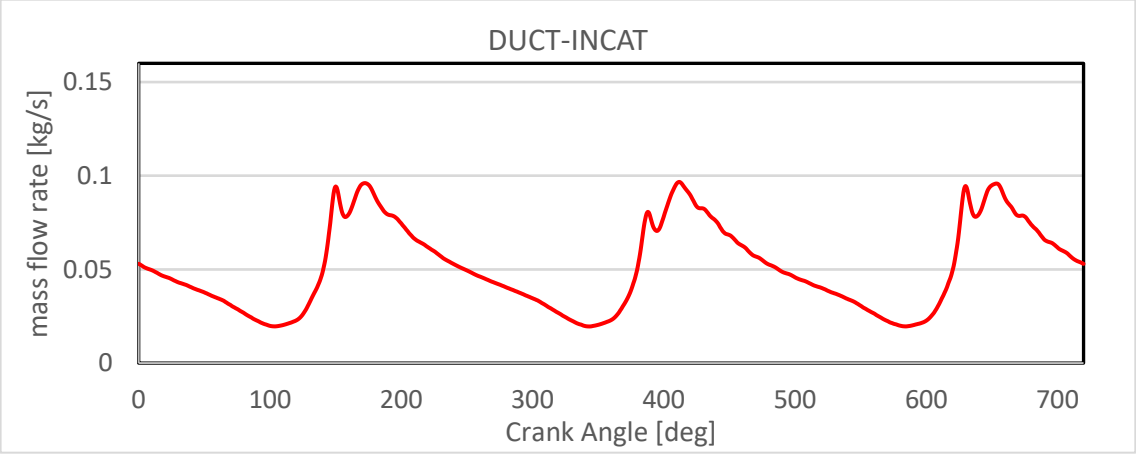

Figure 5.14 :Instantaneous mass flow rate for duct inlet-catalyst using subroutine CPMCAT

5.2.3 Subroutine CPMDUC for Intercooler Junction

The process diagram for the subroutine CPMDUC follows the same path as for the subroutine CPMCAT. In addition to this, the flow chart is the same as well. The only difference for the subroutines for intercooler and that for the catalyst is that in the subroutine for catalyst junction, the number of parallel pipes that are accounted for in are for the catalyst while for the intercooler junction the number of parallel pipes are taken as present in the intercooler. Rest of the subroutine has the same process flow chart and follows the same path. In fact, the subroutine for the catalyst can also be used for the intercooler junction. Hence it is not required to repeat in detail the working procedure of this subroutine.

An intercooler is mostly used in turbocharged engine where the air is compressed and is required to be cooled in the intercooler before entering the cylinder. An example of the intercooler in an engine configuration can be seen in the Figure 5.15. The project is named HRDD10TG, the summary of the project is mentioned already.

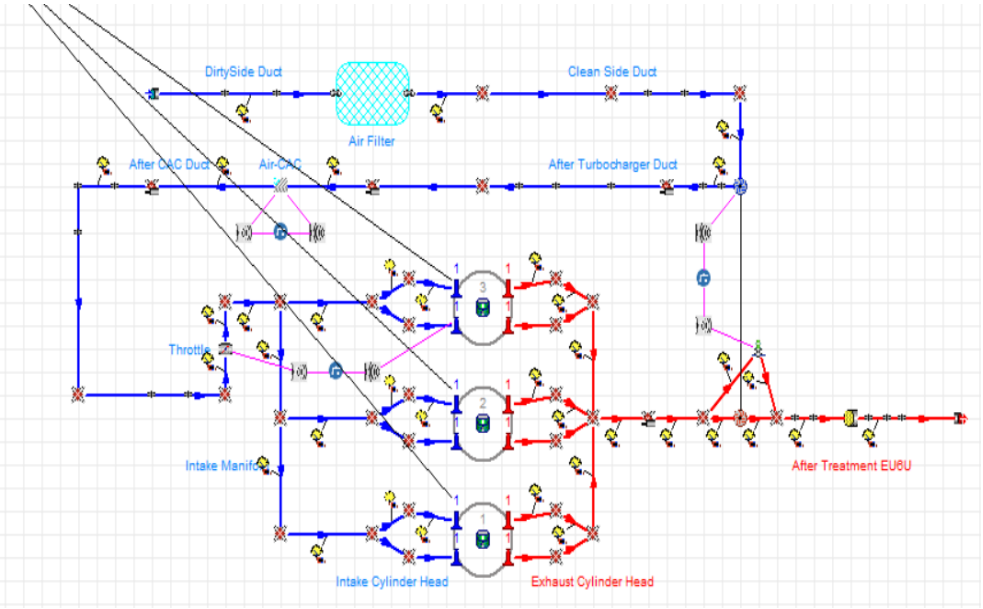

Figure 5.15: Engine configuration with Intercooler –Project: HR10DDTG

The engine simulation was performed for the above-mentioned engine configuration and results were analyzed on the duct connected after the Intercooler. Figure 5.16-Figure 5.18 are the graphical results for the instantaneous values of the characteristic properties .

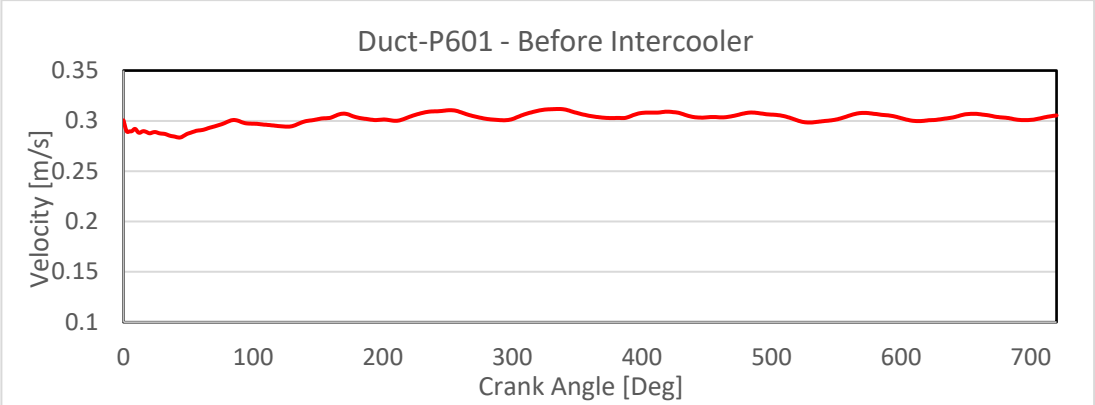

Figure 5.16: Instantaneous velocity for duct connected to Intercooler using subroutine CPMDUC

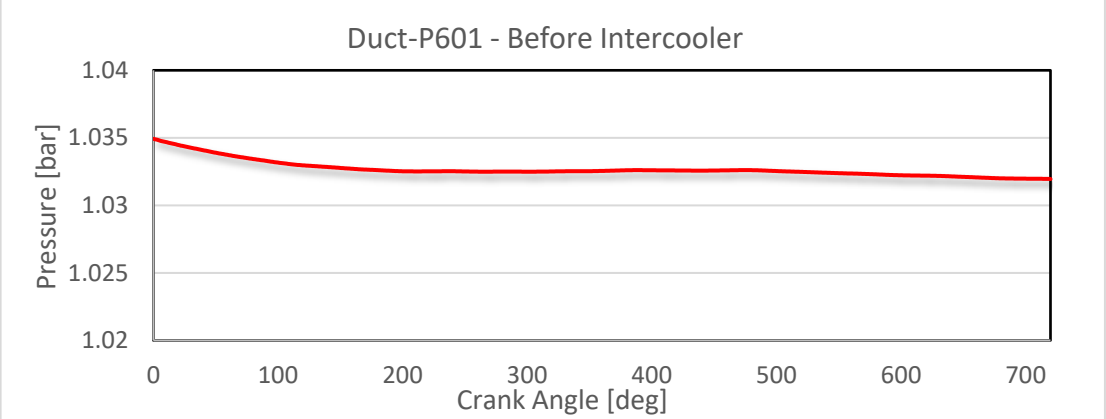

Figure 5.17: Instantaneous pressure for the duct connected to the Intercooler using subroutine CPMDUC

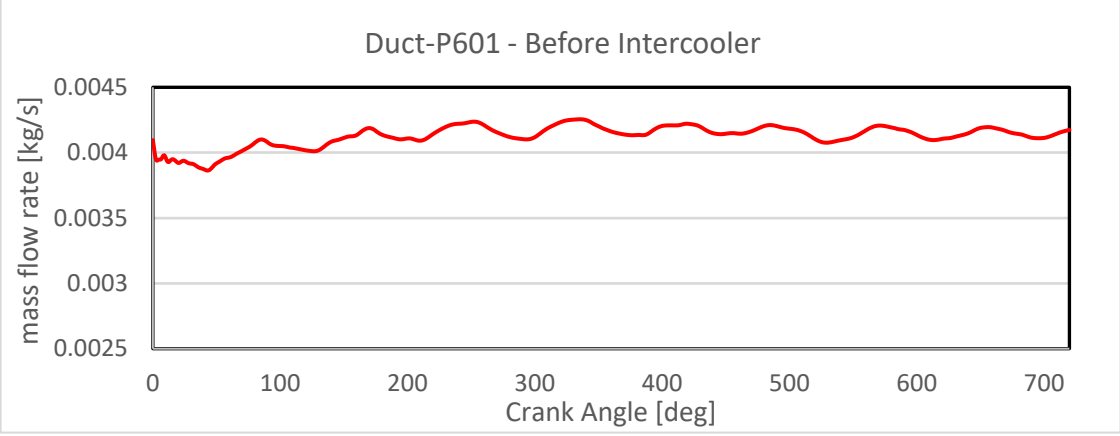

Figure 5.18: Instantaneous mass flow rate for the duct connected to the Intercooler using subroutine CPMDUC

The engine operating point for the Figure 5.16-Figure 5.18 is 2000 rpm & 100 % Load

5.2.4 Subroutine CPMFOR for perforates junction

The subroutine CPMFOR is another constant pressure model-based subroutines. The subroutine is used for the solution of junction connected to a silencer or perforated ducts. It works in the same manner as of other subroutines based on the constant pressure junction model. It means that similar to the subroutine for n pipes, catalyst & intercooler, this subroutine is also called in the main program where inputs for this subroutine are calculated prior to the calling of the subroutine and then in the body of the subroutine, some variables are calculated and sent to the main program for further calculations.

So, the process flow for CPMFOR is the same as of the other subroutines. As far as the body of this subroutine is concerned. The below flow chart in Figure 5.19 explain in general about the working of the subroutine.

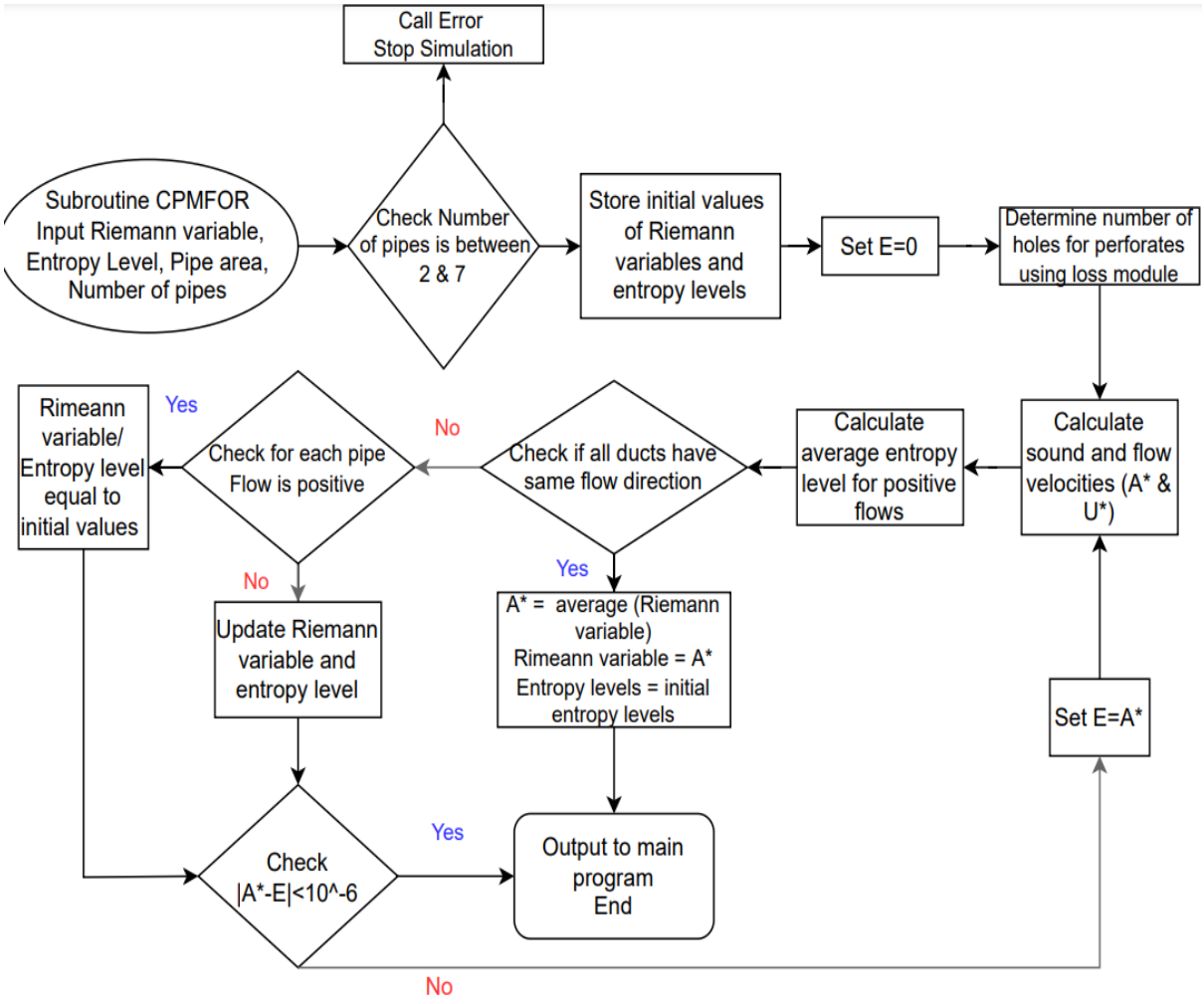

Figure 5.19: Generalized Flow chart for subroutine CPMFOR

An example of the project with the perforated duct in GasdynPre is represented by Figure 5.20. We have applied the subroutine CPMFOR on the same and plotted the instantaneous properties against the crank angle.

The project summary is as follows:

61 exhaust pipes

52 intake pipes

88 junctions

1 silencer

1 Filter

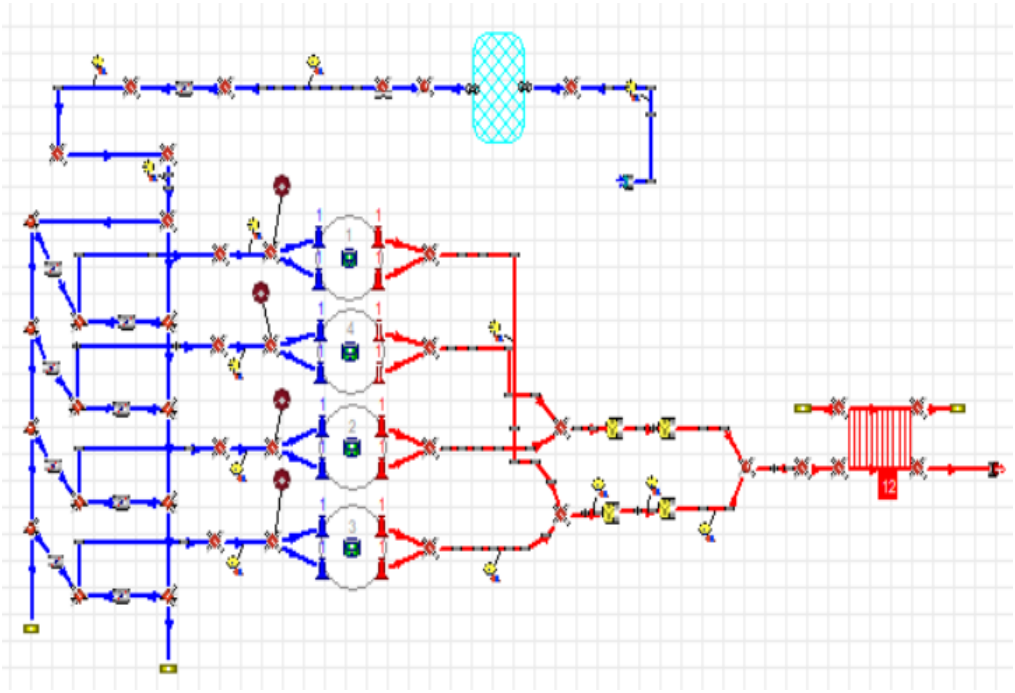

Figure 5.20: Engine configuration with Perforated ducts – Project 2.0_16V

The results of the instantaneous parameters against crank angle after the implementation of the subroutine CPMFOR are represented graphically by Figure 5.21 - Figure 5.23. The results are calculated for the duct-453 connected after the silencer.

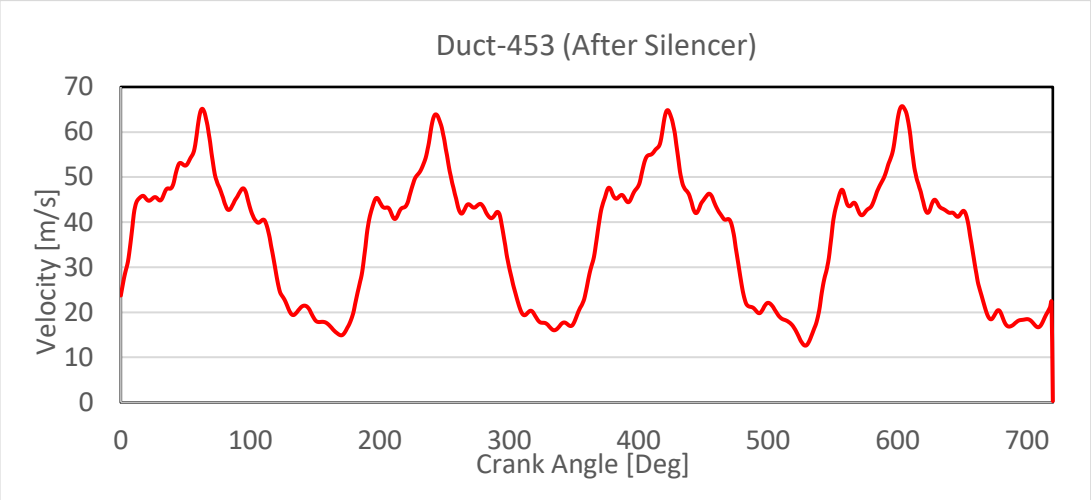

Figure 5.21:: Instantaneous velocity for the duct connected to the Silencer using subroutine CPMFOR

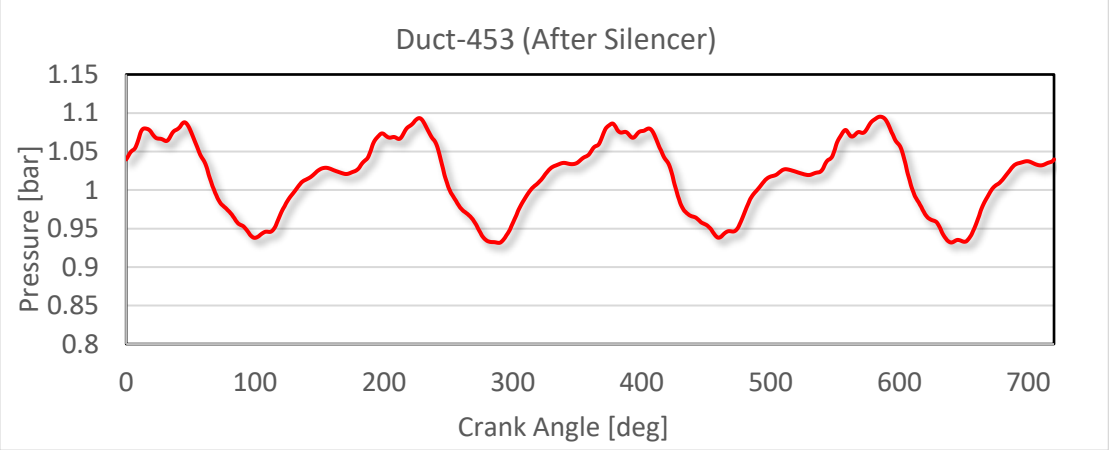

Figure 5.22:: Instantaneous pressure for the duct connected to the Silencer using subroutine CPMFOR

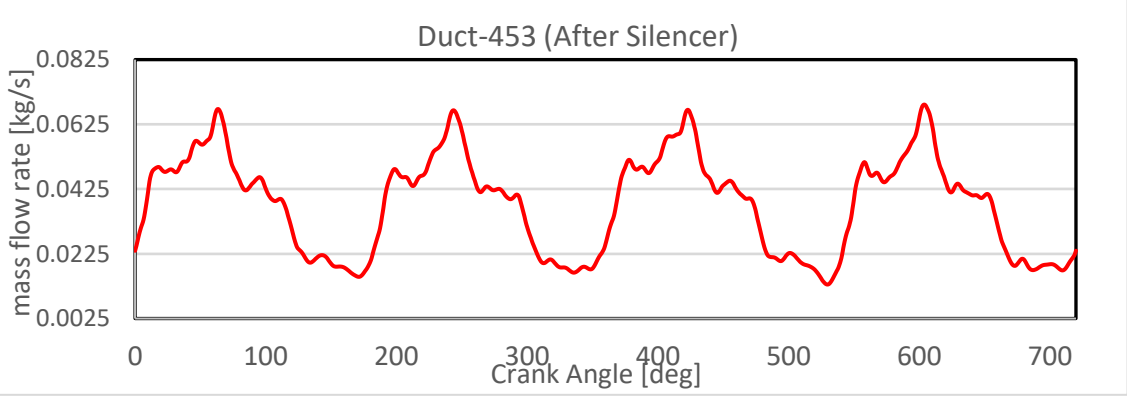

Figure 5.23: Instantaneous pressure for the duct connected to the Silencer using subroutine CPMFOR

5.3 New subroutine bccpmben

5.3.1 Introduction

We had discussed till now several subroutines based on the constant pressure junction model by Benson. The subroutines discussed include the CPMBEN for the junction of n-pipes, CPMCAT for the catalyst junction, CPMDUC for the Intercooler and CPMFOR for the perforates. All of these subroutines have the same theoretical background.

In this thesis work, the main motive was to get rid of the multiple subroutines for different junction types and make a new subroutine that would substitute or replace all the other subroutines based on the constant pressure theory. Thus, in order to do so and create a general subroutine for this this purpose, we first analyzed all the subroutines of different junction types. All the subroutines were implemented, and engine simulation was performed by using the previous subroutines on different engine configurations to obtain the instantaneous properties of the engine during each crankshaft revolution.

After detailed investigation of the previously implemented subroutines and analysis of the results, it was certain that the theoretical background associated with the subroutines is the same and it is possible to make a more generalized subroutine, that would act as a substitution of the other subroutines for constant pressure junctions.

5.3.2 Need of new subroutine

The need for the creation of the new subroutine arises from the fact that in order to implement any sort of change which could be related to any improvement in accuracy of the engine simulation or may be helpful in predicting better performance, the modification would be required on each of the subroutines based on their body and may require multiple trials for the success of each step of improvement. In addition to the modification requirement in each of the computational codes, it would also require verification of the results from each of the subroutines separately and combining them to check for errors repeatedly. Changing the computational codes of each of the subroutines and verifying results from each is rather time consuming and stressful. And thus, if a general subroutine is created for all , it would be an easier task to manage the different junction types. In addition to this, we will not have to test results from each and then combine the results for detailed analysis but instead a

single subroutine will be called for the perforates, catalysts , npipes and the intercooler. Moreover, the previous subroutines showed some instabilities at certain points for some critical configurations which needed to be addressed and resolved by the use of the new subroutine

5.3.3 Development of the subroutine

The development of this general subroutine that would simplify the procedure of implementation of the constant pressure model on the relevant junction types was a complex procedure.

As first task we needed to eliminate the first drawback of the previously used subroutines that was the requirements of several inputs before the calling of the subroutines, and this would not be required in the new subroutine. In fact, the new subroutine would be simple to implement and should work on the minimum number of inputs and should be able to do the simulation and solution based on less inputs from the main program.

The second task was to include in the body of subroutine, relevant codes for the calculation of the variables that were eliminated from the input variables.

The new computational code should be independent and capable to perform all the calculations related to the relevant junctions inside the body of the subroutine itself and that there should be no need to return the output to the main program for further calculations.

Lastly the new subroutine must be capable to work on the difference of criteria in the various subroutines previously used. It should be able to identify the junction type and implement the relevant procedure associated with the particular type for example when the new subroutine is called and the junction type is 'CAT' , then the new code should be capable enough to first identify the junction type and then implement the procedure that was used by the CPMCAT subroutine for the solution of catalyst junction instead of applying the procedure used for the perforates or npipes.

Apart from the inclusion of improvements and simplifications that the new general subroutine should manage, it must also be accurate and robust. Therefore, the results obtained by implementing the subroutine bccpmben should be tested separately in comparison with each of previously used subroutines by substituting the old subroutines at all points in the program where they were called with the bccpmben. This replacement and then comparative analysis should be first performed uniquely for each junction type discussed. In case the results are not accurately similar, the

subroutine code should be adequately revised and modified for improvements until better results were obtained.

After validating results for the replacement of each of the old subroutine separately and performing all checks and modifications, if necessary, the subroutine then should be substituted for all the relevant junction types simultaneously and final scrutiny and comparisons should be performed. The combined and simultaneous substitution of CPMBEN, CPMCAT, CPMDUC, CPMFOR with the new subroutine bccpmben would validate the precise development of the new subroutine.

5.3.4 Body of the subroutine

The subroutine thus created named bccpmben, is the substitution for all the relevant constant pressure model-based duct junctions. The subroutine was developed to follow the unique criteria in order to adopt the correct procedure depending on the junction type by first identifying the junction type and then follow the associated approach related to the junction.

The subroutine takes only one input from the main program that is the number of ducts connected to the junction and then it calculates the other variables necessary inside the body of the subroutine using appropriate commands and the data library. Thus, with number of ducts connected to the junction being the only input, it is able to solve the junction.

The most important step of the new subroutine after the calculation of the other necessary variables for the solution, is the identification of the junction type and setting the multiplier accounting for the parallel ducts in case of catalysts, intercooler, or the holes for perforates. This is performed in the bccpmben by the combination of criteria adopted in each unique subroutine and combining them to set multiplier for each type.

After the relevant calculations performed, the bccpmben generates output for the Riemann variables and the entropy levels in shared form in the program itself and does not need the transfer of outputs to the main program. Hence the solution is performed entirely in the subroutine bccpmben. The flow chart in Figure 5.24 depicts the solution scheme of the subroutine bccpmben

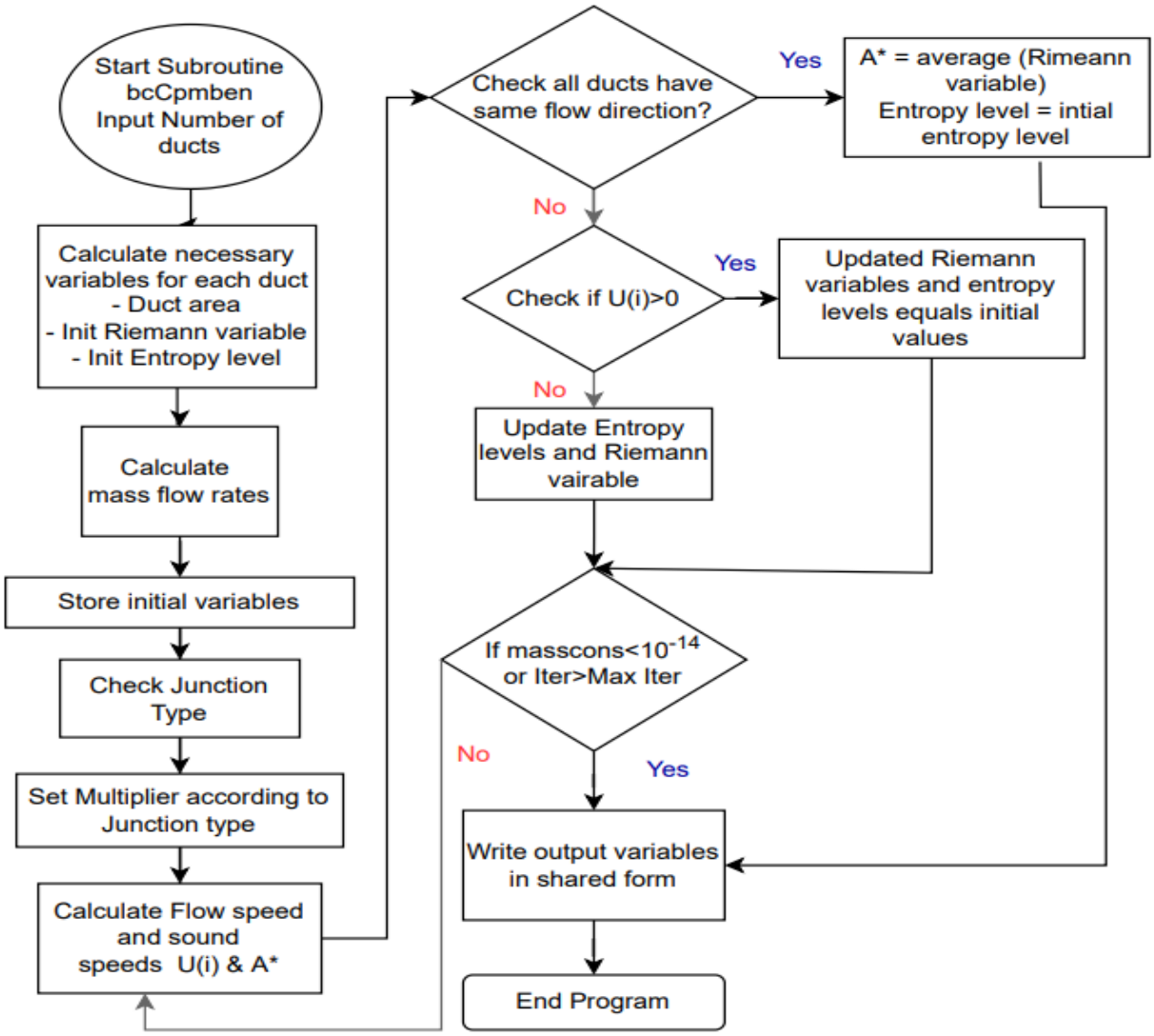

Figure 5.24 : Flow chart for the new subroutine bccpmben

5.3.5 Validation of the new subroutine

5.3.5.1 Substitution of CPMBEN

In order to validate the new created subroutine bccpmben, we had to first start the validation process by substituting step by step one of the old routines by the new subroutine and comparing the results and accuracy of the new subroutine, incorporating any improvements or modifications if needed. Thus, we started by

calling the subroutine bccpmben in the program in all the places where the old subroutine CPMBEN was called. The substitution was performed for various projects and on various ducts so that the results can be accurately verified. In the next paragraph we will discuss one of the projects that was used for the validation of bccpmben in substitution of CPMBEN

The Gasdyn project we discuss here is a six-cylinder turbocharged engine. The engine scheme as in Gasdyn can be seen below, the project has x 23 Nos. of CPMBEN type junctions, hence this was a perfect test for the replacement of the subroutine CPMBEN by bccpmben.

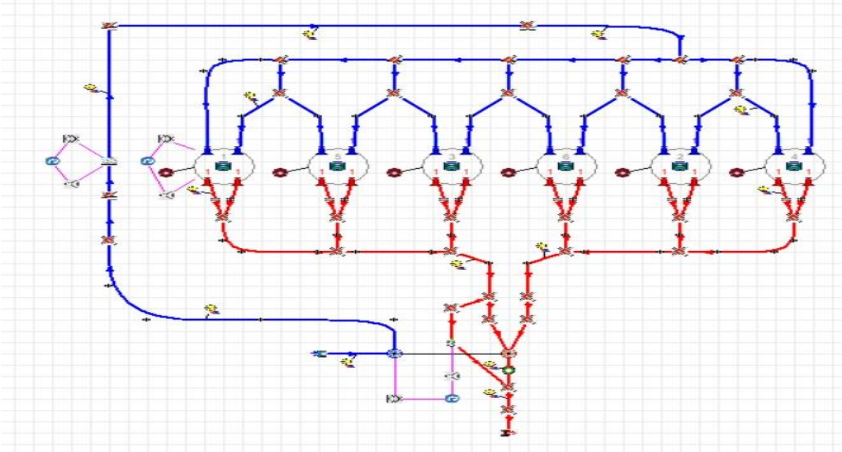

Figure 5.25: Gasdyn configuration for Project 6-cylinder Turbocharged engine

The results as generated by using the old subroutine and the one generated by the new subroutine bccpmben were compared graphically. Plots of temperature, pressure, velocity, mass flow rate were produced to compare the results on different ducts. The graphical results represented here are for the duct-TE, which is located in the exhaust manifold after the turbine.

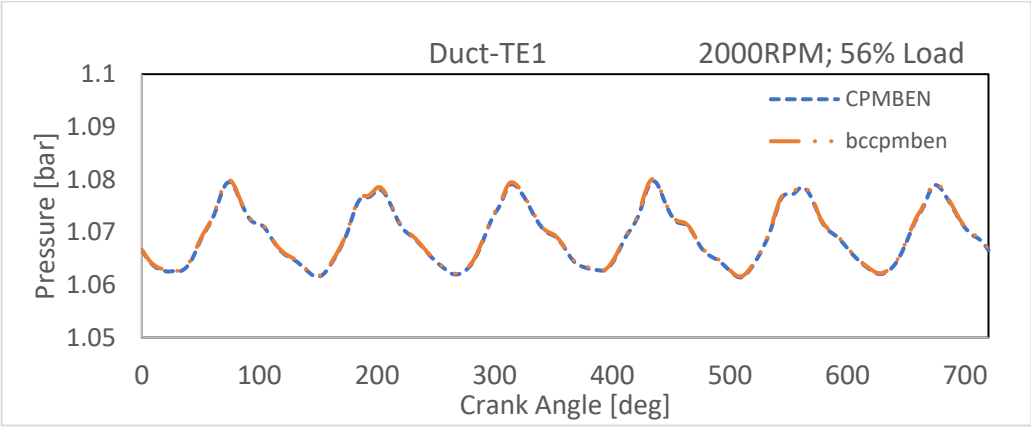

Figure 5.26: Validation of Instantaneous pressure after substitution of CPMBEN

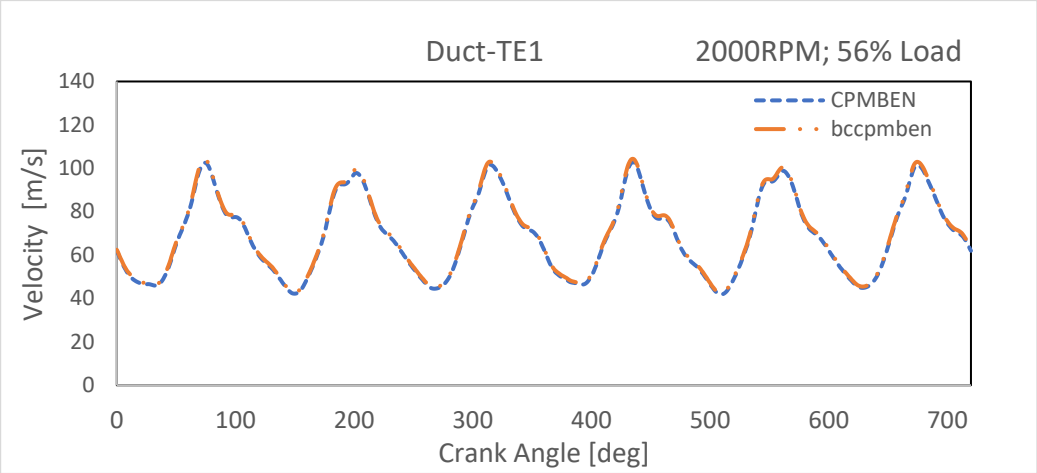

Figure 5.27: Validation of Instantaneous velocity after substitution of CPMBEN

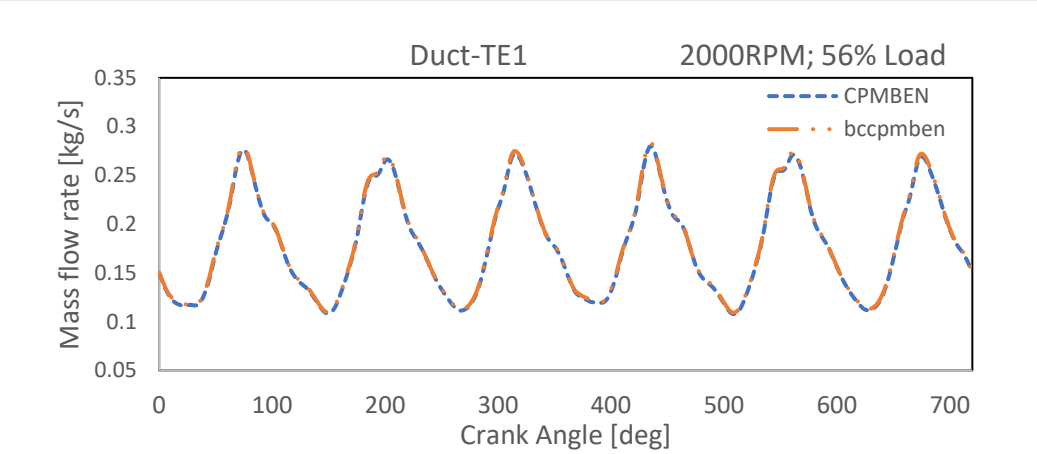

Figure 5.28: Validation of Instantaneous mass flow rate after substitution of CPMBEN

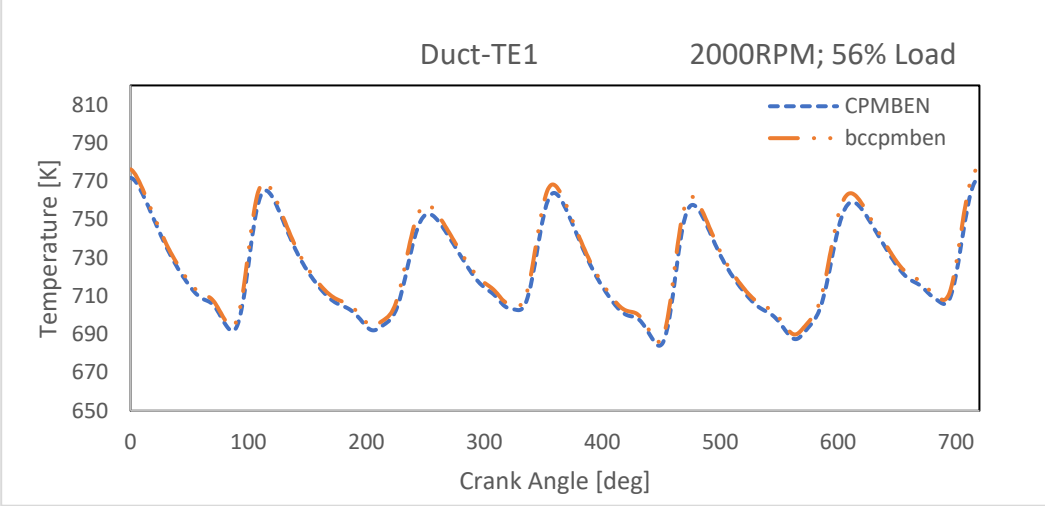

Figure 5.29: Validation of Instantaneous Temperature after substitution of CPMBEN

The simulation of the engine scheme was performed on several operating points. Here we have represented only one of the operating points that is at 2000 rpm and 56 % engine load. Since the graphs for temperature, pressure, velocity, and mass flow rate overlaps with each other this shows that the results generated by bccpmben are exactly the same as generated by the old subroutine CMPBEN at each crank angle, therefore we can say that the bccpmben works as the correct substitution of the subroutine CPMBEN

5.3.5.2 Substitution of CPMCAT

The CPMCAT subroutine is the one used for the junction connected to the catalyst matrix and is also based on the same theoretical structure of constant pressure junction. Thus, the new subroutine bccpmben should be able to replace this subroutine with the same results. This will be tested in the following section.

In order to test the substitution of the new subroutine on a catalyst junction we had to select a project with a catalyst. The Gasdyn project selected for this test was Project: HR10DDTG.

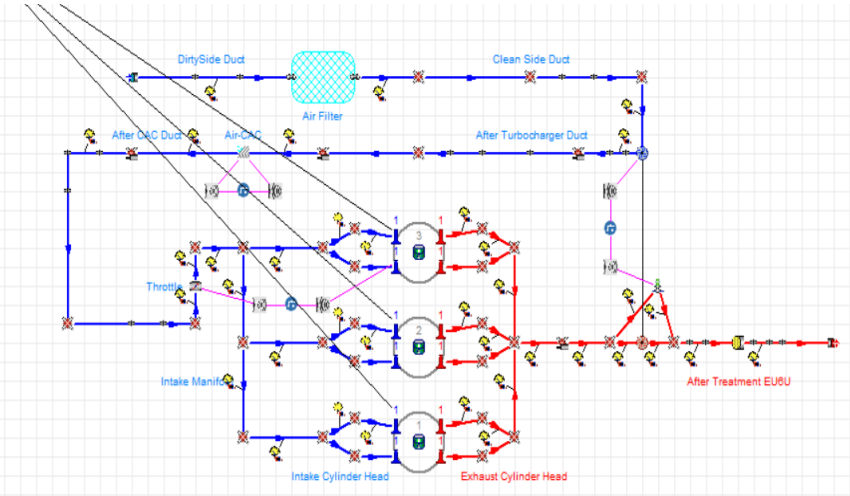

Figure 5.30: Gasdyn configuration for Project HRR10DDTG

The project has a catalyst junction in the exhaust manifold and the same junction was used to test the results of substitution. Similar to the previous work performed for the previous test of substitution, graphical results for instantaneous pressure, temperature, mass flow rate and velocity were plotted against the crank angles using the subroutines CPMCAT & bcpmben. The graphs are plotted for the duct after the catalyst.

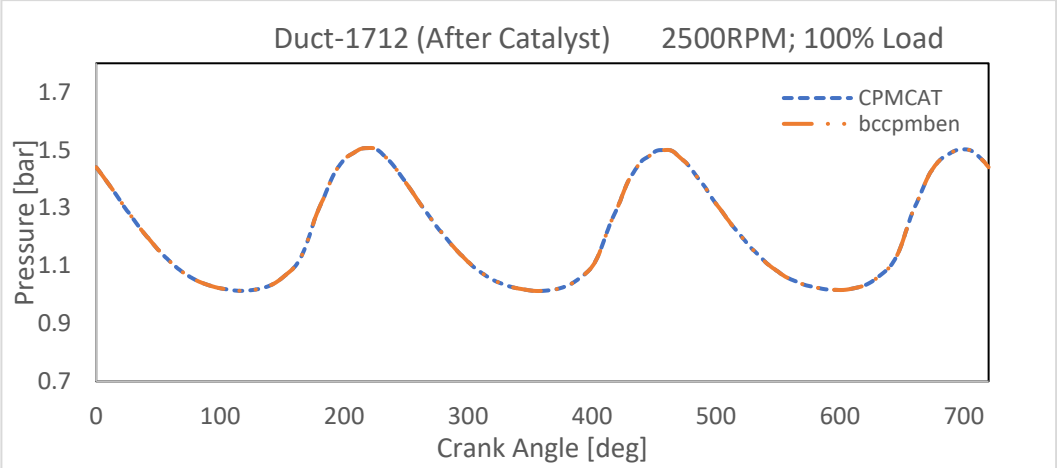

Figure 5.31: Validation of Instantaneous pressure after substitution of CPMCAT

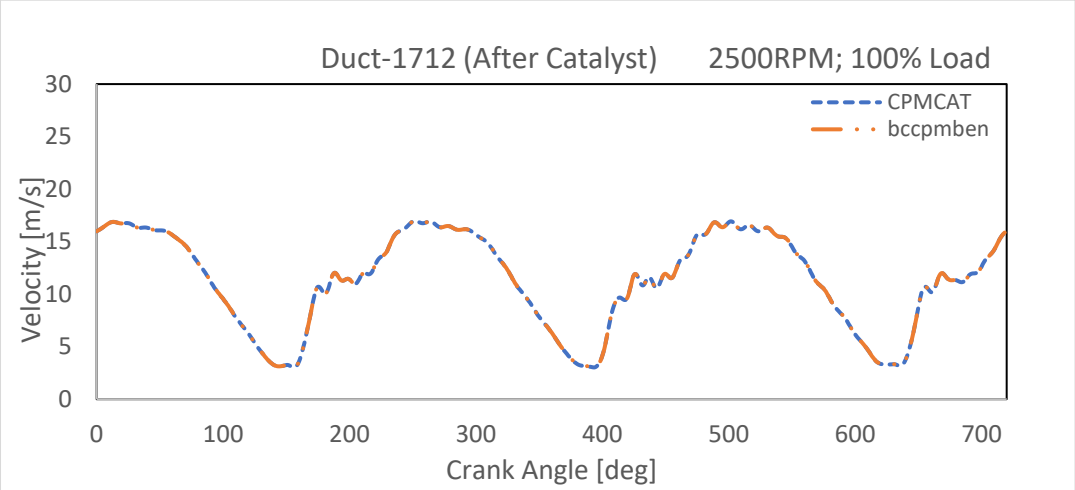

Figure 5.32: Validation of Instanataneous velocity after substitution of CPMCAT

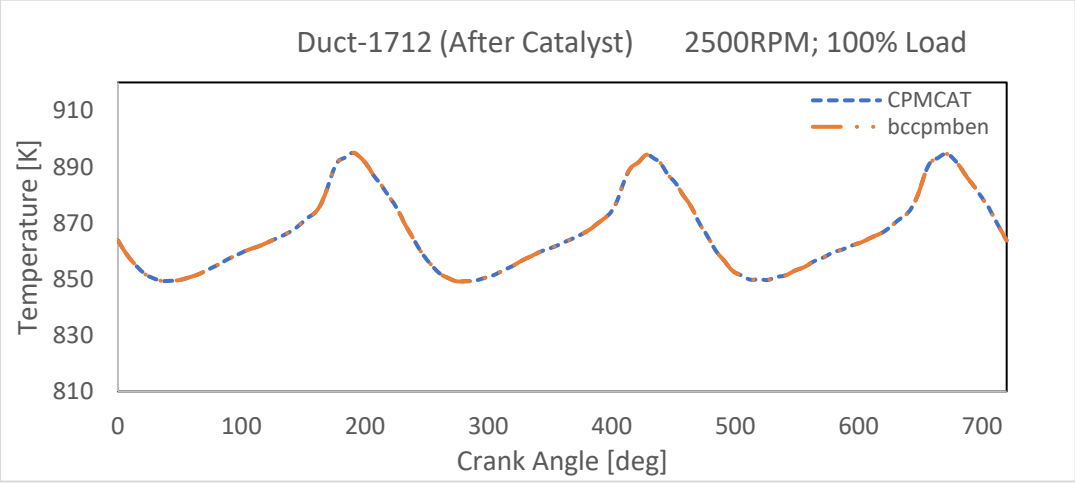

Figure 5.33: Validation of Instanataneous temperature after substitution of CPMCAT

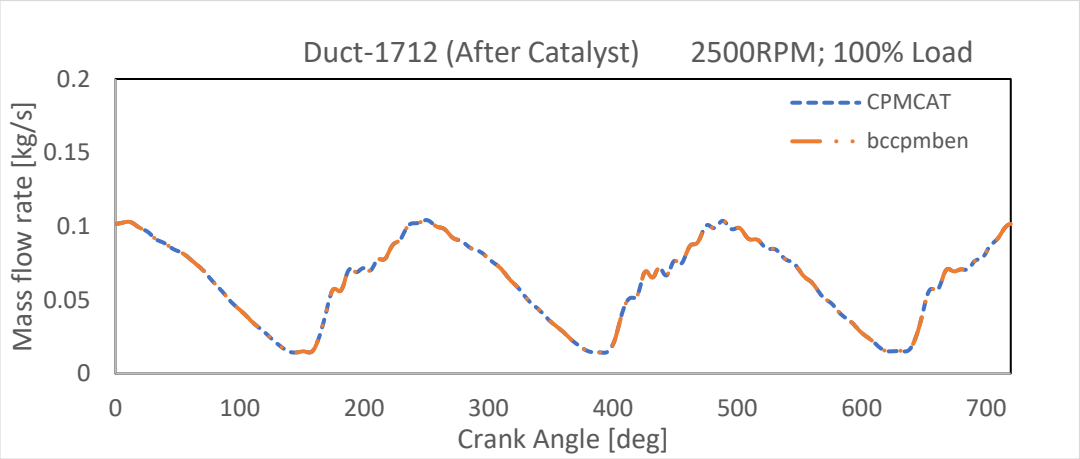

Figure 5.34: Validation of Instanataneous mass flow rate after substitution of CPMCAT

The operating point for the engine simulation results shown in the graph above is 2500 rpm & 100 % load. Moreover, some additional points were tested which showed similar results. The graphs as we see are overlapping which again proves that the new subroutine works perfectly and is a successful substitution of the CPMCAT subroutine

5.3.5.3 Substitution of CPMDUC

The catalyst and the intercooler junction work in the same manner as already explained earlier. Hence it is expected that if the results of substitution of catalyst junction with the new subroutine was a success, then the intercooler junction would too. The test case for this verification is a project that have an intercooler. The same project that HRR10DDTG was used to perform this verification since it does have an intercooler. The graphical results for the instantaneous properties against crank angle are plotted for duct P-604 located after the intercooler represented by the Figure 5.35 - Figure 5.38

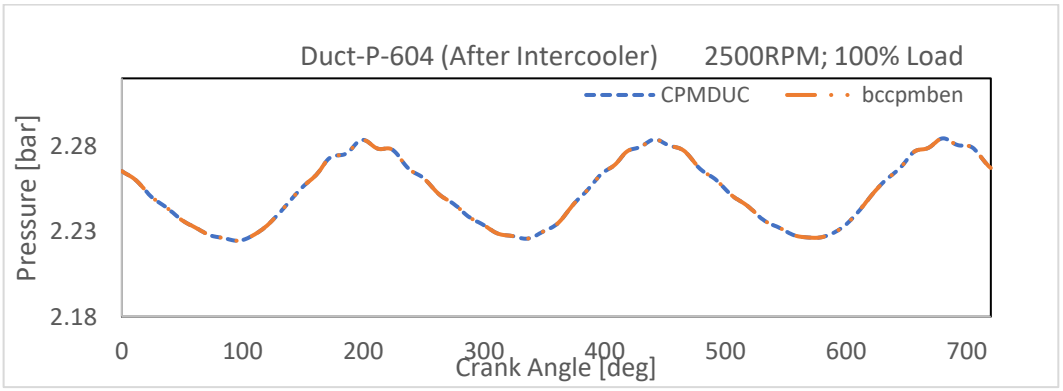

Figure 5.35: Validation of Instanataneous pressure after substitution of CPMDUC

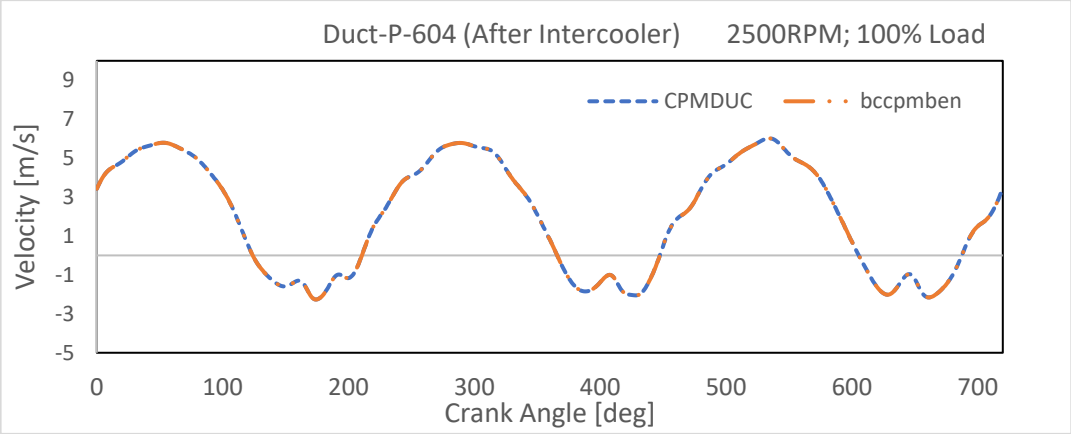

Figure 5.36: : Validation of Instanataneous velocity after substitution of CPMDUC

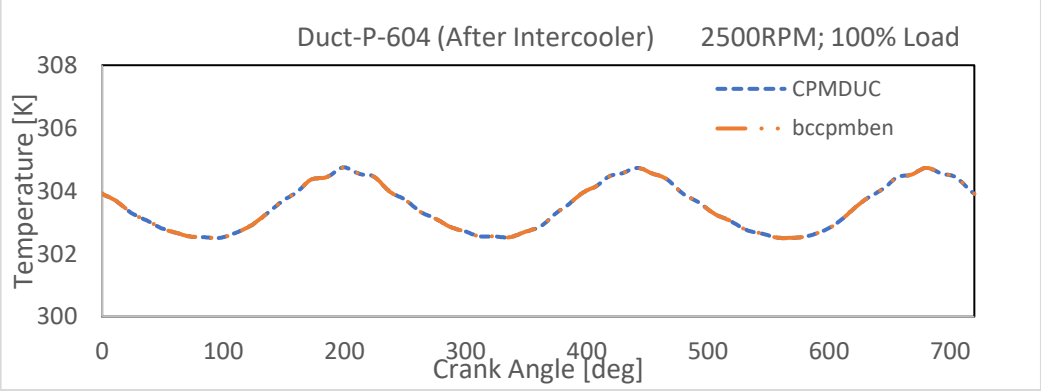

Figure 5.37: Validation of Instanataneous temperature after substitution of CPMDUC

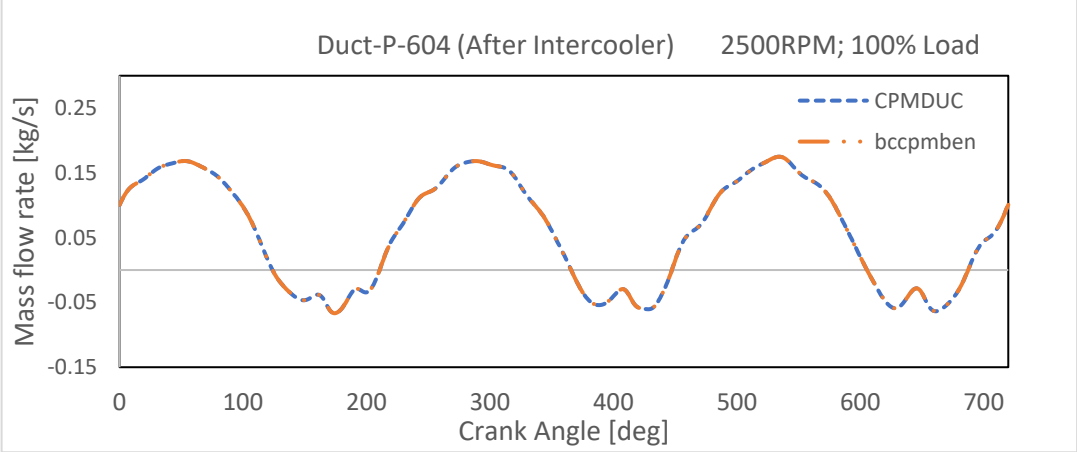

Figure 5.38: Validation of Instanataneous mass flow rate after substitution of CPMDUC

The results as generated by the engine simulation with the old and the new subroutine at operating point of 2500 rpm and 100 % Load, the instantaneous properties are

recorded for the duct-P604 which is located after the intercooler. The graphical results approve that the new subroutine is also valid for the intercooler junctions, and we can call the subroutine bccpmben in place of subroutine CPMDUC when we have an intercooler type junction.

5.3.5.4 Substitution of CPMFOR

The last remaining validation for the new subroutine is for junctions with the perforated ducts/silencers. For this purpose, multiple projects were analyzed. It was observed that initially for some projects the results did not overlap and had minor dissimilarity after which the subroutine was reviewed to check for any corrections needed. It was observed that the new subroutine did not have any errors but in fact the old subroutine used for the perforates gave slightly misaccurate results specially in cases having very low velocity of flow across the junction. The condition used for the positive flows (towards the junction) was not properly inserted in the old subroutine which led to some cases being treated as negative flows despite being in direction towards the junction. This criterion was corrected in the new subroutine which proved to be more robust and accurate and resolved this error and instabilities

Several Gasdyn engine schemes were analyzed for the perforate junction. The critical configurations with the cases mentioned above were studied in detail. One of which is represented in Figure 5.39. The project is called Hybrid Silencer, having two sets of perforated ducts.

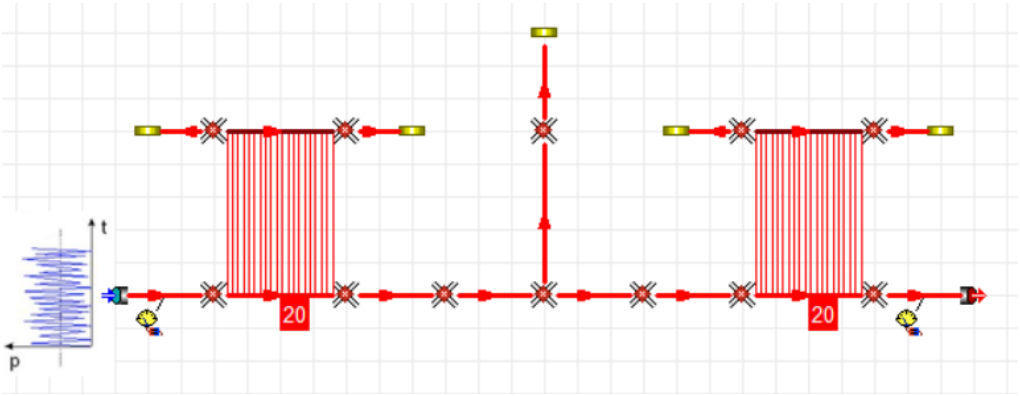

Figure 5.39: Gasdyn Configuration for project - Hybrid Silencer

The graphical results for the instantaneous properties are plotted against crank angles for the duct-8 which is the right most duct after the perforates.

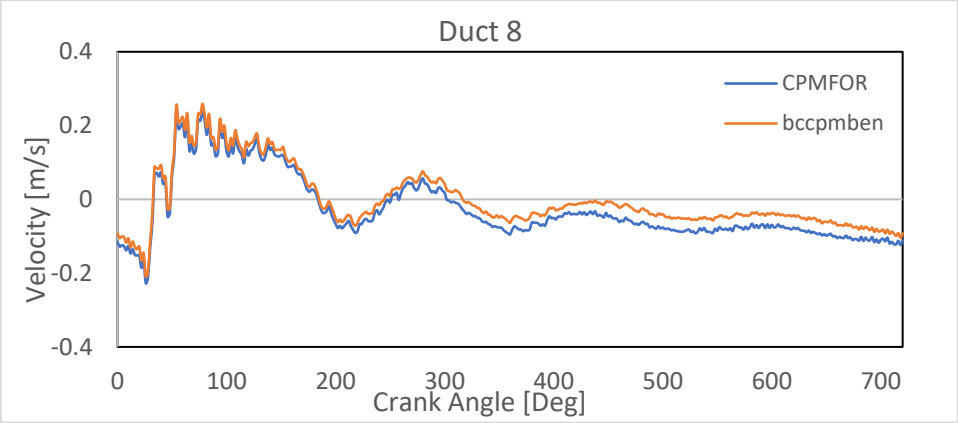

Figure 5.40: Instantaneous velocity results after substitution of CPMFOR

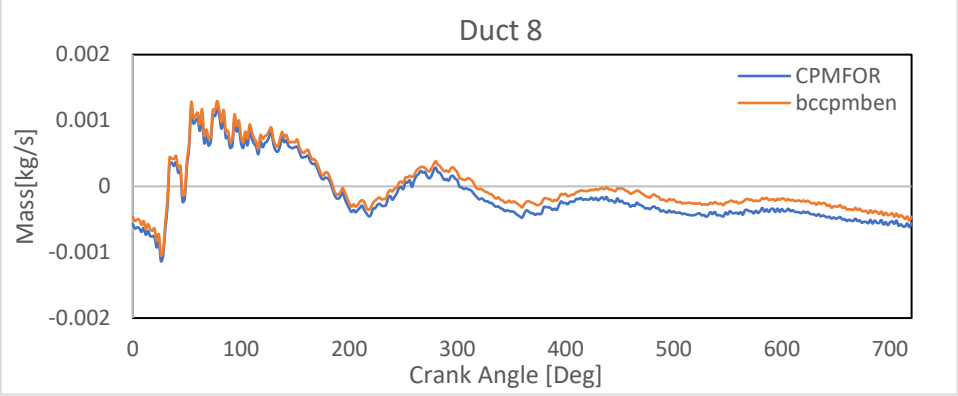

Figure 5.41 : Instantaneous mass flow results after substitution of CPMFOR

Since the substitution for CPMFOR was critical one, we discuss another configuration named Dissipative-D, to analyze the results after substitution. The graph of mass flow rate and velocity is plotted against the crank angle for Duct 10, which is the right most duct located at the outlet.

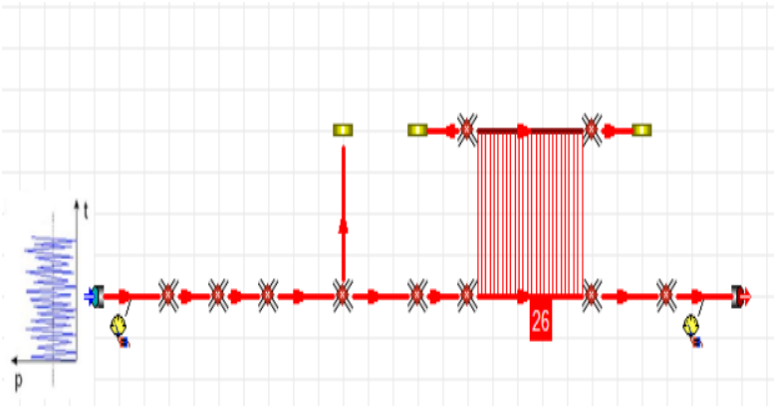

Figure 5.42: Gasdyn Configuration for project - Dissipative-D

The graph of mass flow rate and velocity is plotted against the crank angle for Duct-10 which is the right most duct located at the outlet to compare the results after the implementation of the new subroutine with the previous subroutine

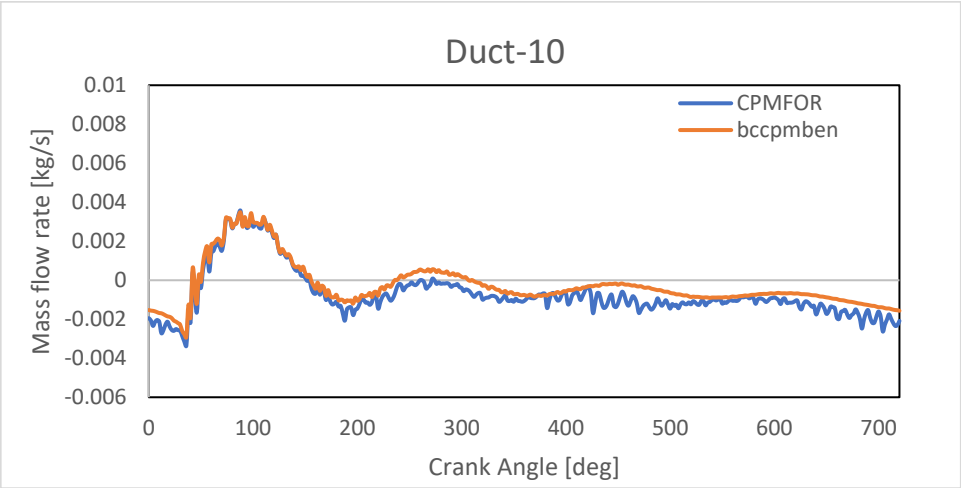

Figure 5.43: Instantaneous mass flow results after substitution of CPMFOR

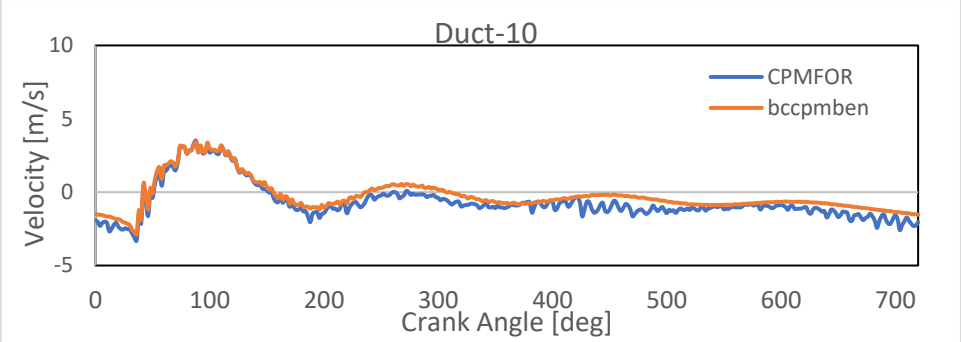

Figure 5.44: Instanataneous velocity results after substitution of CPMFOR

From the graphical comparison of the characteristic properties against crank angles for both the old and new subroutine for the perforates, it is observed that unlike the substitution of other subroutines (CPMBEN,CPMCAT,CPMDUC), the substitution of CPMFOR with bccpmben gives slight difference in results which is due to the fact the original CPMFOR had a minor error which needed to be adjusted and was considered and incorporated by the new subroutine. The new subroutine eliminates the instabilities that were being produced by the old subroutine CPMFOR, this is clearly evident in the graphs for mass flow rate and velocity, as the simulation results generated with bccpmben are smoother unlike the one generated from CPMFOR which predicts unstable results at certain crank angles. Therefore, the new subroutine provides results which are more robust and accurate, and it is convenient to replace the old subroutine for perforates with the new developed subroutine bccpmben.

5.3.6 Validation with simultaneous substitution

It has been concluded till now that the subroutine bccpmben is capable to solve different junction types which include the junction of n-pipes, catalysts, intercooler and perforates. The results with the application of bccpmben instead of each of these subroutines separately was tested in the previous sections which showed successful results. Now we need to verify the results by simultaneously substituting the old routines by the bccpmben, which means that we will call the subroutine bccpmben in all places in the program where the subroutines CPMBEN, CPMCAT, CPMDUC & CPMFOR were called, this should be performed simultaneously.

For this purpose, we need a project which have different junction types in its configuration so that the results of substitution can be validated. The project selected to test the simultaneous substitution is 2.0_16V. This engine configuration of this project is represented by Figure 5.45 and includes the following components:

61 exhaust pipes

52 intake pipes

88 n-pipe junctions

04 Catalysts mesh

01 Silencer

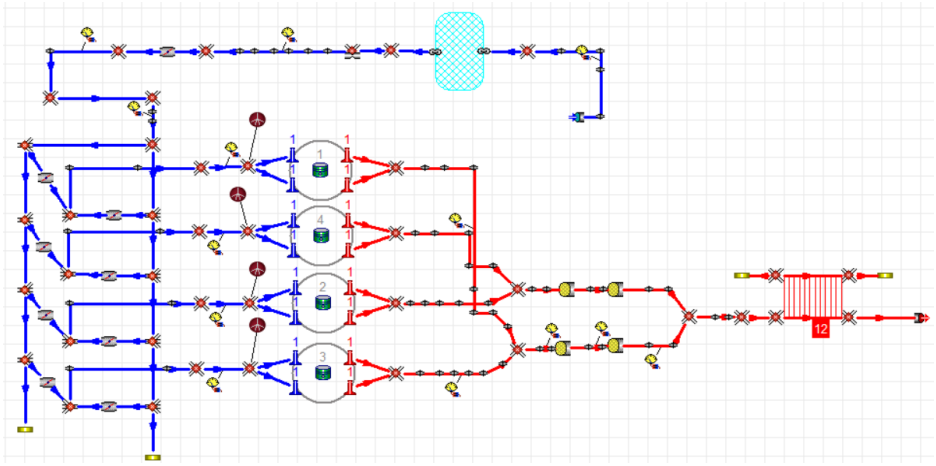

Figure 5.45: Gasdyn Project 2.0_16V

Since the considered configuration of the engine has several junctions of n pipes, junctions with catalysts and perforates, this project is useful to test the simultaneous substitution. The only junction type missing is the intercooler type junction, but we have already stated that the intercooler type junction works in the same manner as of the catalyst so we can test the substitution of the old subroutines simultaneously with bccpmben on this project for validation.

The test was performed on multiple ducts to ensure that the subroutine bccpmben provides accurate results and can substitute the other subroutines with perfection. Also, the simultaneous substitution tests were performed on these ducts using various operating points. Therefore, the results could then be analyzed and checked if there are any errors related to the new subroutine. The results showed that the new subroutine worked perfectly to replace the old subroutines.

The instantaneous properties (pressure, velocity, mass flow rate & Temperature) were plotted against the crank angle for the comparison of results, we have represented the graphs of the duct-433 which is the duct just behind the silencer as it would include the effect of previous junctions as well.

The graphical results of the characteristic properties against crank angle during the engine operating cycle at 2000 rpm & 100 % Load for the duct 433 are represented by Figure 5.46 & Figure 5.47.

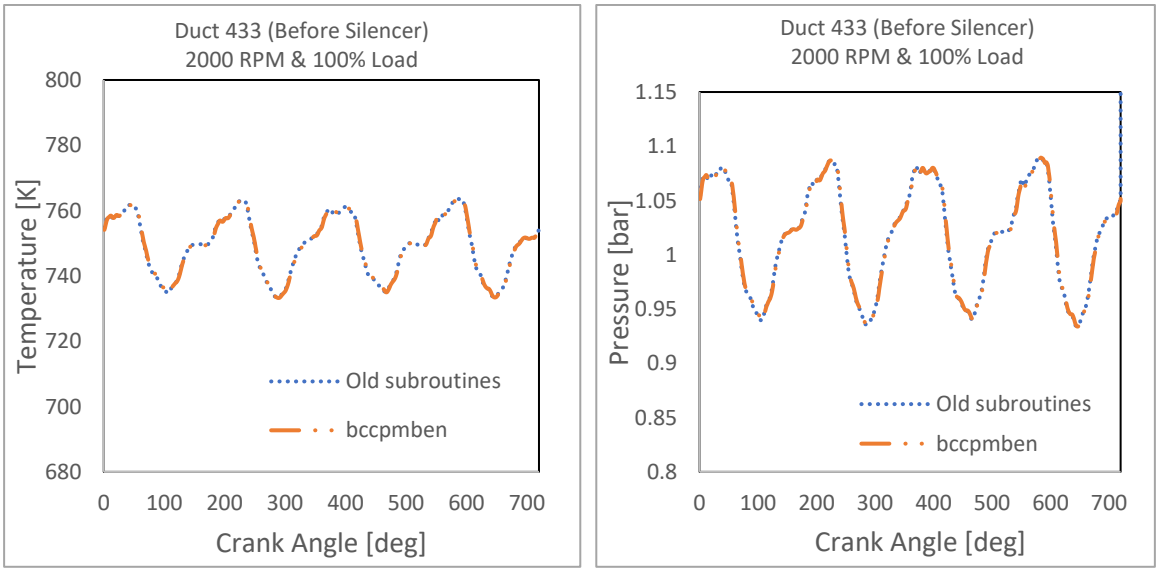

Figure 5.46: Instantaneous Temperature and pressure after simultaneous substitution on duct-433

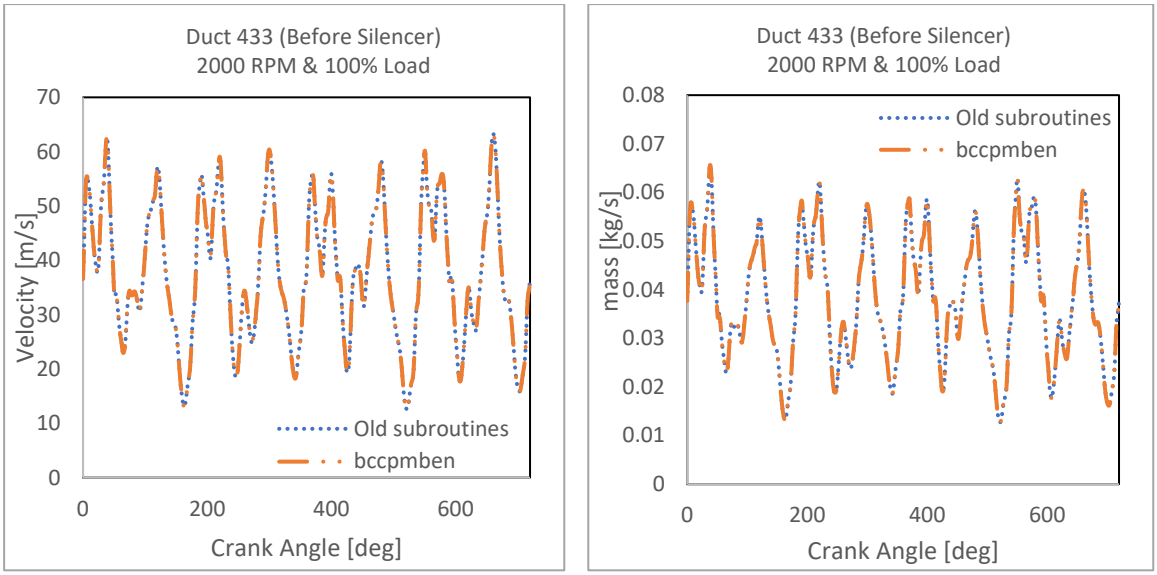

Figure 5.47: Instantaneous velocity and mass flow rates after simultaneous substitution on duct-433

In addition to the duct-433, we have also represented the graphical result of the duct-453, which is the last duct (on the extreme right). This last duct is a good point for comparison as it represents the overall results throughout the engine scheme.

Figure 5.48 & Figure 5.49 are the graphical results of the characteristic properties against crank angle during the engine operating cycle at 2000 rpm & 100 % Load for the duct 453.

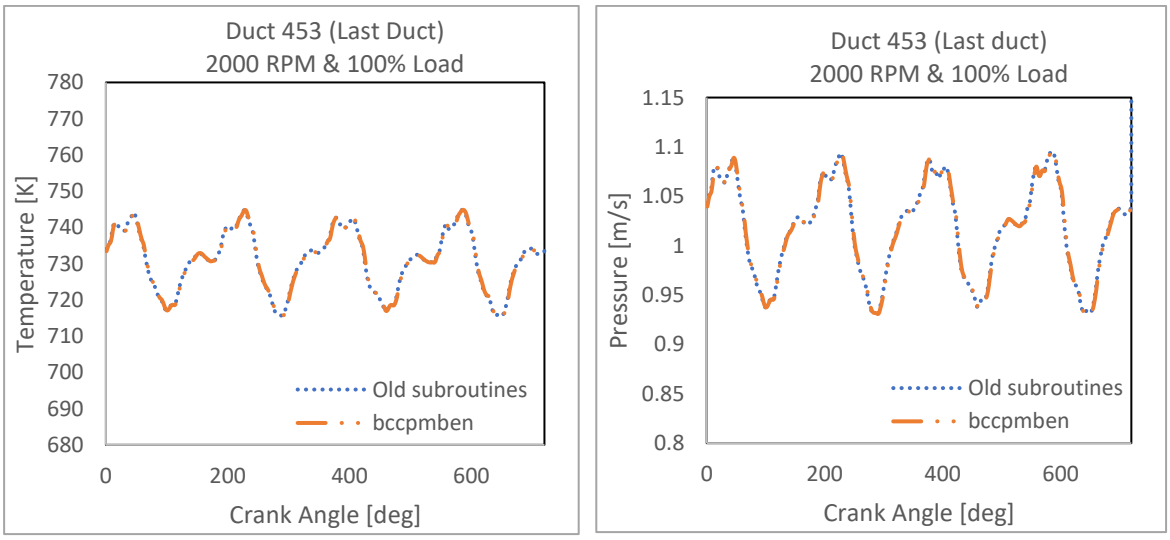

Figure 5.48: Instantaneous Temperature and pressure after simultaneous substitution on duct-453

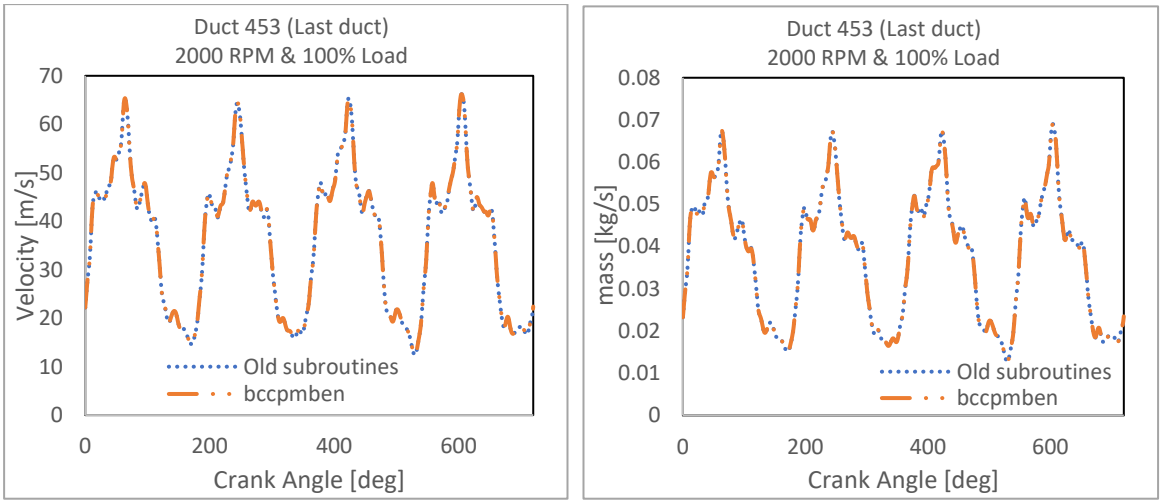

Figure 5.49 Instantaneous velocity and mass flow rates after simultaneous substitution on duct-453

As seen from the graphical results for ducts 453 & 433, it is verified that the results as obtained by using the subroutine bccpmben are in accuracy with the results which we obtained using the old subroutines for different junctions together. Thus, it is correct to claim that the subroutine bccpmben can be used for all the other junction types based on the constant pressure model. The results are validated on different projects and on multiple operating points along different ducts. The verification for substitution test of the new subroutine is successful.

5.3.7 Mass conservation validation

The new subroutine that is developed also takes into account the mass conservation along the junction, which means that it ensures that the total instantaneous mass flow rate that enters the junction is equal to the total instantaneous mass flow rate that flows away from the junction. This is an important aspect that has been included in the new subroutine and should also be verified on an engine configuration. For this purpose, we analyzed the mass conservation on the Gasdyn project discussed above named 2.0_16V, the junction # 13147 was tested for mass conservation.

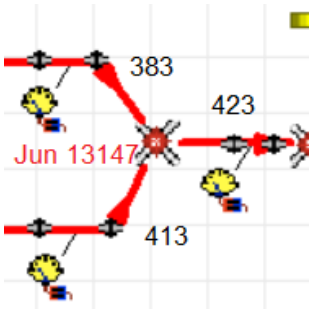

Figure 5.50: Representation of Junction # 13147 with connected ducts

The junction # 13147, as shown in the junction diagram have two # of incoming ducts (Duct 413 and Duct 383), the combined flow from these two ducts is outflows from Duct 423. The table below shows the results for some crank angle the difference in mass flow rates of total incoming flows and outgoing flows at different crank angles. The junction is located after the catalysts. The result shown in the Table 5.1 are for operating point of 2200 RPM & 100 % Load.

Crank Angle (Deg)	**Mass flow in (kg/s) Duct 413 + Duct 383**	**Mass flow out (kg/s) Duct 423**	**Difference (kg/s) (Mass conservation of junction 13147)**
100	0.0411222430000	0.0411222430000	0
250	0.0115817330000	0.0115817320000	0.000000001
320	0.0520645200000	0.0520645200000	0
400	0.0316062570000	0.0316062570000	0
450	0.0301428090000	0.0301428080000	0.000000001
500	0.0436182750000	0.0436182750000	0
600	0.0216223580000	0.0216223580000	0
720	0.0395056570000	0.0395056570000	0

Table 5.1: Mass flow rate conservation applied for the junction-13147 using bccpmben

Table 5.1 represents the mass flow rate in and out to apply the mass conservation at various randomly selected crank angles and it validates the conservation of mass at the selected instances. To check for the entire cycle and prove the validation of the conservation of mass, we plot a graph with mass flow rate in and out of the junction represented against each value of crank angle across the engine cycle.

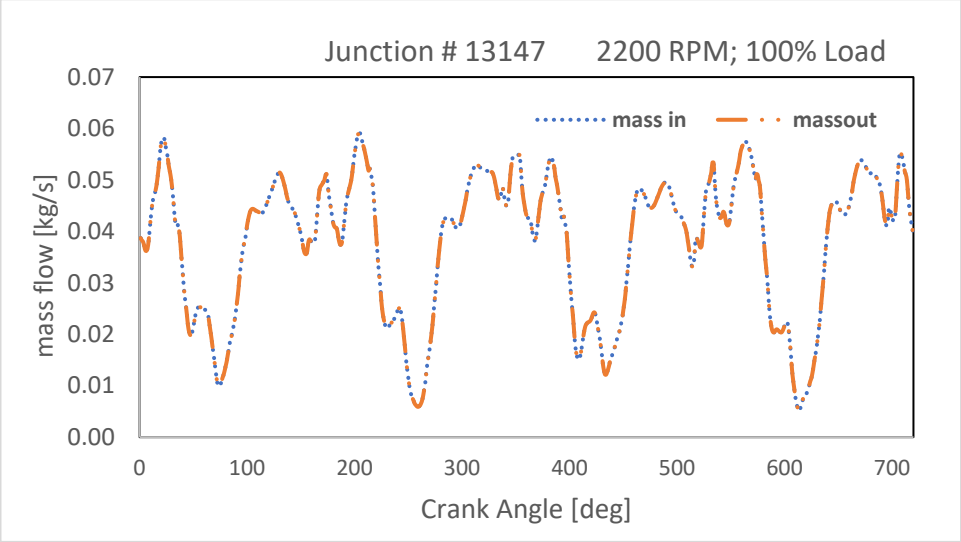

Figure 5.51: Mass flow rate conservation for junction-13147 using bccpmben

Hence it is clear from Figure 5.51 that with the new subroutine the mass flow rate is conserved in the entire cycle for the considered junction at the selected operating point. Multiple tests were performed in a similar way for the other junctions and using various operating points and similar results were obtained which proves that the new subroutine respects the mass conservation with accuracy.

5.3.8 Critical Configurations and combination with pressure loss model

There are junctions where the constant pressure model is not suitable and pressure loss model is essential for the accurate prediction of engine simulation results. There are cases where some of the junctions in the engine configuration are complex and requires the application of the pressure loss subroutine for the solution procedure. In the same configuration most of the other junctions are of the simple type and solved with the constant pressure junction model and thus for these cases for the entire engine simulation we need both the pressure loss and the constant pressure model-based subroutines to predict the behavior at different instances of the engine cycle. One such project is the FPT engine with the configuration as seen in Figure 5.52. The

engine consists of several 'suppwb' type junctions in the intake manifold while the rest of the junctions are of the same constant pressure type junction

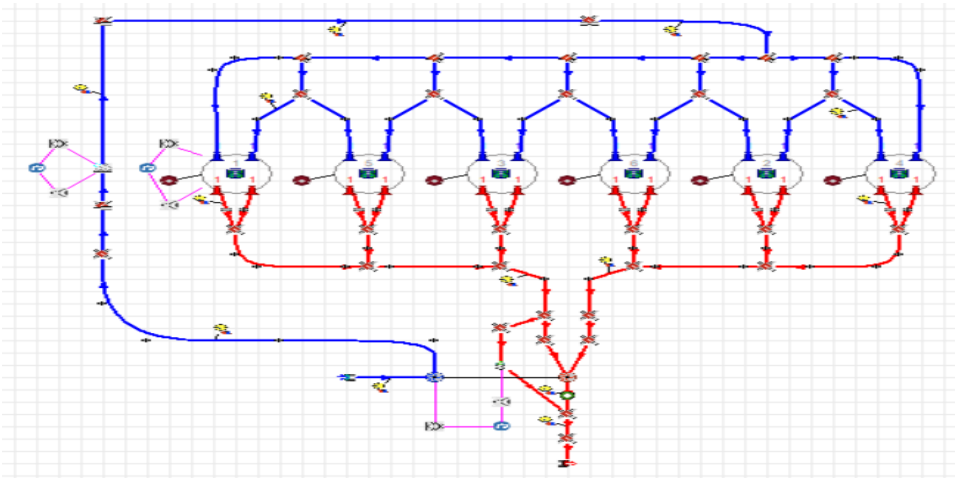

Figure 5.52: Gasdyn Scheme of project FPT – six-cylinder turbocharged engine

The engine simulation for this project is a combination of the application of the subroutine bccpmben and the subroutine for pressure loss model. Let's us analyze the results as produced by the simulation. The instantaneous pressure is observed against crank angles and plotted on the same graph for different operating points. The results represented here are for an intake duct (duct # 11364) which is located in the intake manifold before the first cylinder, with fixed load and varying the engine speed and also with fixed engine speed with varying load

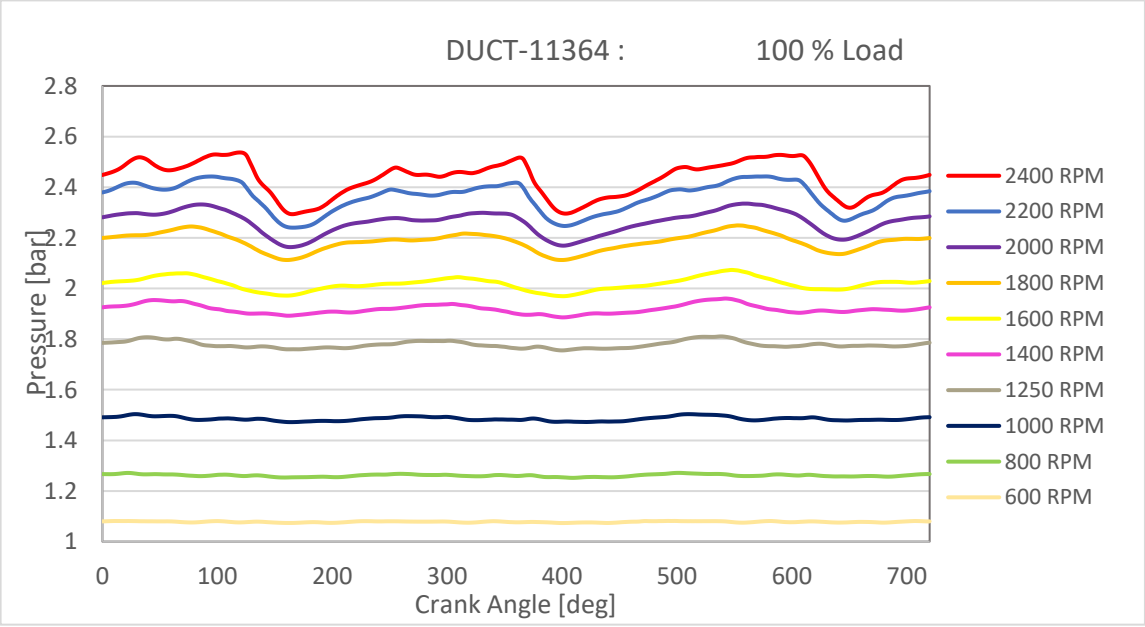

Figure 5.53: Pressure results for project FPT engine at 100 % Load

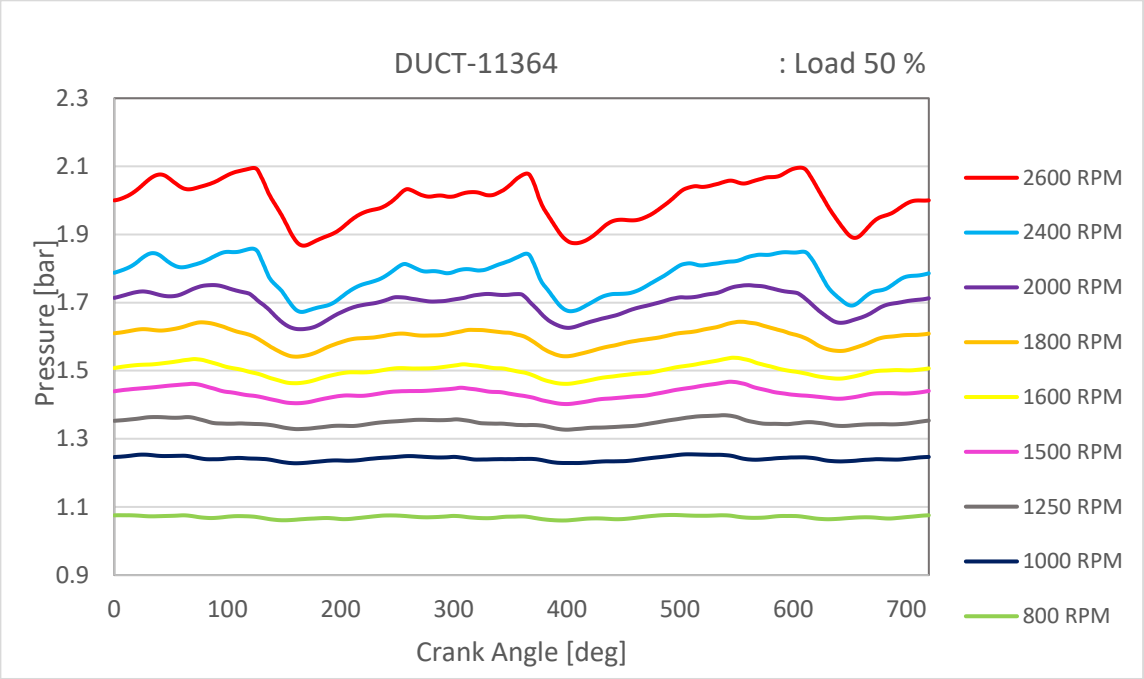

Figure 5.54: Pressure results for project FPT engine at 50 % Load

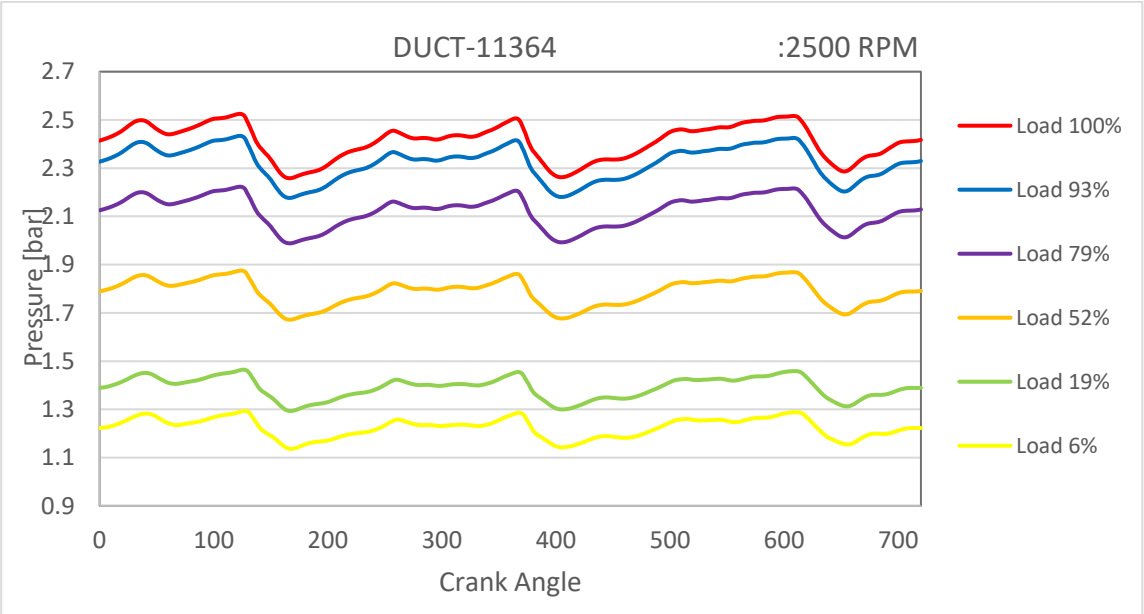

Figure 5.55: Pressure results for project FPT engine at 2500 RPM

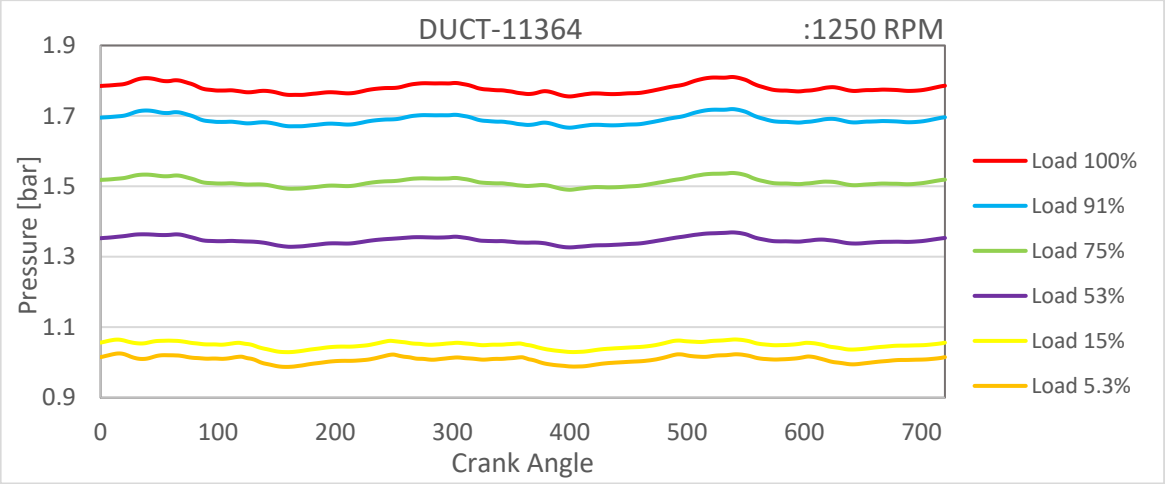

Figure 5.56: Pressure results for project FPT engine at 1250 RPM

The graphical results plotted for instantaneous pressure against the crank angle for the project in consideration respects the trend. The first two graphs represent the instantaneous pressure in the intake duct at fixed load and varying the engine speed while the last two figures represent the instantaneous pressure with varying engine load at fixed speed. We observe that the pressure in the intake manifold increases with the engine speed at fixed load and vice versa, this is expected because of the engine configuration in consideration is a turbocharged engine and the exhaust pressure increases at high speeds which in turn drives the compressor thus increasing the pressure in the intake manifold at high loads and rpms. The trend is respected during the entire range of engine operation which also validates that the subroutine bccpmben also works with the presence of the pressure loss junctions in the engine configuration where the subroutine for pressure loss is applied to the 'collwb' or 'suppwb' type junctions while bccpmben is applied to the other junctions.

Another critical configuration is a single cylinder engine, the gasdyn project for the configuration is represented by the Figure 5.57. The configuration is called 'scighera'

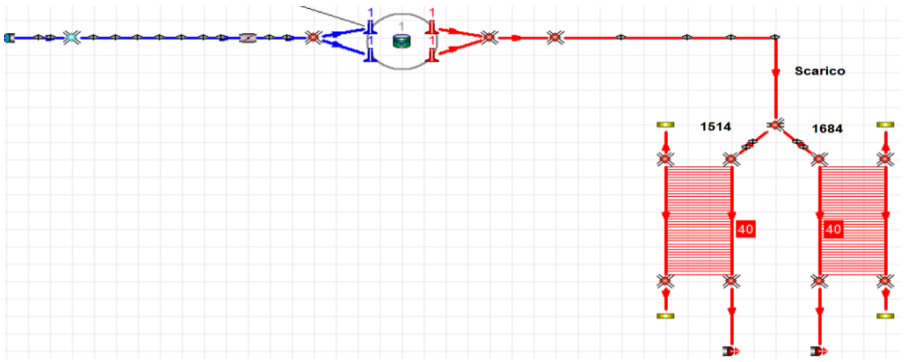

Figure 5.57: Gasdyn configuration for the Project-schighera

The results obtained for this project after implementation of the old subroutines showed instabilities, the configuration of this engine has one pressure loss junction 'suppwb' type where the main exhaust duct supplies flow to two exhaust branches connected to the silencer, the junctions for the silencers are constant pressure type junctions which was previously solved by the old subroutine CPMFOR, which is now replaced by bccpmben. In the intake duct we have a simple 3-duct junction which was previously solved by the subroutine CPMBEN, now replaced by subroutine bccpmben. We compare here the simulations results produced before and after the substitution of the old subroutines with bccpmben. Thus, the simulation is performed in two ways

- As a combination of pressure loss subroutine (nploss) and old subroutines (CPMFOR,CPMBEN)
- As a combination of pressure loss subroutine (nploss) and the new subroutine bccpmben

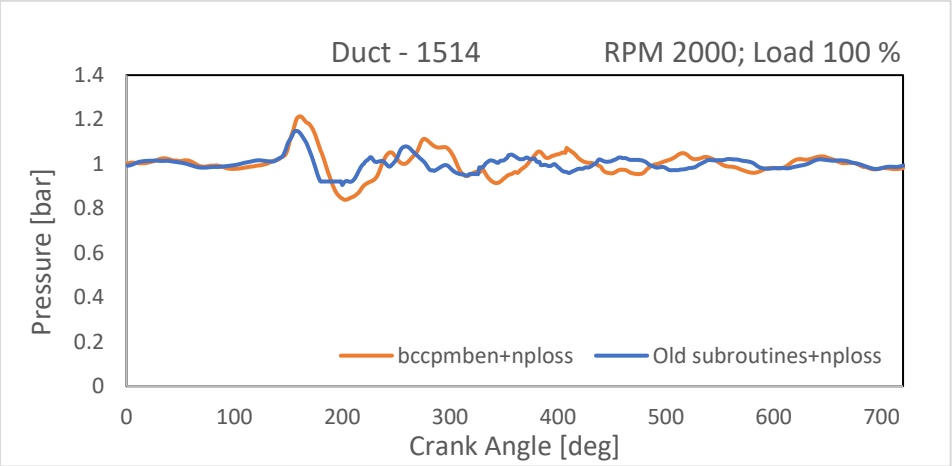

Figure 5.58: Pressure results for project Schighera at 2000 RPM before & after substitution by bccpmben

The instantaneous pressure for duct-1514 is represented at operating point of 2000 rpm & 100 % load. We can see how the old subroutines showed pressure instabilities specially around the crank angle of 180-200 degrees where the pressure is constant on a range of crank angle which is not possible. These instabilities were removed when the simulation was performed with the new subroutine.

The odd behavior can also be observed on the duct 'scarico' which is the exhaust supply duct. The instabilities in the engine simulation for pressure prediction using old subroutines can be seen at large range of crank angles where the pressure remains constant for parts of the crank cycle. Again, the new subroutine bccpmben removes

these instabilities. The graphical representation is plotted at operating point of 4000 rpm & 100 % Load.

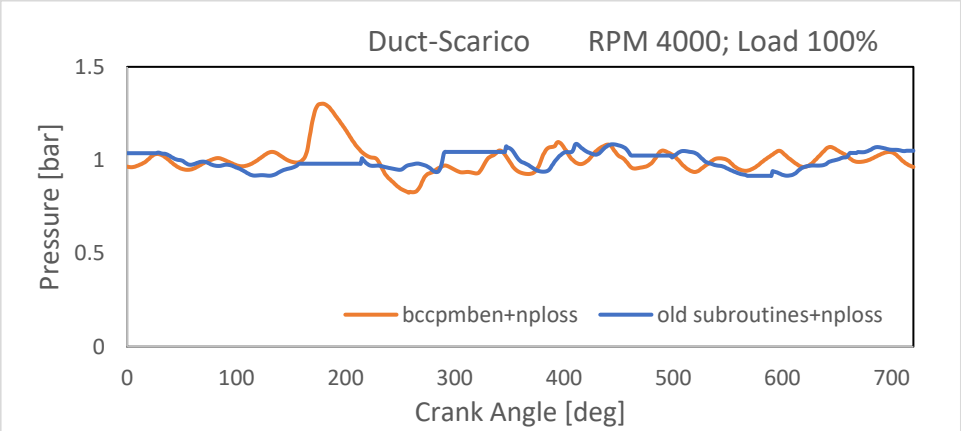

Figure 5.59 : Pressure results on project Schighera at 4000 RPM before & after substitution by bccpmben

Moreover, the mass conservation application was also compared for different operating points, the results for comparison are represented graphically.

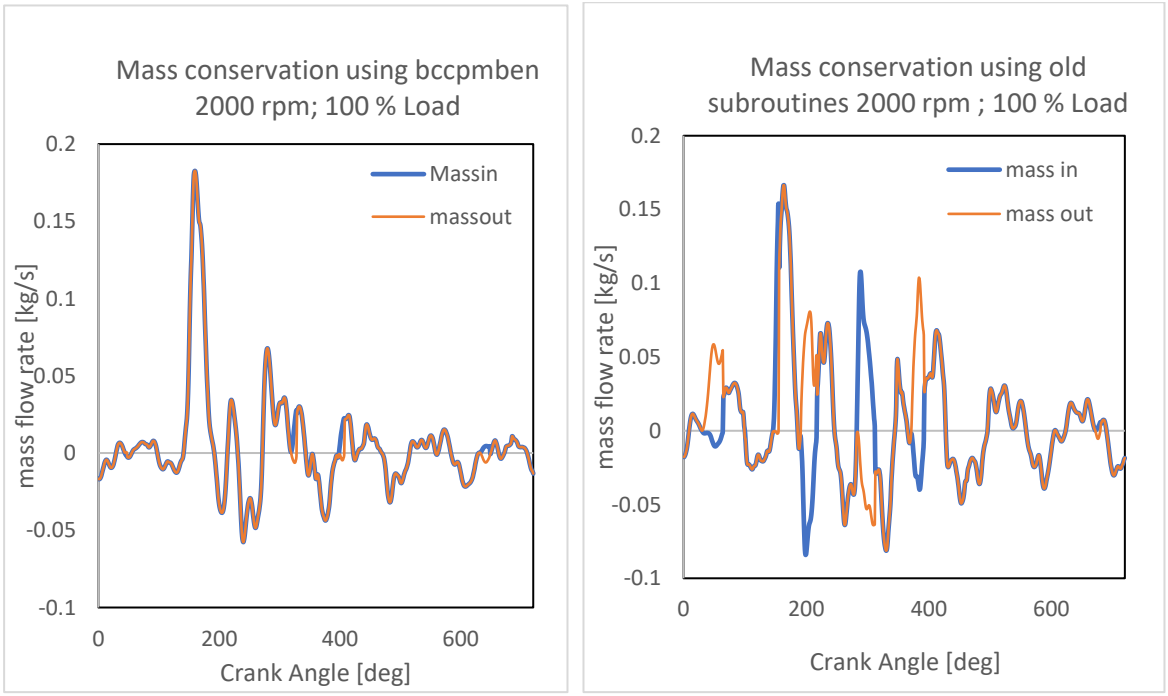

Figure 5.60: Mass conservation on project Schighera at 2000 RPM before & after substitution by bccpmben

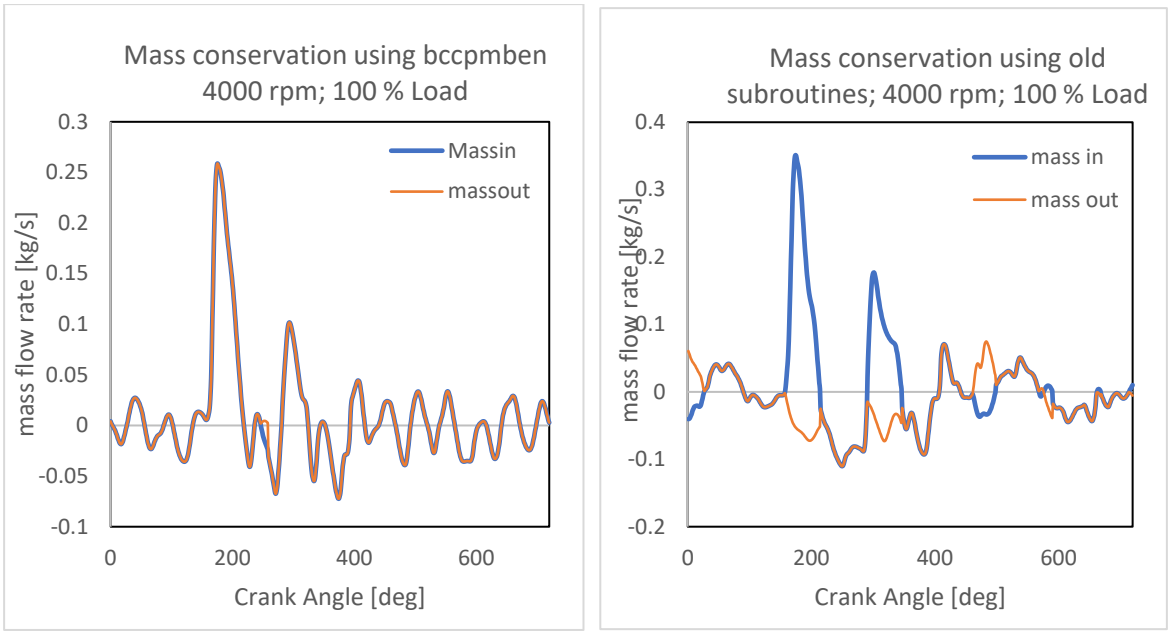

Figure 5.61: Mass conservation on project Schighera at 4000 RPM before & after substitution by bccpmben

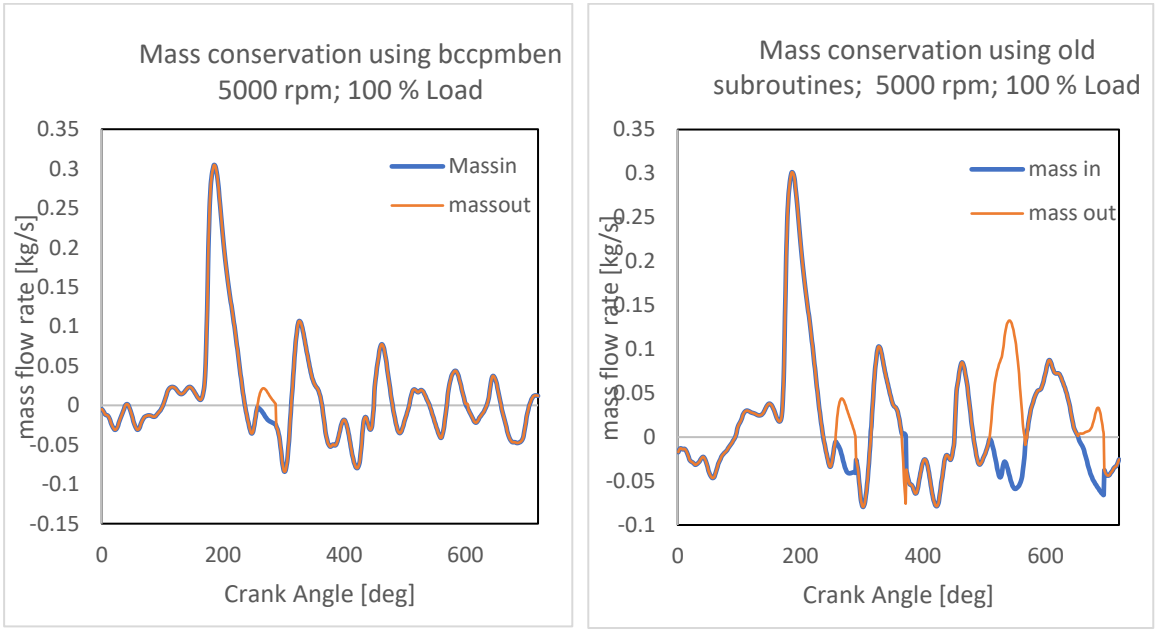

Figure 5.62: Mass conservation on project Schighera at 5000 RPM before & after substitution by bccpmben

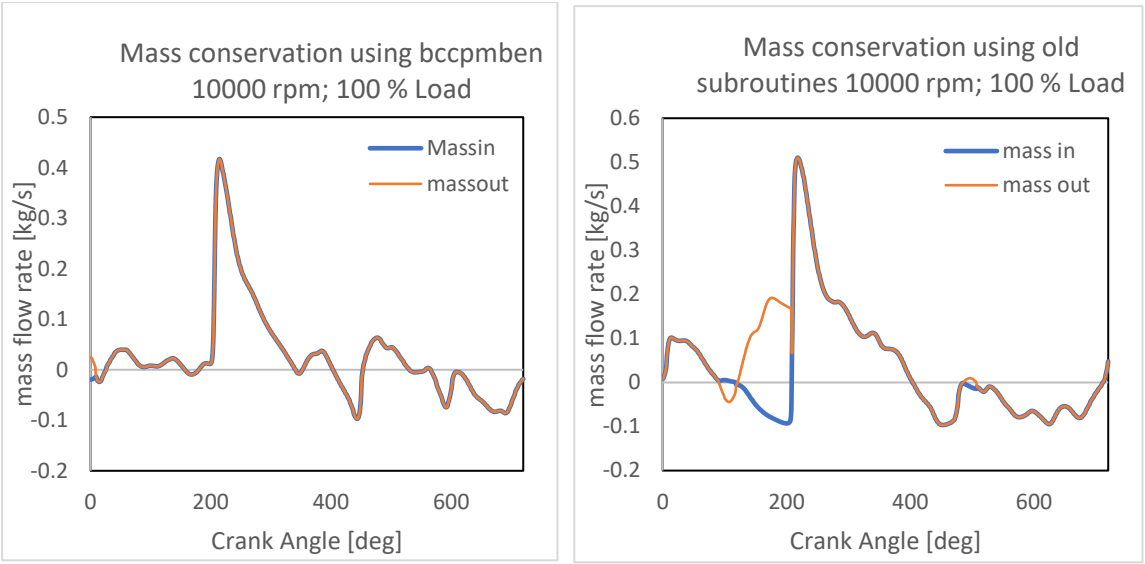

Figure 5.63: Mass conservation on project Schighera at 10000 RPM before & after substitution by bccpmben

It is clear from the graphical results obtained after simulation performed on this critical project, which showed some instabilities in results with the previous subroutines, the new subroutine eliminated the instabilities and respected the mass conservation along the crank cycle at each operating points. The results obtained after using new subroutine bccpmben provide better conservation of mass in comparison to the previous results which is quite significant in the above graphs

5.4 Final conclusions

As the basic objective of this thesis work, a new general subroutine bccpmben was created to replace all the subroutines that are used for the solution of different junction types based on the constant pressure model. The new subroutine bccpmben is a general, more robust and accurate than the previously utilized subroutines. The subroutine was developed by a combination and modification of the characteristics of the old subroutines. Different engine schemes were analyzed to verify the functionality of the new subroutine and the results were compared first individually with the substitution of each of the old subroutine individually and then simultaneously substituting all the subroutines with the new created subroutine. The results of instantaneous properties plotted graphically against the crank angle confirmed the validity of the new subroutine which is now incorporated into Gasdyn

software code for the solution of different junction types. The mass flow conservation is also incorporated into the new subroutine. The validation of mass flow rates being conserved was also performed.

Following is a comparison of using the new subroutine over the old subroutines:

- The new subroutine bccpmben is a general subroutine to solve all types of junctions based on the constant pressure model which includes the catalysts, Intercooler, Perforates & junction of n-pipes. Hence, we do not need further separate subroutines for each junction type
- When the new subroutine is called in the main program, it only requires one input which is the number of ducts connected to the junction, unlike each of the old subroutines which require multiple inputs to be calculated in the main program before they are called.
- The new subroutine bccpmben can perform the calculation of other variables necessary for the solution inside the body of the subroutine.
- The output is written directly in shared form inside the body of the new subroutine unlike the old subroutines
- The new subroutine is independent and does not require the output to be sent to the main program again for further calculations
- If any modifications or precision improvement is required in the constant pressure-based junction models, they can be incorporated into the subroutine bccpmben alone instead of incorporating into separate subroutines.
- The new subroutine overcomes the limitations of the old subroutine and removes the pressure, mass flow rate & velocity instabilities that were observed with the use of old subroutines for particual engine configurations. After implementation of the new subroutine bccpmben, these instabilities were eliminated, this validates the accuracy and robustness of the new subroutine

Bibliography

[1] R. S. Benson, The Thermodynamics and Gas Dynamics of Internal Combustion Engines, Oxford: Claredon Press, 1982.

[2] G. Ferrari, Internal Combustion Engines, 2nd Edition, Esculpia, 2014.

[3] D. E. Winterbone and R. J. Pearson, Design Techniques for Engine Manifolds, London: Professional Enegineering Publishing, 2000.

[4] B. Riemann, Gesammelte Mathematische Werke, University of Michigan, Germany: Leipzig : B.G. Teubner, 1892.

[5] C. Hirsch, Numerical Computation of Internal and External Flows, Brussels: John Wiley & Sons, 1998.

[6] D. E. Winterbone and R. J. Pearson, Numerical Methods for Simulating Gas Dynamics in Engine, University of Manchester, UK, 1994.

[7] R. W. Maccormack, "The effect of viscosity in hypervelocity impact cratering," in *Americal Inst. of Aeronautics & Astronautics, Hypervelocity Impact Conference*, Cincinnati, 1969.

[8] P. D. Lax and B. Wendroff, "Difference Schemes for Hyperbolic Equations with High Order of Accuracy," *Communications on Pure and Applied Mathematics,* 1964.

[9] J. M. Corberan, "A New Constant Pressure Model for N-Branch Junctions," vol. 206, no. 2, 1992.

[10] L. Gascón and J. Corberán, "Construction of second-order TVD schemes for nonhomogeneous hyperbolic conservation laws," *Journal of computational physics,* vol. 172, 2001.

[11] N. List and G. Reyl, "The Scavenging of Internal Combustion Engine," Springer Verlag, Vienna, 1949.

[12] R. S. Benson, "A Simple Algorithm for a Multi-Pipe Junction in Non-Steady Homoentropic Flow," vol. 17, no. Journal of Mechanical Engineers, 1975.

[13] J. R. Nichols, "Techniques for the design of exhaust manifolds with pulse converters," University of Manchester Institute of Science and Technology, 1984.

[14] C. L. Chan, R. J. Nicholas, G. I. Alexander and D. E. Winterbone, "Efficiency of the Manifolds of Turbocharged Engines," *Efficiency of the Manifolds of Turbocharged Engines,* vol. 19, no. Proceedings of the Institution of Mechanical Engineers, 1986.

[15] S. L. Dixon and N. I. Abou-Haider, "Pressure Losses in Combining Subsonic Flows through Branched Ducts," *Trans. ASME,* 1992.

[16] D. D. Corte and M. Deprez, "Studie van de Stroming in een Pulse Converter," *Eindejaarswerk, Rijkuniversiteit Gent,* 1984.

[17] W. H. Hager, "An Approximate Treatment of Flow in Branches and Bends," vol. 198, 1984.

[18] D. E. Winterbone, M. D. Bassett and R. J. Pearson, "A Multi-Pipe Junction Model for One-Dimensional Gas-Dynamic Simulations," *SAE 2003 World Congress & Exhibition,* 2002.

[19] J. F. Bingham and G. Blair, "An Improved Branched Pipe Model for Multi-Cylinder Automotive Engine Calculations," *Proceedings of the Institution of Mechanical Engineers, Part D: Journal of Automobile Engineering,* 1985.

[20] G. Ferrari, A. Onorati and T. Carri, "1D Thermo-Fluid Dynamic Simulation of a High Performance Lamborghini V12 S.I. Engine," *SAE Technical Papers,* 2005.

[21] D. E. Winterbone and R. J. Pearson, Theory of Engine Manifold Design, London: Professional Engineering Publishing, 1999.

Acknowledgements

I would like to thank deeply Politecnico di Milano for providing me a great platform and opportunity to study, explore and experience such a diversified environment. Studying in a multicultural institute from qualified professionals and fellows from all around the world has certainly added value to my interpersonal and professional skills.

Secondly, I would like to thank my family for supporting me in all ways possible to ensure that everything I need is provided to me at all times that allowed me to complete my degree in the best possible way without facing any difficulties.

Lastly, my deepest gratitude to Prof. A. Onorati and Eng. Andrea Massimo for supervising the thesis, and guiding us throughout with their knowledge & wisdom, for providing us all the time, directions and support needed to keep things aligned along with sharing ideas and doubts. Without them, this accomplishment was not possible.